Titre: Title:	Advances in Electromagnetic Reciprocal and Nonreciprocal Bianisotropic Metasurfaces
Auteur: Author:	Guillaume Lavigne
Date:	2022
Type:	Mémoire ou thèse / Dissertation or Thesis
Référence: Citation:	Lavigne, G. (2022). Advances in Electromagnetic Reciprocal and Nonreciprocal Bianisotropic Metasurfaces [Ph.D. thesis, Polytechnique Montréal]. PolyPublie. https://publications.polymtl.ca/10320/

POLYTECHNIQUE MONTRÉAL
affiliée à l'Université de Montréal

Advances in electromagnetic reciprocal and nonreciprocal bianisotropic metasurfaces

GUILLAUME LAVIGNE
Département de génie électrique

Thèse présentée en vue de l'obtention du diplôme de *Philosophiæ Doctor*
Génie électrique

Mai 2022

POLYTECHNIQUE MONTRÉAL
affiliée à l'Université de Montréal

Cette thèse intitulée :

Advances in electromagnetic reciprocal and nonreciprocal bianisotropic metasurfaces

présentée par **Guillaume LAVIGNE**
en vue de l'obtention du diplôme de *Philosophiæ Doctor*
a été dûment acceptée par le jury d'examen constitué de :

Mohammad S. SHARAWI, président
Maksim SKOROBOGATIY, membre et directeur de recherche
Christophe CALOZ, membre et codirecteur de recherche
Stéphane KÉNA-COHEN, membre
Ari SIHVOLA, membre externe

DEDICATION

À Hélo,
pour son support inflexible

RÉSUMÉ

Les métasurfaces électromagnétiques sont de minces structures artificielles composées d'un arrangement de particules conçues pour produire des propriétés électromagnétiques qui ne sont pas présentes naturellement dans les matériaux conventionnels. Au cours des dernières années, les métasurface ont démontré leur capacité sans précédent à contrôler les ondes électromagnétiques. En effet, il a été démontré que les métasurfaces permettent le contrôle de différents aspects fondamentaux des ondes électromagnétiques comme la polarisation, la direction de propagation, la phase, l'amplitude et la forme des faisceaux.

Les métasurfaces étant des structures électromagnétiquement minces, elles peuvent être modélisées comme étant une discontinuité électromagnétique dans l'espace ayant une épaisseur nulle. Sous cette approximation, une généralisation des conditions aux limites conventionnelles qui incluent des courants de polarisation de surface, appelées les Generalized Sheet Transition Conditions (GSTCs), peuvent être utilisées pour modéliser les métasurfaces. Les GSTCs permettent de modéliser non seulement des réponses électriques et magnétiques, mais aussi des réponses électro-magnétiques/magnéto-électriques correspondant à de la bianisotropie. Cette modélisation bianisotropique des métasurfaces est essentielle puisqu'au cours des dernières années, il a été démontré que de nombreuses opérations fondamentales pouvant être effectuées par des métasurfaces nécessitent la présence de réponses bianisotropes pour être réalisées de manière pleinement efficace. Dans cette thèse, nous présentons des avancées liées aux métasurfaces bianisotropes réciproques et non-réciproques.

Dans la première partie, nous étudions le contrôle de la réfraction à l'aide de métasurfaces bianisotropes passives et réciproques. Les premières métasurfaces conçues pour contrôler la réfraction à l'aide de l'approche du gradient de phase avaient des problèmes pour de grands angles de réfraction en raison de l'excitation d'ordres de diffraction indésirables ce qui limitait leur efficacité. Heureusement, il a récemment été démontré théoriquement qu'inclure des réponses bianisotropes permettrait de concevoir des métasurfaces réfractives pour des grands angles avec une efficacité maximale. Dans ce travail, nous présentons la modélisation mathématique, la conception, la simulation et la démonstration expérimentale de métasurfaces bianisotropes réalisant la réfraction à grands angles sans ordres de diffraction indésirables, et donc avec une efficacité optimale. Par la suite, nous étudions la généralisation, avec l'utilisation de métasurfaces bianisotropes, d'un phénomène fondamental lié à la réfraction: l'effet de Brewster. L'effet de Brewster conventionnel consiste en la disparition de la réflexion de la polarisation p à l'interface entre deux diélectriques à un angle spécifique qui

dépend de l'indice de réfraction des deux milieux. Dans ce travail, nous généralisons l'effet de Brewster à n'importe quel angle et à n'importe quelle polarisation en insérant une métasurface bianisotrope correctement conçue à l'interface entre les deux milieux. La modélisation mathématique de ces métasurfaces, leur conception et leurs simulations sont présentées. Les métasurfaces bianisotropes proposées peuvent servir de solution d'adaptation fortement sous longueur d'onde entre différents milieux.

Dans la deuxième partie, nous étudions la réalisation de métasurfaces non-réciproques. La non-réciprocité est une propriété essentielle pour la réalisation de plusieurs opérations fondamentales tels que l'isolation ou la circulation. La non-réciprocité est habituellement obtenue dans les systèmes électromagnétiques à l'aide de matériaux polarisés magnétiquement, par exemple des ferrites, qui produisent le phénomène non-réciproque de rotation de Faraday. Cependant, en raison de l'incompatibilité avec les circuits intégrés, de la grande taille et de l'encombrement de l'aimant nécessaire à la polarisation, la technologie utilisant des matériaux polarisés magnétiquement n'est pas facilement intégrable aux métasurfaces. Les métasurfaces doivent donc utiliser des technologies non-réciproques sans aimant telles que la modulation spatio-temporelle ou l'utilisation de résonateurs chargés de transistors. Dans ce travail, nous présentons plusieurs travaux sur les métasurfaces non-réciproques réalisés à l'aide de résonateurs chargés de transistors. Nous présentons d'abord une métasurface réalisant un isolateur spatial gyrotrope avec la modélisation théorique, la conception des résonateurs chargés de transistors et les simulations associées. Ensuite, nous présentons une étude théorique de métasurfaces réalisant la rotation de Faraday en transmission. Par la suite, nous présentons le concept d'une métasurface à gradient de phase non-réciproque réalisée à l'aide de cellules unitaires bianisotropes réalisant un déphasage non-réciproque. Enfin, nous présentons une métasurface réalisant un isolateur spéculaire non-gyrotrope avec la modélisation théorique, la conception de résonateurs chargés de transistors, la simulation et la démonstration expérimentale associée.

ABSTRACT

Electromagnetic metasurfaces are subwavelengthly thin artificial structures composed of an arrangement of engineered scattering particles that exhibit electromagnetic properties that are beyond those conventionally found in nature. Metasurfaces have been shown to offer an unprecedented control of electromagnetic waves and can be seen as general purpose electromagnetic wave transformers. Indeed, they have been shown to enable the control of fundamental properties of electromagnetic waves such as the polarization, propagation direction, phase, amplitude and beam shapes of electromagnetic waves.

Metasurfaces being electromagnetically thin structures can be modelled as a zero-thickness electromagnetic discontinuity in space. Under this approximation, a generalization of conventional boundary conditions that include surface polarization currents called the Generalized Sheet Transition Conditions (GSTCs) can be used to model, synthesize and analyze metasurfaces. The GSTCs allow the modeling of not only electric and magnetic responses, but also electro-magnetic/magneto-electric responses corresponding to bianisotropy. This bianisotropic modelling is critical since, in recent years, many fundamental metasurface operations have been shown to require bianisotropy to be realized fully efficiently. In this thesis, we present advances related to both reciprocal and nonreciprocal bianisotropic metasurfaces.

In the first part, we investigate the control of refraction with reciprocal and passive bianisotropic metasurfaces. Initial metasurfaces realizing generalized refraction designed with the phase gradient approach had issues for large-angle refraction due to the excitation of undesired diffraction orders and hence limited efficiency. Fortunately, recent theoretical derivations have shown that metasurfaces with bianisotropic responses could realize fully efficient large-angle refraction. In this work, we present the mathematical modelling, design, full-wave simulations and experimental demonstration of bianisotropic metasurfaces realizing large-angle refraction without the excitations of undesired diffraction orders, and hence with optimal efficiency. We next investigate the generalization, with the use of bianisotropic metasurfaces, of a fundamental phenomenon related to refraction: the Brewster effect. The conventional Brewster effect consists on the vanishment of the p-polarized reflection at a dielectric interface at a specific angle that depends on the refractive indexes of both media. In this work, we generalize the Brewster effect to arbitrary angle and polarization by inserting properly designed bianisotropic metasurfaces at the interface between the two media. The mathematical modeling of the metasurfaces, design of the scattering particles at microwave frequencies and full-wave simulations are presented. The proposed bianisotropic metasurfaces

provide deeply subwavelength matching solutions for initially mismatched media.

In the second part, we investigate the realization of nonreciprocal metasurfaces. Nonreciprocity is essential for many fundamental operations such as isolation and circulation, and is conventionally obtained in electromagnetics through magnetically-biased materials (e.g. ferrites) relying on Faraday rotation. However due to the incompatibility with integrated circuits, large size, heavy weight and bulkiness of the magnetized technology, nonreciprocal metasurfaces need to rely on magnetless nonreciprocal technologies such as spacetime-modulation or transistor-loaded resonators. In this work, we present several investigations of magnetless nonreciprocal transistor-loaded metasurfaces. We first present a gyrotropic reflective isolator metasurface with the related theoretical modelling, design of transistor-loaded scattering particles and full-wave simulations. Next, we present a theoretical investigation metasurfaces performing transmissive faraday rotation. We then present the concept of nonreciprocal phase gradient metasurfaces realized using bianisotropic nonreciprocal phase-shifting unit cells. Finally, we present a nongyrotropic specular isolator metasurface with the related theoretical modelling, design of transistor-loaded scattering particles, full-wave simulations and experimental demonstration.

TABLE OF CONTENTS

LIST OF TABLES

LIST OF FIGURES

LIST OF SYMBOLS AND ABBREVIATIONS

Symbols

c_0, c	Speed of light in vacuum
ϵ_0, ϵ	Free space permittivity
μ_0, μ	Free space permeability
η_0, η	Free space impedance
k_0, k	Free space wavenumber
$\overline{\overline{\chi}}_{\mathrm{ee}}$	Electric surface susceptibility tensor
$\overline{\overline{\chi}}_{\mathrm{mm}}$	Magnetic surface susceptibility tensor
$\overline{\overline{\chi}}_{\mathrm{em}}$	Electro-magnetic surface susceptibility tensor
$\overline{\overline{\chi}}_{\mathrm{me}}$	Magneto-electric surface susceptibility tensor

Abbreviations

GSTCs	Generalized Sheet Transition Conditions
FDFD	Finite Difference Frequency Domain
PEC	Perfect Electric Conductor
VNA	Vector Network Analyzer
FSS	Frequency Selective Surface
TE	Transverse Electric
TM	Transverse Magnetic
RGSI	Reflective Gyrotropic Spatial Isolator
FET	Field-Effect Transistor
RF	Radio Frequency

LIST OF APPENDICES

CHAPTER 1 INTRODUCTION

This thesis presents advances in the domain of bianisotropic electromagnetic metasurfaces, with both reciprocal and nonreciprocal applications. This introductory chapter will introduce the research area of electromagnetic metasurfaces and provide the research motivation and objectives of this work. This thesis by article includes three publications in peer-reviewed journals included as chapters 4, 5 and 6.

1.1 Introduction to Metasurfaces

A metamaterial is defined as an artificial structure made of an arrangement of engineered particles that exhibit electromagnetic properties that are beyond those conventionally found in nature [1]. The size of the engineered particles that compose the metamaterials, called metaparticles, scattering particles or meta-atoms, is smaller than the wavelength of the incident wave such that no diffraction is experienced and such that the structure can be homogenized to obtain effective material parameters. In the last couple decades, electromagnetic metamaterials have received a lot of interest due to impressive potential applications such as cloaking [2] and perfect lensing with negative refraction [3]. However, it was soon realized that they suffer from important drawbacks such as high losses, fabrication complexity, bulkiness and limited scalability.

Metasurfaces are the two dimensional equivalent of metamaterials with a deeply subwavelength thickness [4]. They have now received far more interest than their three dimensional counterparts due to their relative ease of fabrication, lower losses and similar, although more restricted, wave manipulation capabilities compared to three dimensional metamaterials. Metasurfaces have been shown to offer an unprecedented control of electromagnetic waves and can be seen as general purpose electromagnetic wave transformers. Indeed, they have been shown to enable the control of fundamental properties of electromagnetic waves such as the phase [5], amplitude [6], polarization [7], propagation direction [5] and beam shapes [8] of electromagnetic waves.

One of the most fundamental operations that can be performed by metasurfaces is that of generalized refraction, since it underlines many other wave transformations like lensing and wavefront manipulations. Initial refractive metasurface were based on the phase-gradient approach [5]. They used metaparticles that provide equal strength electric and magnetic dipole responses to realize fully transmissive unit cells with tunable phase [9]. Distinct unit cells, providing different transmission phases, were then arranged in a periodic pattern, called supercell, which creates a phase-gradient and deflects the wave. However, this approach suffered

from fundamental efficiency limitations for high-angles of deflection due to the excitation of undesired diffraction orders [10]. It was subsequently shown that more sophisticated bianisotropic metasurfaces were required to get rid of those diffraction orders and obtain optimal high-angle wave deflection [11].

Bianisotropic metasurfaces include magnetoelectric coupling in addition to direct electric and magnetic dipole responses [12]. Bianisotropic responses have been theoretically shown to be required for the optimal realization many fundamental wave transformations such as generalized refraction and reflection [11], polarization transformations [7] and isolation. Even more generally, it has been theoretically demonstrated that bianisotropic metasurfaces can realize any wave transformation that respect local power conservation [13].

Most metasurfaces reported to date were limited by Lorentz reciprocity. Such a restriction prohibits the realization of many potential metasurface applications such as spatial isolators and circulators, which require a nonreciprocal response [14]. The realization of nonreciprocal metasurfaces is particularly difficult since it requires a biasing force to break reciprocity. Conventional electromagnetic nonreciprocal devices typically use materials such as ferrites that exhibit Faraday rotation when biased by a magnet [15]. Due to the bulkiness of the required magnet and the non-integrability of this technology with integrated circuits, practical nonreciprocal metasurface need to rely on magnetless nonreciprocal technologies [16] such as nonlinearity, space-time modulation or transistor-loaded structures. The transistor-loaded technology is of particular interest for many monochromatic nonreciprocal operations such as isolation, circulation, or nonreciprocal phase shifting. While a few recent works have investigated the realization of nonreciprocal metasurfaces, there is an opportunity to model, design and implement novel nonreciprocal spatial wave transformations with metasurfaces.

1.2 Motivation and Objectives

Bianisotropic metasurfaces have recently been recognized as possessing the proper characteristics to realize optimally efficient fundamental operations. Specifically, the control of refraction represents an indispensable operation for many metasurface applications. Phase gradient metasurfaces that have realized generalized refraction have fundamental flaws for high-angle deflection due to impedance mismatch between incident and refracted wave, which causes the excitation of undesired diffraction orders. While theoretical works have shown that bianisotropic responses in metasurfaces remove this mismatch and have the potential to realize fully efficient generalized refracting structures, an experimental demonstration of such metasurfaces is still lacking. An complete investigation of the control of refraction, and its related effects, with bianisotropic metasurfaces is hence needed.

Furthermore, given that the vast majority of metasurfaces reported so far have been restricted to reciprocal responses, many nonreciprocal metasurface operations have yet to be realized. The advent of magnetless nonreciprocal technologies now allow the practical implementation of nonreciprocal responses in metasurfaces. The implementation of nonreciprocal metasurfaces responses would allow the design of conventional nonreciprocal circuit operations such as isolation and circulation in a spatial form and also generally increase the capabilities and degrees of freedom of metasurfaces to go beyond simple passive metasurfaces. The transistor-loaded technology is an especially promising magnetless nonreciprocal approach to realize nonreciprocal linear time-invariant metasurfaces due to its simple bias and ease of integration in the microwave regime. Hence, there exists a significant interest in developing transistor-loaded metasurfaces to realize spatial nonreciprocal wave transformations and in general to broaden the already vast capabilities of metasurfaces.

The general objective of this research is to leverage the recent advances in modelling, synthesis and design of bianisotropic metasurface to demonstrate their potential in fundamentally manipulating electromagnetic waves. We shall separate this general objective into two specific objectives: the study of reciprocal and passive bianisotropic metasurfaces applied to controlling refraction and the study of nonreciprocal wave transformations with magnetless transistor-loaded metasurfaces.

First, we investigate the optimal manipulation of refraction using reciprocal and passive bianisotropic metasurface. Specifically, we first aim to demonstrate optimal bianisotropic metasurfaces for large-angle generalized refraction. Next, we shall also study the generalization, with bianisotropic metasurfaces, of a phenomenon closely related to refraction: the Brewster effect.

Secondly, we explore the realization of bianisotropic metasurfaces that break Lorentz reciprocity. Specifically, we will investigate linear time invariant nonreciprocal metasurfaces responses, apply them to realize spatial nonreciprocal operation such as isolation and circulation, and propose related magnetless transistor-loaded metaparticle implementations.

1.3 Thesis Organisation

The thesis by article is organized as follows:

Chapter 2 presents a literature review of metasurfaces.

Chapter 3 presents the mathematical model based that will be subsequently used to synthesize metasurfaces in the rest of the thesis, presents the metasurface design method and introduces the three articles.

The next three chapters are three peer-reviewed articles given here as published.

Chapter 4 is the first article entitled "Susceptibility derivation and experimental demon-

stration of refracting metasurfaces without spurious diffraction". This work presents the synthesis and design of bianisotropic metasurface realizing generalized large-angle refraction with optimal efficiency.

Chapter 5 is the second article entitled "Generalized brewster effect using bianisotropic metasurfaces". This work generalizes the Brewster effect by inserting a properly designed bianisotropic metasurface at the interface between two media allowing to arbitrary control the polarization and angle of incidence of the Brewster effect.

Chapter 6 is the third article entitled "Magnetless reflective gyrotropic spatial isolator metasurface". This work presents a metasurface realizing reflective isolation between the two orthogonal linear polarizations.

Chapter 7 presents complementary results relating to nonreciprocal metasurfaces. It presents three different nonreciprocal metasurface problems. First, a theoretical synthesis of transmissive metasurface realizing Faraday rotation is presented. Second, the concept of nonreciprocal phase-gradient metasurfaces is presented. The related nonreciprocal phase-shifting bianisotropic unit cells are synthesized and a transistor-loaded implementation is proposed and verified by full-wave simulations. Third, a nongyrotropic nonreciprocal specular isolator metasurface is presented. The related susceptibility tensors including normal components are derived, a transistor-loaded metaparticle is proposed and verified by both full-wave simulation and an experimental prototype.

Chapter 8 presents a short general discussion of the entire work.

Finally, chapter 9 concludes the thesis and proposes directions for future works.

CHAPTER 2 LITERATURE REVIEW

Metasurfaces Overview

Electromagnetic metasurfaces are defined as electromagnetically thin structures composed of subwavelength metaparticles that are designed and optimized to exhibit electromagnetic responses beyond those found in conventional materials [4,17–26]. In recent years, metasurfaces have sparked a lot of interest in the electromagnetic community due to their seemingly endless capability to manipulate electromagnetic waves with applications ranging from microwaves to optics. The idea of controlling electromagnetic waves with electrically thin structures has obviously been around for a long time with frequency selective surfaces (FSS) [27–31], reflectarrays [32–34], transmitarrays [35,36] and gratings [37–39]. Metasurfaces are, in many ways, the successors of those technologies, with the main difference being that metasurfaces are necessarily composed of subwavelengthly sized metaparticles, which allows these surfaces to be homogenized and characterized by spatially varying surface parameters.

Metasurfaces have been applied to a vast number of applications due to their ability to act as general purpose electromagnetic wave transformers. On a fundamental level, they have been shown to enable precise manipulation of polarization [7, 40–46], reflection [11, 47, 48], refraction [5, 49–53] and absorption [6, 54–59].

We shall next present a non-exhaustive overview of metasurface applications to illustrate their versatility. The ability of metasurfaces to control the direction of propagation of waves in both reflection and transmission through the use of phase gradients, conceptualized as the so-called generalized law of refraction and reflection [5], lead to the realization of flat lenses [5, 60–64], beam shaping techniques [65–67], the generation of vortex beams carrying orbital angular momentum [68–74] and the generation of holograms [8, 75–77]. Metasurfaces have also been applied to different antenna applications [78–85], reconfigurable intelligent surfaces [86–88], energy harvesting and wireless power transfer [89–91], radar cross section reduction [92–94] and cloaking [2,95–101]. Another promising area of applications is that of analog computation with metasurfaces [102,103] for applications including image processing [104–106], performing mathematical operations [102, 107–109] and machine learning [110–113].

Overall, metasurfaces have demonstrated great versatility in their ability to control electromagnetic waves for a plethora of applications all over the electromagnetic spectrum.

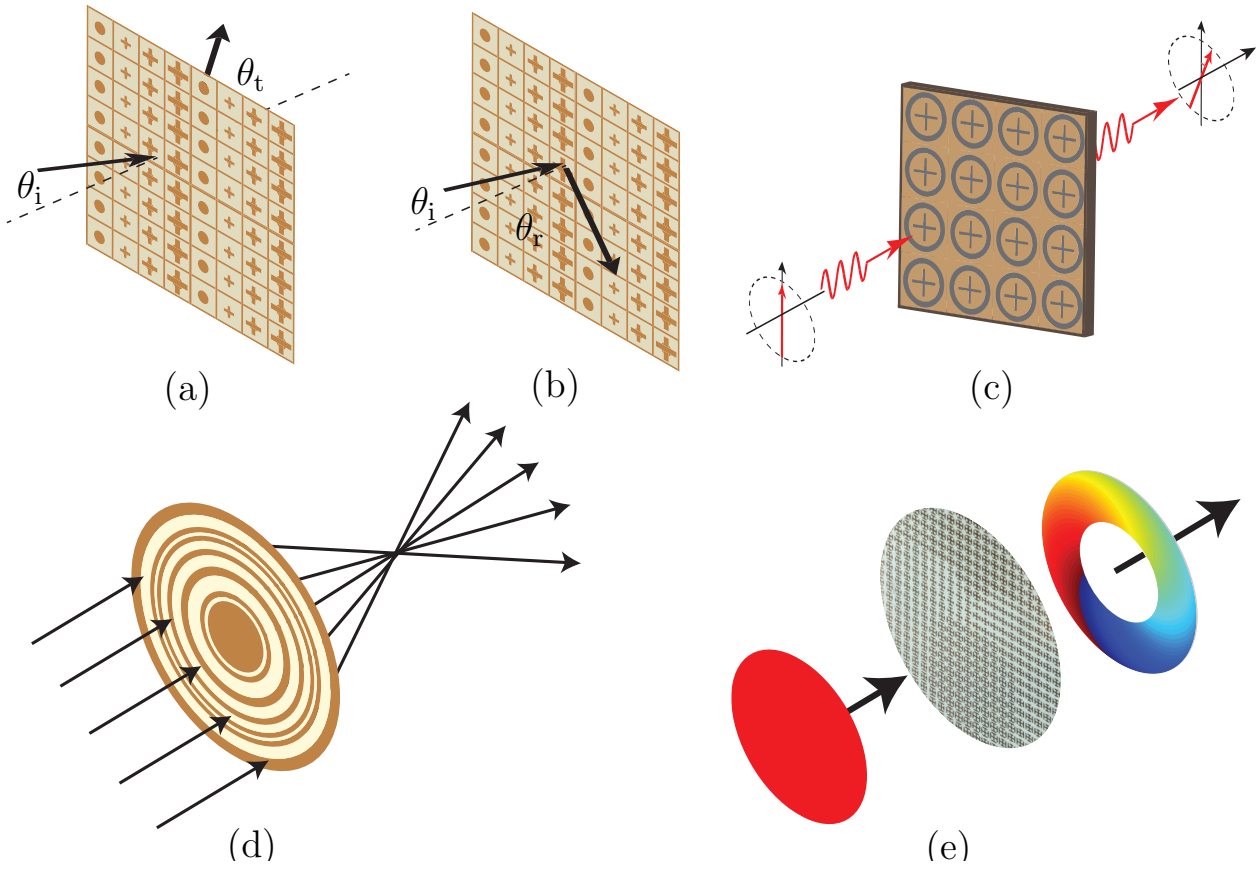

Figure 2.1 Examples of metasurface wave transformations (a) Generalized refraction (b) Generalized reflection (c) Polarization control (d) Flat lensing (e) Generation of vortex beams carrying orbital angular momentum

Metasurfaces Modelling, Synthesis and Analysis

The vast interest in the capabilities of metasurfaces naturally lead to a need to properly model, synthesize and analyze their responses. Given that metasurfaces are electromagnetically thin structures with deeply subwavelength thickness, and hence do not support significant phase shifts or Fabry-Perot resonances, they are appropriately modeled as zero thickness electromagnetic discontinuities in space. Such electromagnetic field discontinuities, according to the Huygens principle, induce surface polarization current sheets on the metasurface and these surface polarization currents can then be related to metasurface surface properties. There exists three main perspectives to model these surface properties: the impedance [10, 20, 26, 114, 115], polarizability [11, 42, 116–122] and susceptibility approaches [4, 25, 68, 123–128]. Those three approaches are often equivalent with the major exception that the sheet impedance model is restricted to metasurfaces having no normal polarization densities, which play an important role in certain metasurfaces [129–132]. The

susceptibility model is arguably the most general of the three since it takes into account both tangential and normal polarizations, intrinsically includes coupling between the different cells composing the metasurface, can easily be extended to nonlinear [133, 134] and time-varying metasurfaces [135], and leads to a powerful and straightforward metasurface synthesis technique [25, 124, 126].

The susceptibility model is based on the General Sheet Transition Conditions (GSTCs) [123, 136, 137], which provide rigourous boundary conditions for discontinuities in the electromagnetic field. The fields averages and differences on both sides of the metasurfaces are related through the GSTCs through its characteristic surface susceptibility tensors. A general synthesis procedure which consists in specifying the desired fields on both sides of the metasurface and calculating the required susceptibility tensors [124]. Once the susceptibility tensors are found, they are discretized into subwavelength unit cells and appropriate scattering particles are designed to realize the required responses. The susceptibility tensor description allows an in-depth investigation of the different susceptibility responses in terms of the symmetries and angular response of the metasurface [131,138,139]. Furthermore, several computational analysis tools have been developed that include the susceptibility-based GSTCs allowing to computationally verify metasurface designs and analyze them for unspecified excitations. Theses computational tools include susceptibility GSTCs-based finite-difference frequency-domain (FDFD) [140, 141], finite-difference time-domain (FDTD) [142], fine-element method [143] and integral equation [132, 144] field solvers.

A particular strength of the aforementioned boundary conditions is the modeling of not only electric and magnetic responses, but also electro-magnetic/magneto-electric responses corresponding to bianisotropy [12, 145, 146]. The presence of bianisotropic responses is directly linked to the asymmetry of the structure [12,131]. In recent years, many fundamental metasurface functionalities such as perfect control of refraction [11, 147–149], reflection [11], polarization [7], surface wave conversion [150] and isolation [151] have been shown to require bianisotropic responses to be realized fully efficiently. More fundamentally, it has been shown that any arbitrary wave transformations that respects local power conservation can be realized by a passive, lossless and reciprocal bianisotropic metasurface [13]. The local power conservation restriction can even be overcome by more sophisticated designs either by specifying additional auxiliary evanescent waves on the metasurface [115] or by using a pair of bianisotropic metasurface with multiple reflections between them [152,153], hence allowing the realization of wave transformations that do not respect local power conservation.

Following the mathematical synthesis of a metasurface and its characterization in terms of surface properties, appropriate scattering particles to realize the different unit cells of the metasurfaces need to be designed. Typical unit cells can be based on cascaded metallic

layers [41, 68, 114, 149] or purely dielectric resonators [45, 154–157] with the later being especially preferred at optical frequencies to avoid high plasmonic losses. It has been shown that a scattering particle made of a cascade of three metallic layers can provide the necessary degrees of freedom to obtain full transmission and a 2π phase coverage [9, 41]. A technique based on transmission line theory and the modelling of each metallic layer as an admittance was proposed to design bianisotropic unit cells in [41]. However, this technique is limited in its accuracy since the metallic layers in metasurfaces are close to one another allowing large evanescent coupling between them. A more sophisticated method to include the evanescent coupling has been proposed [158], but the task of designing the scattering particles remains computationally costly and often involves brute force optimization.

Generalized Refraction with Metasurfaces

One of the most fundamental operation that can be performed by metasurfaces is generalized refraction, which consists in deflecting an incident towards an arbitrary direction, since it underpins many other operations such as lensing or beamforming. The first generalized refracting metasurfaces were based on the phase gradient concept [5,49,50,159] where multiple subwavelength unit cells providing different transmission phases are appropriately arranged to form a phase gradient which can control the wavefront of the incident wave [160] as illustrated in Fig. 2.2. Considering an metasurface with a phase gradient along the x-direction, the generalized law of refraction is written as

$$n_\mathrm{t} \sin\theta_\mathrm{t} - n_\mathrm{i} \sin\theta_\mathrm{i} = \frac{\lambda_0}{2\pi} \frac{d\Phi}{dx}, \tag{2.1}$$

where n_t and n_i are the refractive indices of the transmitted and incident media respectively, θ_i is the angle of incidence, θ_t is the angle of transmission and $d\Phi/dx$ is the phase gradient along x. Note that the phase gradient concept is very similar to phased-array antenna techniques that have been known for a long time [161] and to grating structures [37], especially binary blazed gratings [162]. Still the nicely conceptualized generalized law of reflection and refraction [49] based on phase gradients has had a significant impact on the field of metasurfaces. The design procedure of a phase-gradient metasurface is first to determine the phase function to be realized by the metasurface for the desired wave transformation, discretize this function into subwavelength unit cells and then find appropriate scattering particles able to provide full transmission and a 2π phase coverage. A suitable scattering particle geometry to realize full transmission and a 2π phase coverage is using a cascade of three patterned metallic sheets with the first and third layer being the same making the structure symmetric [9] as shown in Fig. 2.2 (b). Such structures can realize the 2π

phase coverage by providing equal strength magnetic and electric resonances which can be understood in terms of odd and even modes of the structure as illustrated in Fig. 2.2 (c).

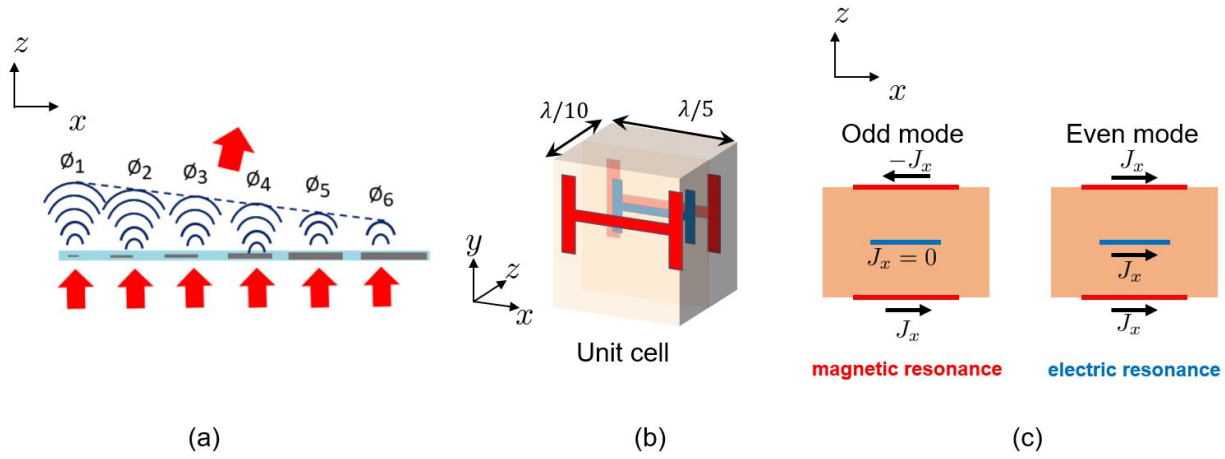

Figure 2.2 Phase gradient metasurface concept (a) Supercell composed of different unit cells providing different transmission phases (b) Symmetric 3-layered metallic unit cell able to provide full transmission and 2π phase coverage (c) Illustration of the magnetic and electric resonances of the unit cell in (b)

However, it was soon realized that those simple designs had limited efficiency for large angle of deflection due to scattering losses in undesired diffraction orders [10]. This was caused by the fact that the incident and transmitted waves have different tangential wave impedances that would need to be simultaneously matched by the metasurface. However, initial phase-gradient metasurfaces were symmetric structures which could at best match only one of the two waves. One technique to suppress those diffraction orders was to add dissipative losses in the metasurface [163] in order to suppress the undesired diffraction orders, however, this limited the power redirected in the desired diffraction order. It was then theoretically shown that passive and reciprocal bianisotropic metasurfaces could get rid of the undesired diffraction orders and realize optimally efficient refracting metasurfaces [11,147]. The asymmetric nature of bianisotropic metasurfaces was shown to allow simultaneously matching both the incident and transmitted waves [11,147–149]. Another technology that has recently emerged to realize generalized refraction are the so-called metagratings [164–168], which replace the multiple subwavelength unit cells of metasurfaces with a single (or a small number of) polarizable particle(s).

A fundamental phenomenon closely related to refraction is the Brewster effect [169]. The conventional Brewster effect relates to the vanishment of the reflection of a p-polarized wave when incident at a specific angle on a dielectric interface [170–172]. At the Brewster angle, which, at a dielectric interface, is given by $\theta_{\mathrm{B}} = \arctan(n_2/n_1)$, where n_1 and n_2 are the refractive indexes of the two media, all the energy of the incident wave is refracted into the second media. The Brewster effect also exists in a more general form in magneto-electric materials, which support either TM-polarization or TE-polarization Brewster transmission, with both simultaneously possible only for normal incidence [173].

The recent advent of metasurfaces has created novel opportunities to extend the Brewster effect. They have recently been shown to support Brewster-like, i.e., reflection-less, transmission when surrounded at both sides by air in planar optical silicon nanodisk configuration [174], high-refractive-index nanorod metasurfaces [175], non-planar microwave split-ring resonator configuration [176,177] and all-angle Brewster transmission in a terahertz metasurface [178]. Moreover, they have been demonstrated to allow general Brewster transmission, i.e., between two different media, in the particular case of normal incidence in a non-planar bianisotropic loop-dipole configuration [152]. Recently, the Brewster effect at a dielectric interface was generalized using destructive interference by placing a metasurface composed of electric dipoles on top of the interface [179], similarly to anti-reflection coatings.

Nonreciprocal Metasurfaces

Nonreciprocity is a fundamental concept in science and technology that is essential to realize many useful operations such as isolation, circulation and nonreciprocal phase shifting [14,180]. A nonreciprocal system is defined as a system that exhibits different received-transmitted field rations when its sources and detectors are exchanged. The breaking of Lorentz reciprocity requires a biasing force, which for electromagnetic systems has conventionally been through magnetized materials, such as ferrites [15] or terbium garnet crystals [181], that exhibit the Faraday effect. The polarization of a wave traveling through such magnetically biased materials will rotate in a direction dictated by the applied static magnetic field independently of the direction of propagation [169]. However, magnetized materials have severe drawbacks such as incompatibility with integrated circuit technologies and bulkiness due to the required biasing magnets, which make them especially impractical for their implementation in metasurfaces. Hence, the vast majority of metasurfaces reported to date have been restricted to following Lorentz reciprocity.

Fortunately, the recent advent of magnetless nonreciprocal technologies [16,182] offer promising solutions to the drawbacks of magnetic-based nonreciprocal technology and have allowed the realization of some nonreciprocal metasurfaces. Magnetless nonreciprocity can be

achieved either in linear or nonlinear forms. However, the nonlinear form is restricted to fixed intensity ranges and non-simultaneous excitations in opposite directions [183–185], and hence does not represent a generally viable solution for practical nonreciprocal devices [16]. In contrast, linear nonreciprocity may be highly efficient, while bearing potential for novel types of nonreciprocities. In the microwave and millimeter-wave regimes, it subdivides into space-time modulated systems (dynamic bias) [186–193] and transistor-loaded systems (static bias) [151, 194–206].

Introducing nonreciprocity in metasurfaces has the potential to extend conventional nonreciprocal operations such as isolation and circulation, usually applied to guided waves, to spatial wave manipulations, and to lead to novel metasurface-based wave transformations. Nonreciprocal metasurfaces using both the space-time modulation route [193, 207–212] and the transistor-loaded route [151, 200–206] have recently been demonstrated. The transistor approach is particularly suitable for typical, monochromatic nonreciprocal operations (isolation, circulation and nonreciprocal phase-shifting), given their simple, low consumption and inexpensive (DC) biasing scheme, and immunity to spurious harmonics and intermodulation products. Transistor-loaded nonreciprocal metasurfaces have been recently reported realizing nonreciprocal polarization rotation in reflection [197, 198] and in transmission [201, 206], reflective spatial circulation [203], transmissive isolation [151, 205] and nonreciprocal reflective beamsteering [204].

CHAPTER 3 APPROACH OF THE WHOLE RESEARCH

The different works that will be presented in this thesis will all rely on a modeling of the metasurfaces using the susceptibility-based GSTCs. This chapter presents the related metasurface synthesis and design method, and introduces the three published articles of Chapters 3, 4 and 5.

3.1 Susceptibility-based Generalized Sheet Transition Conditions

A metasurface is a two-dimensional structure with a deeply subwavelength thickness ($\delta \ll \lambda$) making it negligible compared to the wavelength of its operating frequency. It is composed of an arrangement of transversely subwavelength metaparticles (also referred to as scattering particles or meta-atoms) that transforms incident waves into synthesizable reflected and transmitted waves.

Figure 3.1 shows the metasurface synthesis problem. In general, we wish to determine the susceptibility tensors of a metasurface that will transform a given incident field, $\mathbf{\Phi}_\mathrm{i}$, into specified reflected, $\mathbf{\Phi}_\mathrm{r}$, and transmitted, $\mathbf{\Phi}_\mathrm{t}$, fields. A set of related incident, reflected and transmitted fields will be referred to as a wave transformation. As we will show, a general bianisotropic metasurface can be synthesized to realize multiple independent wave transformations simultaneously.

As an electromagnetically thin structure, metasurfaces can be modelled as a zero-thickness electromagnetic discontinuity in space. Under this approximation, rigourous boundary conditions called the Generalized Sheet Transition Conditions (GSTCs) can be used to model metasurfaces. Those conditions are a generalization of the conventional boundary conditions via the addition of surface polarization currents. A derivation of the GSTCs for a flat metasurface is given in appendix A. They were first derived by Idemen [136] and were later applied to metasurface structures by Kuester [123]. A general metasurface synthesis technique based on susceptibility tensors was later developed by Achouri [124]. Those conditions, assuming the time convention $e^{j\omega t}$, are written as follows

$$\hat{z} \times \Delta\mathbf{H} = j\omega\mathbf{P}_\parallel - \hat{z} \times \nabla M_z, \tag{3.1a}$$

$$\hat{z} \times \Delta\mathbf{E} = -j\omega\mu\mathbf{M}_\parallel - \frac{1}{\epsilon}\hat{z} \times \nabla P_z, \tag{3.1b}$$

where the Δ symbol represents the difference of the fields on both side of the metasurface, $\mathbf{P}$ and $\mathbf{M}$ are the electric and magnetic surface polarization densities respectively. Those polarization densities can be expressed as function of the average fields on both sides of the

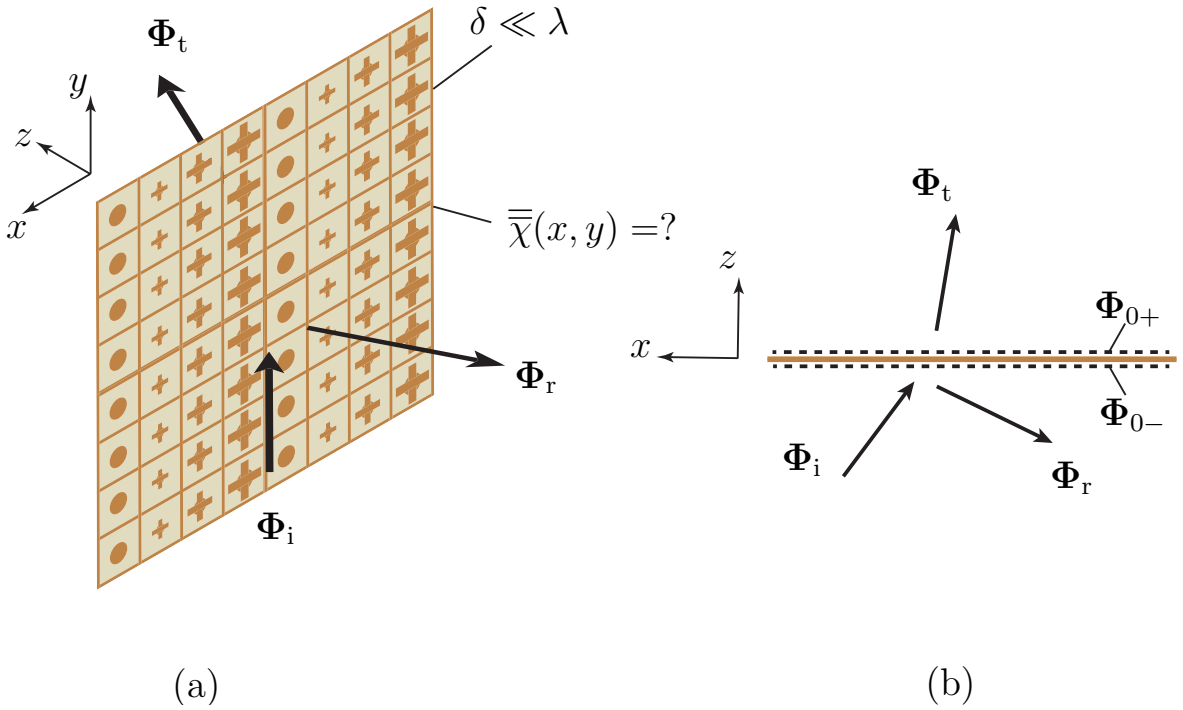

Figure 3.1 General metasurface synthesis problem (a) Perspective view of a metasurface transforming an incident field $\boldsymbol{\Phi}_\mathrm{i}$ into a reflected field $\boldsymbol{\Phi}_\mathrm{r}$ and a transmitted field $\boldsymbol{\Phi}_\mathrm{t}$ (b) Top view of the metasurface problem

metasurface through surface susceptibility tensors that fully characterize the metasurface as

$$\mathbf{P} = \epsilon \overline{\overline{\chi}}_\mathrm{ee} \mathbf{E}_\mathrm{av} + \frac{1}{c} \overline{\overline{\chi}}_\mathrm{em} \mathbf{H}_\mathrm{av}, \tag{3.2a}$$

$$\mathbf{M} = \frac{1}{\eta} \overline{\overline{\chi}}_\mathrm{me} \mathbf{E}_\mathrm{av} + \overline{\overline{\chi}}_\mathrm{mm} \mathbf{H}_\mathrm{av}. \tag{3.2b}$$

Assuming that the metasurface is placed in the xy-plane at $z = 0$, the field differences and averages are

$$\boldsymbol{\Phi}_\mathrm{av} = \frac{\boldsymbol{\Phi}_{0+} + \boldsymbol{\Phi}_{0-}}{2}, \tag{3.3a}$$

$$\Delta\boldsymbol{\Phi} = \boldsymbol{\Phi}_{0+} - \boldsymbol{\Phi}_{0-}, \tag{3.3b}$$

where $\boldsymbol{\Phi}$ denotes either the electric or magnetic field. It can be useful to express the field differences and averages directly as a function of the incident, transmitted and reflected fields.

For an incident wave propagating in the $+z$-direction as in Fig. 3.1, the field differences and averages are

$$\boldsymbol{\Phi}_{\mathrm{av}} = \frac{\boldsymbol{\Phi}_{\mathrm{i}} + \boldsymbol{\Phi}_{\mathrm{r}} + \boldsymbol{\Phi}_{\mathrm{t}}}{2}, \tag{3.4a}$$

$$\Delta\boldsymbol{\Phi} = \boldsymbol{\Phi}_{\mathrm{t}} - (\boldsymbol{\Phi}_{\mathrm{i}} + \boldsymbol{\Phi}_{\mathrm{r}}). \tag{3.4b}$$

In the most general case, each susceptibility tensor is composed of 9 independent components for a total of 36 independent susceptibility components between all the tensors. They read

$$\overline{\overline{\chi}}_{\mathrm{ee}} = \begin{bmatrix} \chi_{\mathrm{ee}}^{xx} & \chi_{\mathrm{ee}}^{xy} & \chi_{\mathrm{ee}}^{xz} \\ \chi_{\mathrm{ee}}^{yx} & \chi_{\mathrm{ee}}^{yy} & \chi_{\mathrm{ee}}^{yz} \\ \chi_{\mathrm{ee}}^{zx} & \chi_{\mathrm{ee}}^{zy} & \chi_{\mathrm{ee}}^{zz} \end{bmatrix}, \quad \overline{\overline{\chi}}_{\mathrm{mm}} = \begin{bmatrix} \chi_{\mathrm{mm}}^{xx} & \chi_{\mathrm{mm}}^{xy} & \chi_{\mathrm{mm}}^{xz} \\ \chi_{\mathrm{mm}}^{yx} & \chi_{\mathrm{mm}}^{yy} & \chi_{\mathrm{mm}}^{yz} \\ \chi_{\mathrm{mm}}^{zx} & \chi_{\mathrm{mm}}^{zy} & \chi_{\mathrm{mm}}^{zz} \end{bmatrix}, \tag{3.5a}$$

$$\overline{\overline{\chi}}_{\mathrm{em}} = \begin{bmatrix} \chi_{\mathrm{em}}^{xx} & \chi_{\mathrm{em}}^{xy} & \chi_{\mathrm{em}}^{xz} \\ \chi_{\mathrm{em}}^{yx} & \chi_{\mathrm{em}}^{yy} & \chi_{\mathrm{em}}^{yz} \\ \chi_{\mathrm{em}}^{zx} & \chi_{\mathrm{em}}^{zy} & \chi_{\mathrm{em}}^{zz} \end{bmatrix}, \quad \overline{\overline{\chi}}_{\mathrm{me}} = \begin{bmatrix} \chi_{\mathrm{me}}^{xx} & \chi_{\mathrm{me}}^{xy} & \chi_{\mathrm{me}}^{xz} \\ \chi_{\mathrm{me}}^{yx} & \chi_{\mathrm{me}}^{yy} & \chi_{\mathrm{me}}^{yz} \\ \chi_{\mathrm{me}}^{zx} & \chi_{\mathrm{me}}^{zy} & \chi_{\mathrm{me}}^{zz} \end{bmatrix}. \tag{3.5b}$$

Each of the 36 susceptibility components represent a specific response due to a given excitation. The second subscript and superscript describe the excitation, while the first subscript and superscript describe the response. For instance, χ_{me}^{yx} represents a magnetic response along the y-direction due to an electric excitation along the x-direction, and so on for all other components. Each specified wave transformation yields 4 scalar equations from the GSTCs in (3.1). Hence, it is possible to specify up to 9 independent wave transformations and obtain a full rank system of $4 \times 9 = 36$ scalar equations for 36 unknowns susceptibility components. In practice, for a given metasurface, some of those susceptibility components would generally be zero.

The susceptibility characterization of metasurfaces is particularly useful since it can immediately inform us on properties of the metasurface such as reciprocity and the presence of gain or loss [128]. A reciprocal system is one that exhibits the same field transmit to receive ratios when its sources and detectors are exchanged. Following the Lorentz reciprocity theorem [229], a metasurface is reciprocal if its susceptibility tensors respect the conditions

$$\overline{\overline{\chi}}_{\mathrm{ee}} = \overline{\overline{\chi}}_{\mathrm{ee}}^{T}, \quad \overline{\overline{\chi}}_{\mathrm{mm}} = \overline{\overline{\chi}}_{\mathrm{mm}}^{T} \quad \text{and} \quad \overline{\overline{\chi}}_{\mathrm{em}} = -\overline{\overline{\chi}}_{\mathrm{me}}^{T}. \tag{3.6}$$

Furthermore, the presence of gain or loss can be verified through the computation of the bianisotropic Poynting theorem [145]. It can be shown that a metasurface will be gainless and lossless if the following conditions are [128] respected

$$\overline{\overline{\chi}}_{\mathrm{ee}}^{\mathrm{T}} = \overline{\overline{\chi}}_{\mathrm{ee}}^{*}, \quad \overline{\overline{\chi}}_{\mathrm{mm}}^{\mathrm{T}} = \overline{\overline{\chi}}_{\mathrm{mm}}^{*} \quad \text{and} \quad \overline{\overline{\chi}}_{\mathrm{em}}^{\mathrm{T}} = \overline{\overline{\chi}}_{\mathrm{me}}^{*}. \tag{3.7}$$

In the case of a metasurface including normal susceptibility components, the spatial derivatives in (3.1) leads to a system of coupled partial differential equations which greatly complexifies the synthesis problem and will generally prohibit analytical susceptibility solutions. However, the case of *uniform* metasurfaces including normal susceptibility components can still be easily handled, since the susceptibilities are no longer a function of position on the metasurface, and are hence no longer affected by the spatial derivatives in (3.1).

For many applications, considering only tangential susceptibility components is sufficient to synthesize and design the required metasurfaces. This can be explained from the Huygens principle, since electromagnetic fields can always be expressed in terms of tangential components. Hence, a metasurface possessing both normal and tangential susceptibility components may always be transformed into an equivalent metasurface with only tangential susceptibility components [129] when considering a specific incident wave. However, this reduces the available degrees of freedom from 36 to 16, which reduces the number of independent wave transformations being able to be specified from 9 to 4. Furthermore, certain operations where the metasurface is required to realize different operations at different angles of incidence will require normal susceptibilities [130,131]. An example of such a metasurface operation will be presented in Sec. 7.3 with the nongyrotropic metasurface specular isolator. The rest of the works presented in this thesis will use purely tangential susceptibility components. Under such an assumption, inserting (3.2) into the GSTCs equations of (3.1) yields the simplified purely tangential susceptibility GSTCs

$$\hat{z} \times \Delta\mathbf{H} = j\omega\epsilon\overline{\overline{\chi}}_{\mathrm{ee}}\mathbf{E}_{\mathrm{av}} + jk\overline{\overline{\chi}}_{\mathrm{em}}\mathbf{H}_{\mathrm{av}}, \tag{3.8a}$$

$$\hat{z} \times \Delta\mathbf{E} = -j\omega\mu\overline{\overline{\chi}}_{\mathrm{mm}}\mathbf{H}_{\mathrm{av}} - jk\overline{\overline{\chi}}_{\mathrm{me}}\mathbf{E}_{\mathrm{av}}, \tag{3.8b}$$

where the susceptibility tensors $\overline{\overline{\chi}}_{\mathrm{ee}}$, $\overline{\overline{\chi}}_{\mathrm{em}}$, $\overline{\overline{\chi}}_{\mathrm{me}}$ and $\overline{\overline{\chi}}_{\mathrm{mm}}$ are now each composed of $2 \times 2 = 4$ components related only to the tangential components in the xy-plane given the synthesis problem shown in Fig. 3.1.

Equations (3.8) are two vectorial equations, whose projection onto the xy-plane yields four scalar equations that can be conveniently written in matrix form as

$$\begin{bmatrix} \Delta H_y \\ \Delta H_x \\ \Delta E_y \\ \Delta E_x \end{bmatrix} = \begin{bmatrix} -j\omega\epsilon\chi_{\mathrm{ee}}^{xx} & -j\omega\epsilon\chi_{\mathrm{ee}}^{xy} & -jk\chi_{\mathrm{em}}^{xx} & -jk\chi_{\mathrm{em}}^{xy} \\ j\omega\epsilon\chi_{\mathrm{ee}}^{yx} & j\omega\epsilon\chi_{\mathrm{ee}}^{yy} & jk\chi_{\mathrm{em}}^{yx} & jk\chi_{\mathrm{em}}^{yy} \\ jk\chi_{\mathrm{me}}^{xx} & jk\chi_{\mathrm{me}}^{xy} & j\omega\mu\chi_{\mathrm{mm}}^{xx} & j\omega\mu\chi_{\mathrm{mm}}^{xy} \\ -jk\chi_{\mathrm{me}}^{yx} & -jk\chi_{\mathrm{me}}^{yy} & -j\omega\mu\chi_{\mathrm{mm}}^{yx} & -j\omega\mu\chi_{\mathrm{mm}}^{yy} \end{bmatrix} \begin{bmatrix} E_{x,\mathrm{av}} \\ E_{y,\mathrm{av}} \\ H_{x,\mathrm{av}} \\ H_{y,\mathrm{av}} \end{bmatrix}. \tag{3.9}$$

In this work, we propose a classification of the different types of susceptibility responses of metasurfaces in terms of homoanisotropy, heteroanisotropy and bianisotropy as shown in Fig. 3.2. An homoanisotropic response, from the latin prefix *homo* meaning the same, is one whose field excitation and response are related the same field (either electric excitation to electric response $\overline{\overline{\chi}}_{\mathrm{ee}}$ or magnetic excitation to magnetic response $\overline{\overline{\chi}}_{\mathrm{mm}}$). In contrast, an heteroanisotropic response, from the latin prefix *hetero* meaning different, is one whose field excitation and response are related to different fields (either electric excitation to magnetic response $\overline{\overline{\chi}}_{\mathrm{me}}$ or magnetic excitation to electric response $\overline{\overline{\chi}}_{\mathrm{em}}$). Finally, we shall call a metasurface that includes both homoanisotropic and heteroanisotropic responses as bianisotropic.

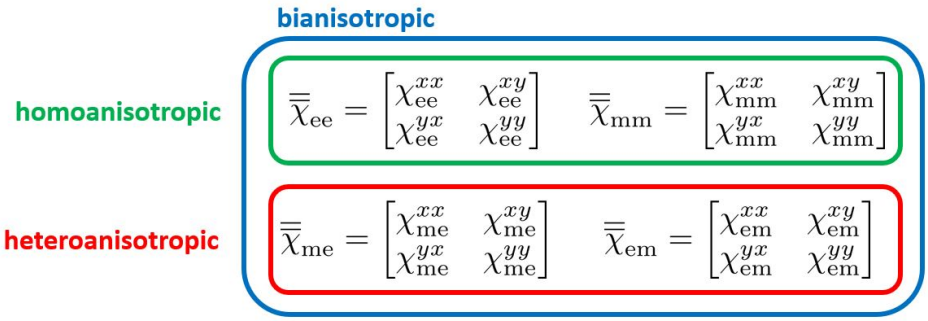

Figure 3.2 Classification of susceptibility responses in terms of homoanisotropy, heteroanisotropy and bianisotropy

Furthermore, we shall characterize metasurfaces as either *gyrotropic* or *nongyrotropic*. We define a gyrotropic as a metasurface whose scattering when excited by a linearly polarized wave (either p- or s-polarization) produces some fields that are orthogonally polarized to the incident wave. In contrast, a nongyrotropic metasurface is one whose scattering and excitation are all co-polarized when excited by a linearly polarized wave. For a purely tangential metasurface, the susceptibility components producing a gyrotropic response are $\chi_{\mathrm{ee}}^{xy}, \chi_{\mathrm{ee}}^{yx}, \chi_{\mathrm{mm}}^{xy}, \chi_{\mathrm{mm}}^{yx}, \chi_{\mathrm{em}}^{xx}, \chi_{\mathrm{em}}^{yy}, \chi_{\mathrm{me}}^{xx}$ and χ_{me}^{yy}.

As previously mentioned, the purely tangential GSTCs contain 16 degrees of freedom that allow up to 4 wave transformations to be performed independently. Extending equations (3.9) to include multiple transformations yields a general system of equations including all 4 wave transformations which can be used for synthesizing the susceptibilities

$$\begin{bmatrix} \Delta H_{y1} & \Delta H_{y2} & \Delta H_{y3} & \Delta H_{y4} \\ \Delta H_{x1} & \Delta H_{x2} & \Delta H_{x3} & \Delta H_{x4} \\ \Delta E_{y1} & \Delta E_{y2} & \Delta E_{y3} & \Delta E_{y4} \\ \Delta E_{x1} & \Delta E_{x2} & \Delta E_{x3} & \Delta E_{x4} \end{bmatrix} = \\ \begin{bmatrix} -j\omega\epsilon\chi_{\mathrm{ee}}^{xx} & -j\omega\epsilon\chi_{\mathrm{ee}}^{xy} & -jk\chi_{\mathrm{em}}^{xx} & -jk\chi_{\mathrm{em}}^{xy} \\ j\omega\epsilon\chi_{\mathrm{ee}}^{yx} & j\omega\epsilon\chi_{\mathrm{ee}}^{yy} & jk\chi_{\mathrm{em}}^{yx} & jk\chi_{\mathrm{em}}^{yy} \\ jk\chi_{\mathrm{me}}^{xx} & jk\chi_{\mathrm{me}}^{xy} & j\omega\mu\chi_{\mathrm{mm}}^{xx} & j\omega\mu\chi_{\mathrm{mm}}^{xy} \\ -jk\chi_{\mathrm{me}}^{yx} & -jk\chi_{\mathrm{me}}^{yy} & -j\omega\mu\chi_{\mathrm{mm}}^{yx} & -j\omega\mu\chi_{\mathrm{mm}}^{yy} \end{bmatrix} \begin{bmatrix} E_{x1,\mathrm{av}} & E_{x2,\mathrm{av}} & E_{x3,\mathrm{av}} & E_{x4,\mathrm{av}} \\ E_{y1,\mathrm{av}} & E_{y2,\mathrm{av}} & E_{y3,\mathrm{av}} & E_{y4,\mathrm{av}} \\ H_{x1,\mathrm{av}} & H_{x2,\mathrm{av}} & H_{x3,\mathrm{av}} & H_{x4,\mathrm{av}} \\ H_{y1,\mathrm{av}} & H_{y2,\mathrm{av}} & H_{y3,\mathrm{av}} & H_{y4,\mathrm{av}} \end{bmatrix}, \tag{3.10}$$

where the subscripts 1, 2, 3 and 4 indicate the electromagnetic fields of the 4 different independent wave transformations. Under this matrix form, the required susceptibilities can be easily obtained by matrix inversion after calculating the fields differences and averages of each specified wave transformation with (3.3). Depending on the requirements of the metasurface to be synthesized, the matrix equations of (3.10) can be reduced to include less than 4 wave transformations. In this case, some susceptibility components can be set to zero to maintain a full rank system with a unique solution.

Using the previous equations, we can now perform the mathematical synthesis of a metasurface which yields the susceptibility tensors required to realize the specified wave transformations. Depending on the operation, the susceptibility tensors can be a function of position on the metasurface, which will then be discretized into subwavelength unit cells. The next step of the metasurface design is to find suitable scattering particles, or metaparticles, to realize the required susceptibility tensors of each unit cell separately. The different unit cells can then be assembled together to create the metasurface.

To design the different unit cells, a particularly useful mapping can be done between the susceptibilities and the scattering parameters. We consider a single unit cell placed in periodic boundary conditions, which takes into account the interactions and coupling between adjacent scatterers. This periodic array of scattering particles is uniform with subwavelength periodicity, hence no propagating diffraction orders will be excited. We define ports 1 and 2 placed on either side of the metasurface for both x and y polarization and express the field differences and averages in terms of the related scattering parameters for normal incidence.

The system of equations (3.10) becomes

$$\overline{\overline{\Delta}} = \overline{\overline{\tilde{\chi}}} \cdot \overline{\overline{A}}_{\mathrm{v}}, \tag{3.11a}$$

where

$$\overline{\overline{\Delta}} = \begin{bmatrix} -\mathbf{m}/\eta + \mathbf{m}\mathbf{S}_{11}/\eta + \mathbf{m}\mathbf{S}_{21}/\eta & -\mathbf{m}/\eta + \mathbf{m}\mathbf{S}_{12}/\eta + \mathbf{m}\mathbf{S}_{22}/\eta \\ -\mathbf{n}\mathbf{m} - \mathbf{n}\mathbf{m}\mathbf{S}_{11} + \mathbf{n}\mathbf{m}\mathbf{S}_{21} & \mathbf{n}\mathbf{m} - \mathbf{n}\mathbf{m}\mathbf{S}_{12} + \mathbf{n}\mathbf{m}\mathbf{S}_{22} \end{bmatrix}, \tag{3.11b}$$

$$\overline{\overline{A}}_{\mathrm{v}} = \frac{1}{2} \begin{bmatrix} \mathbf{I} + \mathbf{S}_{11} + \mathbf{S}_{21} & \mathbf{I} + \mathbf{S}_{12} + \mathbf{S}_{22} \\ \mathbf{n}/\eta - \mathbf{n}\mathbf{S}_{11}/\eta + \mathbf{n}\mathbf{S}_{21}/\eta & -\mathbf{n}/\eta - \mathbf{n}\mathbf{S}_{12}/\eta + \mathbf{n}\mathbf{S}_{22}/\eta \end{bmatrix} \tag{3.11c}$$

and

$$\overline{\overline{\tilde{\chi}}} = \begin{bmatrix} -j\omega\epsilon\chi_{\mathrm{ee}}^{xx} & -j\omega\epsilon\chi_{\mathrm{ee}}^{xy} & -jk\chi_{\mathrm{em}}^{xx} & -jk\chi_{\mathrm{em}}^{xy} \\ j\omega\epsilon\chi_{\mathrm{ee}}^{yx} & j\omega\epsilon\chi_{\mathrm{ee}}^{yy} & jk\chi_{\mathrm{em}}^{yx} & jk\chi_{\mathrm{em}}^{yy} \\ jk\chi_{\mathrm{me}}^{xx} & jk\chi_{\mathrm{me}}^{xy} & j\omega\mu\chi_{\mathrm{mm}}^{xx} & j\omega\mu\chi_{\mathrm{mm}}^{xy} \\ -jk\chi_{\mathrm{me}}^{yx} & -jk\chi_{\mathrm{me}}^{yy} & -j\omega\mu\chi_{\mathrm{mm}}^{yx} & -j\omega\mu\chi_{\mathrm{mm}}^{yy} \end{bmatrix}, \tag{3.11d}$$

with

$$\mathbf{m} = \begin{bmatrix} 1 & 0 \\ 0 & -1 \end{bmatrix}, \quad \mathbf{n} = \begin{bmatrix} 0 & -1 \\ 1 & 0 \end{bmatrix}, \quad \mathbf{I} = \begin{bmatrix} 1 & 0 \\ 0 & 1 \end{bmatrix} \quad \text{and} \quad \mathbf{S}_{ab} = \begin{bmatrix} S_{ab}^{xx} & S_{ab}^{xy} \\ S_{ab}^{yx} & S_{ab}^{yy} \end{bmatrix}. \tag{3.11e}$$

Hence, using Eqs. (3.11), we can relate a given set of susceptibilities to its scattering parameters at normal incidence, which can be used to design the unit cell geometries. The scattering parameters of a unit cell can be simulated using full-wave simulators (such as CST, HFSS or COMSOL) and a proper scattering particle geometry for each unit cell can be optimized.

3.2 Metasurface Synthesis and Design Method

This section will outline the general method for the mathematical synthesis of metasurface using the susceptibility-based model and the design of the scattering particles from these susceptibilities. A metasurface can be designed following the next 10 steps:

1) Specify the required number of wave transformations for the desired operation of the metasurface. This involves specifying the electric and magnetic field on both sides of the metasurface for each independent wave transformation. Note that to obtain a proper solution from the following synthesis technique, the wave transformations specified need to be properly posed. Some specifications can lead to an unsolvable system or wrong results. For instance, specifying two different wave transformations for the same incident wave will not yield a proper solution.

2) Select appropriate susceptibility components to realize the metasurface operation. We are often interested in finding a unique analytical solution to the synthesis problem, which depending on the number of specified wave transformations involves selecting a limited number of susceptibility components as degrees of freedom to obtain a full-rank system of equations. Certain properties of the desired metasurface such as non/gyrotropy, non/reciprocity or a/symettry can suggest the use of certain susceptibility components [128, 131, 139]. For instance, specifying a gyrotropic wave transformation would require susceptibility terms coupling excitations and responses of orthogonal polarizations (e.g. χ_{ee}^{xy}, χ_{em}^{xx}, etc...). However, it may not always be clear which susceptibility components to use to synthesize the metasurface and often there exists multiple solutions for the same metasurface operation that utilizes different susceptibility components. Hence, using an heuristic approach at this step is often justified. After finishing the mathematical synthesis with a chosen set of susceptibilities, we shall analyze the results to verify first if we found a proper solution and second if it respects certain desired properties such as non/reciprocity or passivity and losslessness.

3) Compute the field differences and averages of the electric and magnetic fields following equations (3.3) for each wave transformation.

4) Arrange the computed field differences and averages into a matrix form, such as in equations (3.10).

5) Solve the system of equations by matrix inversion to find the susceptibility components.

6) Verify the correctness of the resulting susceptibility tensors. First, if the system of equations yielded no solution, the desired wave transformations are either ill-posed or the susceptibility components chosen heuristically were not appropriate. Next, computational tools such as FDFD or FDTD simulations specifically designed to include the susceptibility GSTCs [140] can be used to simulate the resulting metasurface and verify its response at the specified incidences and analyze it for other unspecified wave incidences. In the case of uniform meta-

surfaces, the reflection and transmission coefficients as a function of the incidence angle for a given set of susceptibilities can be analytically computed [128, 138] and compared with the desired response.

7) Discretize the susceptibility functions into subwavelength unit cells to be designed independently.

8) Map the susceptibility tensors of each unit cell to the normal incidence scattering parameters of a perfectly periodic structure having the same uniform susceptibility tensors as the unit cell using Eqs. (3.11).

9) Design of each unit cell separately using a commercial full-wave software such as CST or HFSS. This design is done by optimizing the scattering particle geometry to realize the scattering parameters mapped from the required susceptibilities. Each unit cell is simulated in periodic boundary conditions to take into account coupling to adjacent cells. Figure 3.3 shows examples of unit cells for both reciprocal and passive metasurfaces in Fig. 3.3 (a) and for nonreciprocal transistor-loaded unit cells in Fig. 3.3 (b).

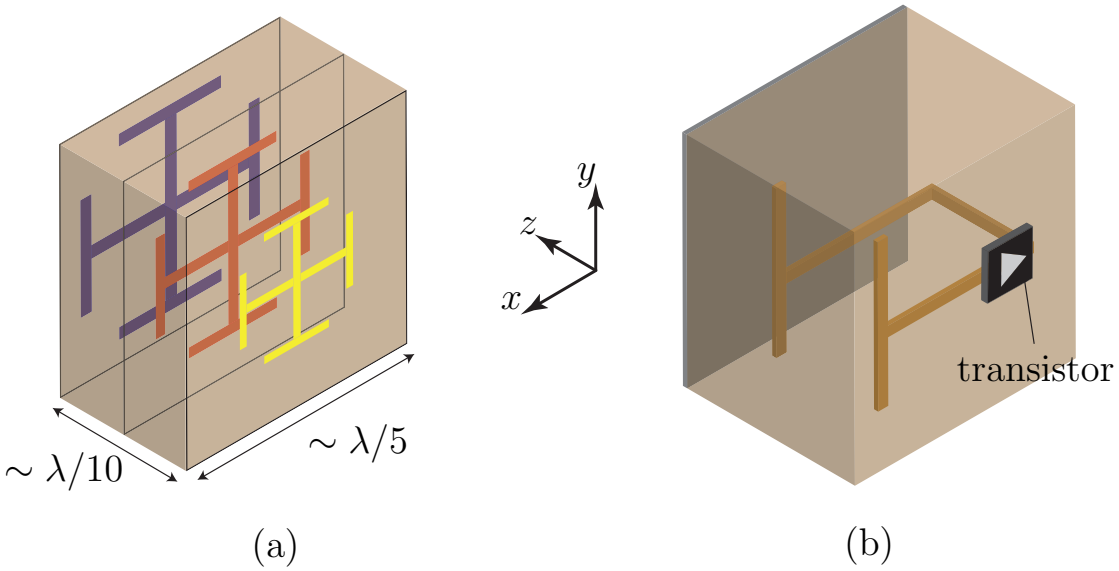

Figure 3.3 Examples of unit cells realizing bianisotropic responses (a) Reciprocal unit cell composed of three metallic jerusalem crosses separated by dielectric slabs (b) Nonreciprocal transistor-loaded unit cell

10) In the case of a nonuniform periodic metasurface, arrange the different unit cell into a supercell and simulate its response. Further optimization of the whole supercell can be performed to take into account the different coupling between adjacent unit cells compared to their respective simulations in periodic boundary conditions.

Finally, we obtained the required physical dimensions of the metasurface. We can now fabricate it and proceed with the experimental validation of the metasurface design.

3.3 Articles Introduction

The next three chapters are composed of three peer-reviewed journal publication that are included here as they were published.

Chapter 4 is the first article entitled "Susceptibility derivation and experimental demonstration of refracting metasurfaces without spurious diffraction". Generalized refraction is a fundamental operation that metasurfaces have initially been realized using the phase gradient concept. However, it was soon realized that such simple designs had limited efficiency for high-angle refraction due to the excitations of spurious diffraction orders. It was subsequently theoretically derived that bianisotropy was required to realize a reciprocal, passive and lossless metasurface realizing high-angle generalized refraction without spurious diffraction. This work presents the mathematical synthesis and design of bianisotropic metasurfaces realizing this operation with optimal efficiency. It presents related simulation results and the first experimental demonstration of overcoming the theoretical efficiency limit of lossless homoanisotropic metasurfaces with bianisotropic metasurfaces for high-angle generalized refraction[1].

Chapter 5 is the second article entitled "Generalized Brewster effect using bianisotropic metasurfaces". The conventional Brewster effect is the vanishment of the reflection of TM-polarized wave at the interface between two dielectric media a specific angle of incidence, which depends on the refractive indexes of the two media. This work generalizes the Brewster effect by inserting a properly designed bianisotropic metasurface at the interface between the two media to arbitrary control the incidence angle and polarization of the Brewster effect. The corresponding metasurface susceptibility tensors are derived and the generalized Brewster angle is demonstrated by full-wave electromagnetic simulation.

The first two articles tackle the first specific research objective with the aim of controlling refraction with bianisotropic metasurfaces.

Chapter 6 is the third article entitled "Magnetless reflective gyrotropic spatial isolator metasurface". This work presents a birefringent metasurface that reflects vertically polarized incident waves into horizontally polarized waves, and absorbs horizontally polarized incident waves. Thus, this metasurface realizes reflective isolation between the two orthogonal polarization. We present the corresponding metasurface susceptibility tensors, propose a mirror-backed transistor-loaded metaparticle implementation and demonstrate the metasurface by

[1]The metasurfaces were fabricated at Polytechnique Montréeal by the technicians of Poly-Grames and the experiment was conducted by Guillaume Lavigne.

full-wave simulations.

The third article and the complementary results of chapter 7 tackle the second specific research objective aiming at designing magnetless nonreciprocal metasurfaces based on the transistor-loaded technology.

CHAPTER 4 ARTICLE 1: SUSCEPTIBILITY DERIVATION AND EXPERIMENTAL DEMONSTRATION OF REFRACTING METASURFACES WITHOUT SPURIOUS DIFFRACTION

Authors: Guillaume Lavigne, Karim Achouri, Viktar Asadchy, Sergei Tretyakov, and Christophe Caloz

This work was published in the IEEE Transactions on Antennas and Propagation, Volume 66, Issue 3, pages 1321-1330, in March 2018.

Abstract

Refraction represents one of the most fundamental operations that may be performed by a metasurface. However, simple phase-gradient metasurface designs suffer from restricted angular deflection due to spurious diffraction orders. It has been recently shown, using a circuit-based approach, that refraction without spurious diffraction, or diffraction-free, can fortunately be achieved by a transverse (or in-plane polarizable) metasurface exhibiting either loss-gain, nonreciprocity or bianisotropy. Here, we rederive these conditions using a medium-based – and hence more insightfull – approach based on Generalized Sheet Transition Conditions (GSTCs) and surface susceptibility tensors, and experimentally demonstrate, for the first time beyond any doubt, two diffraction-free refractive metasurfaces that are essentially lossless, passive, bianisotropic and reciprocal.

4.1 Introduction

Metasurfaces represent a powerful electromagnetic technology that has experienced spectacular development over the past lustrum [20, 21, 213]. They have already lead to a diversity of applications, including single-layer perfect absorption [54], polarization twisting [214], power harvesting [89], orbital angular momentum multiplexing [71, 126], spatial processing [215] and flat lensing [216], and there seems to be much more to be discovered and developed in this area.

One of the most fundamental operations that a metasurface may perform is generalized refraction and reflection [49], as most metasurface field transformations involve these phenomena. Such operations have been achieved in *blazed gratings* [38, 39], and later in *planar phase-gradient metasurfaces* [49], however with restriction to small angle differences between the incident and refracted or reflected beams and with the presence of spurious diffraction orders [126, 160].

Fortunately, it is possible to achieve refraction without spurious diffraction, that we shall hereafter refer to as *diffraction-free* refraction for short, by introducing more complexity in the metasurface design [11, 13]. This has been clearly demonstrated in [11], which shows that such operation may be accomplished by a *transverse*[1] metasurface if that metasurface exhibits any one of the following three properties:

1. monoisotropy with loss and gain [163],
2. nonreciprocity [11], or
3. bianisotropy [147, 148, 217].

Among these properties, the practically most convenient is certainly the third one, since it allows to achieve diffraction-free generalized refraction with a metasurface that is purely lossless and passive, avoiding complex amplification, and at the same time reciprocal, avoiding non-integrable magnetic materials [15] or complex magnetless structures [151, 197, 198].
The work reported in [147], and related experimentation [148], represents the first synthesis of a diffraction-free generalized bianisotropic refractive metasurface. In that paper, the authors use a *circuit-based* approach with generalized scattering parameters to match the impedances of the oblique incident and transmitted waves across a *layered* metasurface structure. As a result, they obtain analytical expressions for the admittances of each of the layers constituting the metasurface. Here, as an extension of the short report [217], we present a fundamentally different and also more general approach of the same problem. This approach uses surface susceptibilities synthesized [68, 124, 133] by Generalized Sheet Transition Conditions (GSTCs) [136], and is therefore a *medium-based* rather than a circuit-based approach, which inherently brings about greater insight into the physics of the problem. Moreover, it treats the metasurface as a *global entity*, without any restriction regarding its structure, and may therefore accommodate different implementations, via subsequent scattering parameter mapping [124]. Secondly, starting from a completely general bianisotropic metasurface, this approach naturally reveals the three diffraction-free conditions derived in [11], and ultimately leads to closed-form expressions for the bianisotropic susceptibility tensors. Finally, using a novel supercell optimization technique, we design and experimentally demonstrate two diffraction-free bianisotropic reciprocal refractive metasurfaces which reach higher performances than previously reported ones.

[1] A transverse metasurface is a metasurface characterized only by tensor components that are parallel to the plane of the metasurface (i.e. "in-plane" or $\parallel$) or, equivalently, perpendicular to the normal of the metasurface. Including longitudinal (i.e. "off-plane" or $\perp$) tensor components, i.e. components in the direction of the normal of the metasurface, immediately brings about much greater complexity because, as shown in [124], this transforms otherwise algebraic GSTC equations into differential equations. The reduction of the general to a transverse metasurfaces reduces the four bianisotropic constitutive parameters from 3×3 tensors ($4 \times 9 = 36$ elements) to 2×2 tensors ($4 \times 4 = 16$ elements).

The paper is organized as follows. Section 4.2.2 presents the GSTC synthesis of the metasurface susceptibility tensors and discusses the physics of the metasurfaces corresponding to the three above options. Next, Sec. 4.3.3 maps the synthesized susceptibilities onto scattering parameters as an intermediate step to discretize the metasurface. Using this mapping, Sec. 4.4.4 determines the scattering particles corresponding to each metasurface cell. Simulation and experimental validations are provided in Sec. 4.5.5. Finally, conclusions are given in Sec. 4.6.6.

4.2 Refractive Transverse Metasurface Synthesis

4.2.1 Generalized Refraction and GSTC Synthesis

The problem of diffraction-free generalized refraction by a metasurface is represented in Fig. 4.1. The metasurface is placed at $z = 0$ in the xy-plane of a cartesian coordinate system. We denote a and b the media, possibly having different electromagnetic properties, bounding the metasurface at $z < 0$ and $z > 0$, respectively. A plane wave, with electric and magnetic fields $\mathbf{E}_{a1}$ and $\mathbf{H}_{a1}$, respectively, impinges from medium a at angle θ_a onto the metasurface. The metasurface transforms, without any spurious reflection and scattering, this wave into a plane wave, with fields $\mathbf{E}_{b1}$ and $\mathbf{H}_{b1}$, propagating in medium b at angle θ_b.

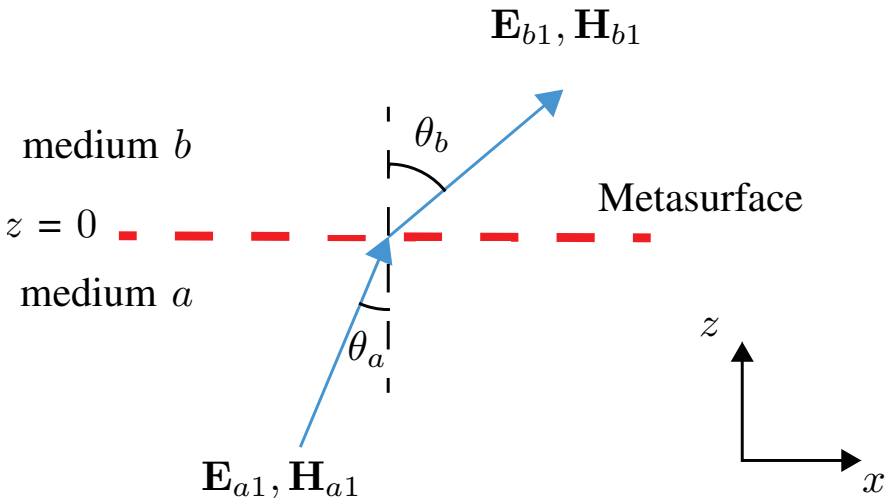

Figure 4.1 Problem of diffraction-free generalized refraction by a metasurface

We shall next perform the synthesis of the diffraction-free generalized refractive metasurface in Fig. 4.1 using the GSTC-susceptibility technique presented in [124]. This technique consists in specifying the incident, reflected and transmitted fields and computing the corresponding metasurface susceptibility tensors via GSTCs. According to the definition of diffraction-free generalized refraction, the reflected field will be specified to be zero and the transmitted field

will be specified as a pure plane wave without any spurious diffraction orders. In the case of a general transverse bianisotropic metasurface, the GSTCs, defined at $z = 0$, are given as

$$\hat{z} \times \Delta\mathbf{H} = j\omega\epsilon_0\overline{\overline{\chi}}_{\mathrm{ee}}\mathbf{E}_{\mathrm{av}} + j\omega\overline{\overline{\chi}}_{\mathrm{em}}\sqrt{\mu_0\epsilon_0}\mathbf{H}_{\mathrm{av}}, \tag{4.1a}$$

$$\Delta\mathbf{E} \times \hat{z} = j\omega\mu_0\overline{\overline{\chi}}_{\mathrm{mm}}\mathbf{H}_{\mathrm{av}} + j\omega\mu_0\overline{\overline{\chi}}_{\mathrm{me}}\sqrt{\epsilon_0/\mu_0}\mathbf{E}_{\mathrm{av}}, \tag{4.1b}$$

where the Δ symbol and 'av' subscript represent the differences and averages of the tangential electric or magnetic fields on both sides of the metasurface, and $\overline{\overline{\chi}}_{\mathrm{ee}}$, $\overline{\overline{\chi}}_{\mathrm{em}}$, $\overline{\overline{\chi}}_{\mathrm{me}}$, $\overline{\overline{\chi}}_{\mathrm{mm}}$ are the bianisotropic susceptibility tensors describing the metasurface. In order to realize the simplest and most fundamental generalized refraction operation, we require the metasurface to be *non-gyrotropic* so as to avoid polarization alteration. As a result, the s-polarization and p-polarization problems are independent from each other and can therefore be treated separately.

4.2.2 Monoisotropic Metasurface

We heuristically start with a metasurface having the simplest possible constitutive parameters, namely a *monoisotropic* metasurface, which is characterized solely by the two scalar parameters χ_{ee} and χ_{mm}. However, such a metasurface is inadequate since it does not allow independent syntheses for p-polarization and s-polarization, in contradiction with the last statement of Sec. 4.2.1. Indeed, independent syntheses would require distinct χ_{ee}^{xx}–χ_{mm}^{yy} and χ_{ee}^{yy}–χ_{mm}^{xx} pairs for p-polarization and s-polarization, respectively.

4.2.3 Monoanisotropic Metasurface

The next simplest metasurface is thus a *monoanisotropic* metasurface. Note that similar derivations for monoanisotropic metasurfaces were originally presented in [114,126]. In the p-polarization case, for which the metasurface appears monoisotropic, the fields corresponding to the scenario of Fig. 4.1 are

$$\mathbf{E}_{a1} = (\cos\theta_a\hat{x} + \sin\theta_a\hat{z})e^{-j(k_{ax}x+k_{az}z)}, \mathbf{H}_{a1} = \frac{e^{-jk_{ax}x}}{\eta_a}\hat{y}, \tag{4.2a}$$

$$\mathbf{E}_{b1} = T_{\mathrm{p}}(\cos\theta_b\hat{x} + \sin\theta_b\hat{z})e^{-j(k_{bx}x+k_{bz}z)}, \mathbf{H}_{b1} = T_{\mathrm{p}}\frac{e^{-jk_{bx}x}}{\eta_b}\hat{y}, \tag{4.2b}$$

where T_{p} is the (parallel-polarization) transmission coefficient, $\eta_{(a,b)} = \sqrt{\mu_{(a,b)}/\epsilon_{(a,b)}}$, and

$$k_{(a,b)x} = k_{a,b}\sin\theta_{a,b}, \tag{4.3a}$$

$$k_{(a,b)z} = k_{a,b}\cos\theta_{a,b}, \tag{4.3b}$$

where $k_{(a,b)} = \sqrt{\mu_{(a,b)}\epsilon_{(a,b)}}k_0$ with $k_0 = \omega/c_0$.

Based on the above assumption of a transverse metasurface, the GSTCs (4.1) involve only the x and y components of these fields, evaluated at $z = 0$, which, also accounting for the p-polarization monoisotropy, results into

$$\chi_{\rm ee}^{xx} = \frac{-\Delta H_{y1}}{j\omega\epsilon_0 E_{x,\rm av1}}, \tag{4.4a}$$

$$\chi_{\rm mm}^{yy} = \frac{-\Delta E_{x1}}{j\omega\mu_0 H_{y,\rm av1}}, \tag{4.4b}$$

with

$$\Delta E_{x1} = E_{bx1} - E_{ax1} = T_{\rm p}\cos\theta_b e^{-jk_{bx}x} - \cos\theta_a e^{-jk_{ax}x}, \tag{4.5a}$$

$$\Delta H_{y1} = H_{by1} - H_{ay1} = T_{\rm p}e^{-jk_{bx}x}/\eta_b - e^{-jk_{ax}x}/\eta_a, \tag{4.5b}$$

$$E_{x,\rm av1} = \frac{E_{ax1} + E_{bx1}}{2} = \frac{\cos\theta_a e^{-jk_{ax}x} + T_{\rm p}\cos\theta_b e^{-jk_{bx}x}}{2} \tag{4.5c}$$

$$H_{y,\rm av1} = \frac{H_{ay1} + H_{by1}}{2} = \frac{e^{-jk_{ax}x}/\eta_a + T_{\rm p}e^{-jk_{bx}x}/\eta_b}{2} \tag{4.5d}$$

where the subscript '1' has been introduced for later convenience. The only unknown in these relations is the transmission coefficient, $T_{\rm p}$. This coefficient may be obtained by enforcing power conservation across the metasurface,

$$\frac{1}{2}{\rm Re}\left((E_{ax1}\hat{x}) \times (H_{ay1}^*\hat{y})\right) = \frac{1}{2}{\rm Re}\left((E_{bx1}\hat{x}) \times (H_{by1}^*\hat{y})\right), \tag{4.6}$$

whose resolution for $T_{\rm p}$ with (4.2) yields

$$T_{\rm p} = \sqrt{\frac{\eta_b\cos\theta_a}{\eta_a\cos\theta_b}} \tag{4.7}$$

which is thus a fundamental *condition for power conserving diffraction-free refraction.*

Inserting (4.5) into (4.4) yields the periodic complex susceptibility functions

$${\rm Re}(\chi_{\rm ee}^{xx}) = \frac{-2k_a k_b T_{\rm p}(\eta_a k_b k_{az} + \eta_b k_a k_{bz})\sin(\alpha x)}{\epsilon_0\omega\eta_a\eta_b(k_b^2k_{az}^2 + k_a^2k_{bz}^2T_{\rm p}^2 + 2k_a k_{az}k_b k_{bz}T_{\rm p}\cos(\alpha x))}, \tag{4.8a}$$

$$\begin{aligned}&{\rm Im}(\chi_{\rm ee}^{xx}) = \\ &\frac{2k_a k_b(\eta_a k_a k_{bz}T_{\rm p}^2 - \eta_b k_{az}k_b + T_{\rm p}(\eta_a k_b k_{az} - \eta_b k_a k_{bz})\cos(\alpha x)))}{\epsilon_0\omega\eta_a\eta_b(k_b^2k_{az}^2 + k_a^2k_{bz}^2T_{\rm p}^2 + 2k_a k_{az}k_b k_{bz}T_{\rm p}\cos(\alpha x))},\end{aligned} \tag{4.8b}$$

$$\mathrm{Re}(\chi_{\mathrm{mm}}^{yy}) = \frac{-2\eta_a\eta_b(eta_a k_{az}k_b + \eta_b k_a k_{bz})T_{\mathrm{p}}\sin(\alpha x)}{k_a k_b \mu_0\omega(\eta_b^2\eta_a^2 T_{\mathrm{p}}^2 + 2\eta_a\eta_b T_{\mathrm{p}})\cos(\alpha x)}, \tag{4.8c}$$

$$\mathrm{Im}(\chi_{\mathrm{mm}}^{yy}) = \frac{2\eta_a\eta_b(\eta_a k_a k_{bz}T_{\mathrm{p}}^2 - \eta_b k_{az}k_b + (\eta_a k_a k_{bz}T_{\mathrm{p}}^2 - \eta_b k_b k_{az})T_{\mathrm{p}}^2\cos(\alpha x))}{k_a k_b \mu_0\omega(\eta_b^2\eta_a^2 T_{\mathrm{p}}^2 + 2\eta_a\eta_b T_{\mathrm{p}})\cos(\alpha x)}, \tag{4.8d}$$

with $\alpha = k_{ax} - k_{bx}$. Plots of these functions may be found in [126]. The non-zero imaginary parts of χ_{ee}^{xx} and χ_{mm}^{yy}, tensorially corresponding to the loss and gain relations $\overline{\overline{\chi}}_{\mathrm{ee}}^{T} \neq \overline{\overline{\chi}}_{\mathrm{ee}}^{*}$ and $\overline{\overline{\chi}}_{\mathrm{mm}}^{T} \neq \overline{\overline{\chi}}_{\mathrm{mm}}^{*}$, where the superscripts T and $*$ denote the transpose and conjugate operation respectively [218], indicate the presence of loss (negative imaginary part) and gain (positive imaginary part) alternating along the metasurface. This synthesis corresponds to the first way of obtaining a diffraction-free refractive metasurface, as shown in [11].

4.2.4 Bianisotropic Metasurface

Since specifying a monoanisotropic (or monoisotropic) metasurface leads only to the loss and gain option for diffraction-free refraction, as just found, complexity must be added to the metasurface to obtain the nonreciprocity and bianisotropy options. The non-gyrotropy assumption requires $\chi_{\mathrm{ee,mm}}^{xy} = \chi_{\mathrm{ee,mm}}^{yx} = \chi_{\mathrm{em,me}}^{xx} = \chi_{\mathrm{em,me}}^{yy} = 0$, and hence eliminates 8 of the 16 terms of a transverse metasurface, and, among the remaining 8 terms, 4 are for p-polarization and 4 are for s-polarization. Therefore, still assuming p-polarization, only the *bianisotropic* two terms χ_{em}^{xy} and χ_{me}^{yx} can be added to χ_{ee}^{xx} and χ_{mm}^{yy}. This 4-element susceptibility set allows for two fundamentally new possibilities: a) $\chi_{\mathrm{em}}^{xy} \neq -\chi_{\mathrm{me}}^{yx}$, and b) $\chi_{\mathrm{em}}^{xy} = -\chi_{\mathrm{me}}^{yx}$. The latter tensorially generalizes to $\overline{\overline{\chi}}_{\mathrm{em}} = -\overline{\overline{\chi}}_{\mathrm{me}}^{T}$, where the superscript 'T' represents the transpose operation, which is the only condition for *reciprocity* in the prevailing non-gyrotropic situation [218], and the former corresponds thus to a *nonreciprocal* metasurface. These two possibilities correspond to options 2) and 3), respectively, in [11]. In each of the two cases, one has to describe the phenomenon (reciprocity or nonreciprocity) by also specifying the transformation in the reverse direction, namely the direction from medium b to medium a, which brings about two additional equations, leading to a full-rank matrix system of order 4.

In the nonreciprocal case, one may specify any reverse transformation, such as for instance refraction in different directions or absorption. However, as mentioned in Sec. 6.1, we are primarily interested here in realizing a reciprocal metasurface. The corresponding reverse transformation, involving the same angles as in Fig. 4.1, is shown in Fig. 4.2.

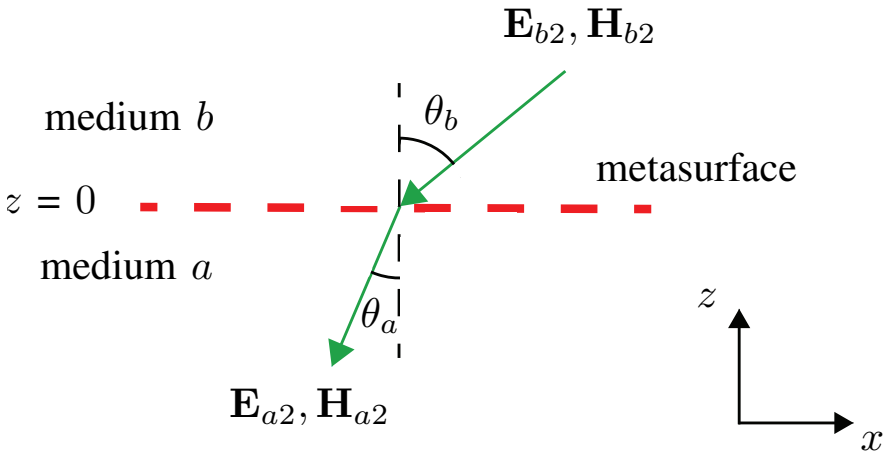

Figure 4.2 Reverse transformation reciprocal to that of Fig. 4.1

Thus, the proper synthesis equations, including both the reciprocal direct (subscript '1') and reverse (subscript '2') transformations, may be compactly written as

$$\begin{bmatrix} \Delta H_{y1} & \Delta H_{y2} \\ \Delta E_{x1} & \Delta E_{x2} \end{bmatrix} = \begin{bmatrix} -j\omega\epsilon_0\chi_{\mathrm{ee}}^{xx} & -jk_0\chi_{\mathrm{em}}^{xy} \\ -jk_0\chi_{\mathrm{me}}^{yx} & -j\omega\mu_0\chi_{\mathrm{mm}}^{yy} \end{bmatrix} \begin{bmatrix} E_{x1,\mathrm{av}} & E_{x2,\mathrm{av}} \\ H_{y1,\mathrm{av}} & H_{y2,\mathrm{av}} \end{bmatrix}, \tag{4.9}$$

whose first and second columns correspond to the direct and reverse transformations, respectively. The fields corresponding to the reverse transformation [Fig. 4.2] read

$$\mathbf{E}_{a2} = -(\cos\theta_a\hat{x} + \sin\theta_a\hat{z})e^{j(k_{ax}x+k_{az}z)}, \mathbf{H}_{a2} = \frac{e^{jk_{ax}x}}{\eta_a}\hat{y}, \tag{4.10a}$$

$$\mathbf{E}_{b2} = -T_{\mathrm{p}}(\cos\theta_b\hat{x} + \sin\theta_b\hat{z})e^{j(k_{bx}x+k_{bz}z)}, \mathbf{H}_{b2} = T_{\mathrm{p}}\frac{e^{jk_{bx}x}}{\eta_b}\hat{y}, \tag{4.10b}$$

corresponding to

$$\Delta E_{x2} = E_{bx2} - E_{ax2} = -T_{\mathrm{p}}\cos\theta_b e^{jk_{bx}x} + \cos\theta_a e^{jk_{ax}x}, \tag{4.11a}$$

$$\Delta H_{y2} = H_{by2} - H_{ay2} = T_{\mathrm{p}}e^{jk_{bx}x}/\eta_b - e^{jk_{ax}x}/\eta_a, \tag{4.11b}$$

$$E_{x,\mathrm{av}2} = \frac{E_{ax2} + E_{bx2}}{2} = \frac{-\cos\theta_a e^{jk_{ax}x} - T_{\mathrm{p}}\cos\theta_b e^{jk_{bx}x}}{2}, \tag{4.11c}$$

$$H_{y,\mathrm{av}2} = \frac{H_{ay2} + H_{by2}}{2} = \frac{e^{jk_{ax}x}/\eta_a + T_{\mathrm{p}}e^{jk_{bx}x}/\eta_b}{2}. \tag{4.11d}$$

Inserting (4.5) and (4.11) into (4.9) finally yields the sought after transverse susceptiblity

functions

$$\chi_{\mathrm{ee}}^{xx} = \frac{-4k_a k_b T_\mathrm{p} \sin(\alpha x))}{\epsilon_0 \omega \left(T_\mathrm{p}(\eta_a k_b k_{az} + \eta_b k_a k_{bz}) \cos(\alpha x)) + \eta_a k_b k_{az} + \eta_b k_a k_{bz} T_\mathrm{p}^2\right)}, \tag{4.12a}$$

$$\chi_{\mathrm{em}}^{xy} = \frac{2j \left(T_\mathrm{p}(\eta_a k_b k_{az} - \eta_b k_a k_{bz}) \cos(\alpha x)) - \eta_b k_b k_{az} + \eta_a k_a k_{bz} T_\mathrm{p}^2\right)}{k_0 \left(T_\mathrm{p}(\eta_a k_b k_{az} + \eta_b k_a k_{bz}) \cos(\alpha x)) + \eta_a k_b k_{az} + \eta_b k_a k_{bz} T_\mathrm{p}^2\right)}, \tag{4.12b}$$

$$\chi_{\mathrm{me}}^{yx} = \frac{2j \left(T_\mathrm{p}(\eta_b k_a k_{bz} - \eta_a k_b k_{az}) \cos(\alpha x)) - \eta_b k_b k_{az} + \eta_a k_a k_{bz} T_\mathrm{p}^2\right)}{k_0 \left(T_\mathrm{p}(\eta_a k_b k_{az} + \eta_b k_a k_{bz}) \cos(\alpha x)) + \eta_a k_b k_{az} + \eta_b k_a k_{bz} T_\mathrm{p}^2\right)}, \tag{4.12c}$$

$$\chi_{\mathrm{mm}}^{yy} = \frac{-4\eta_a \eta_b k_{az} k_{bz} T_\mathrm{p} \sin(\alpha x))}{\mu_0 \omega \left(T_\mathrm{p}(\eta_a k_b k_{az} + \eta_b k_a k_{bz}) \cos(\alpha x)) + \eta_a k_b k_{az} + \eta_b k_a k_{bz} T_\mathrm{p}^2\right)}, \tag{4.12d}$$

with $\alpha = k_{ax} - k_{bx}$. These relations are plotted in Fig. 4.3 for $\theta_a = 0°$ and $\theta_b = 70°$, and considering air on both sides of the metasurface.

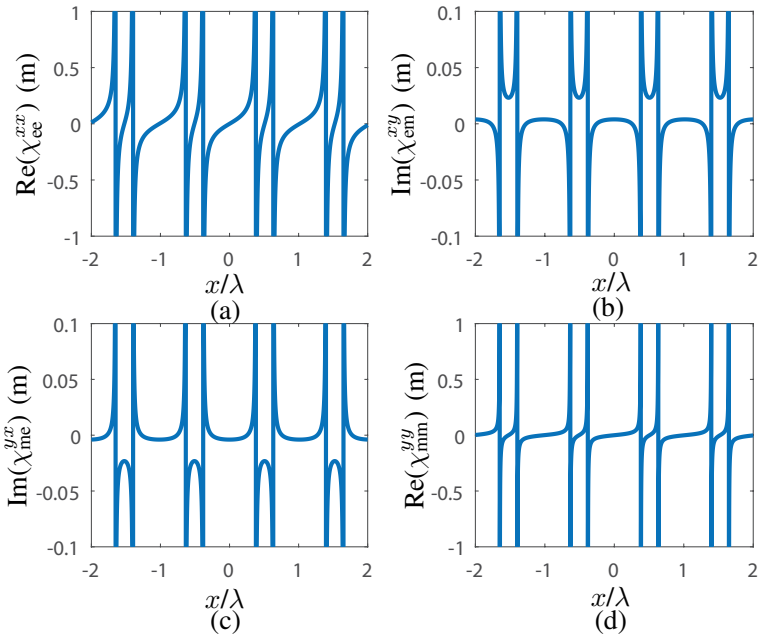

Figure 4.3 Susceptibility functions (4.12) for $\theta_a = 0°$ and $\theta_b = 70°$ (a) χ_{ee}^{xx} (purely real) (b) χ_{em}^{xy} (purely imaginary) (c) χ_{me}^{yx} (purely imaginary) (d) χ_{mm}^{yy} (purely real)

4.2.5 Properties of the Synthesized Metasurface

The metasurface characterized by the susceptibilities in (4.12) possesses the following properties:

- It is *bianisotropic*, as already noted in Sec. 4.2.4.2, since $\chi_{\text{em}}^{xy} \neq 0$ and $\chi_{\text{me}}^{yx} \neq 0$.
- As a result of bianisotropy, it is *asymmetric*, as will be shown in the corresponding scattering parameters to be given in Sec. 4.3.3.
- It is *reciprocal*, as noted in Sec. 4.2.4.2, since $\chi_{\text{em}}^{xy} = -\chi_{\text{me}}^{yx}$, which is equivalent to $T_{\text{p}} = \sqrt{\eta_b \cos\theta_a / \eta_a \cos\theta_b}$ (power conservation), tensorially corresponding to the relation $\overline{\overline{\chi}}_{\text{me}}^{T} = -\overline{\overline{\chi}}_{\text{em}}$.
- It is *passive* and *lossless*, since $\chi_{\text{ee}}^{xx}, \chi_{\text{mm}}^{yy} \in \mathbb{R}$ and $\chi_{\text{em}}^{xy}, \chi_{\text{me}}^{yx} \in \mathbb{I}$, tensorially corresponding to the relations $\overline{\overline{\chi}}_{\text{ee}}^{T} = \overline{\overline{\chi}}_{\text{ee}}^{*}$, $\overline{\overline{\chi}}_{\text{mm}}^{T} = \overline{\overline{\chi}}_{\text{mm}}^{*}$ and $\overline{\overline{\chi}}_{\text{me}}^{T} = \overline{\overline{\chi}}_{\text{em}}^{*}$ [218].
- It is *periodic* in x with period $k_{ax} - k_{bx}$, as seen in Fig. 4.3, corresponding to the periodic field momentum transformation [219] operated by the metasurface.

4.3 Scattering Parameter Mapping

The task now is to establish a proper link between the mathematical transverse susceptibility functions (4.12) and the corresponding real metasurface, composed of an array of scattering particles. Specifically, this includes discretizing these susceptibility functions in subwavelength cells and determining the appropriate particle geometries for all the cells.
To build a metasurface with the assumed purely transverse susceptibility, $\overline{\overline{\chi}}_{\mathrm{t}}$, we shall proceed as follows:

1. Map the synthesized susceptibility parameters onto *normal-incidence* scattering parameters. The reason to use normal incidence *in the design procedure* is twofold. First, this is a necessary condition to ensure that only the *transverse* terms of the particle susceptibilities or, more precisely, polarizabilities, get excited. Second, this will lead to the *simplest* possible simulation set-up for each specific particle (step 3 below), obliqueness being produced by the phase gradient between cells. For p-polarization, and assuming that the metasurface is reciprocal and surrounded by air, the corresponding relations are found, following the procedure in [124], as

$$S_{11}^{xx} = \frac{-2j\left(2k_0\eta_0\chi_{\mathrm{me}}^{yx} + \mu_0\omega\chi_{\mathrm{mm}}^{yy} - \eta_0^2\epsilon_0\omega\chi_{\mathrm{ee}}^{xx}\right)}{D^{xx}}, \tag{4.13a}$$

$$S_{22}^{xx} = \frac{2j\left(2k_0\eta_0\chi_{\mathrm{me}}^{yx} - \mu_0\omega\chi_{\mathrm{mm}}^{yy} + \eta_0^2\epsilon_0\omega\chi_{\mathrm{ee}}^{xx}\right)}{D^{xx}}, \tag{4.13b}$$

$$S_{21}^{xx} = S_{12}^{xx} = \frac{-j\eta_0\left(4 + k_0^2(\chi_{\mathrm{me}}^{yx})^2 + \mu_0\epsilon_0\omega^2\chi_{\mathrm{ee}}^{xx}\chi_{\mathrm{mm}}^{yy}\right)}{D^{xx}}. \tag{4.13c}$$

with

$$\begin{aligned} D^{xx} = &-2j\mu_0\omega\chi_{\mathrm{mn}}^{yy} \\ &+ \eta_0\left(-4 + k_0^2(\chi_{\mathrm{me}}^{yx})^2 + \epsilon\omega\chi_{\mathrm{ee}}^{xx}\left(-2j\eta_0 + \mu_0\omega\chi_{\mathrm{mm}}^{yy}\right)\right), \end{aligned} \tag{4.13d}$$

where the x's in the superscript xx correspond to the transverse component of the p-polarized fields [Eqs. (4.2) and (4.10)], assuming also non-gyrotropy. We have thus obtained the scattering matrix periodic functions $\overline{\overline{S}}^{xx}(x,y)$ corresponding to $\overline{\overline{\chi}}_{\parallel}(x,y)$. As announced in Sec. 4.2.5.2, Eqs. (4.13a) and (4.13a) reveal that the metasurface is asymmetric, since $S_{11}^{xx} \neq S_{22}^{xx}$. This requirement of an asymmetric unit cell is in agreement with previous works [11, 13].

2. Discretize the periodic functions (4.13), or $\overline{\overline{S}}^{xx}(x,y)$, in subwavelength cells in order to ensure their safe sampling in terms of Nyquist theorem. This leads to the discrete function $\overline{\overline{S}}^{xx}(x_i,y_j)$, for $i,\ldots,N_x$ and $j,\ldots,N_y$, where N_x and N_y represent the number

of cells along the x and y directions, respectively.

3. Select a generic particle structure and geometry that may be adjusted to cover the phase and amplitude range of $\overline{\overline{S}}^{xx}(x_i, y_j)$ across the entire metasurface. For simplicity and computational efficiency, compute the scattering parameters (under normal incidence) of each cell separately and within *periodic boundary conditions*. Even though the final metasurface will be locally aperiodic, i.e. made of different adjacent cells, periodic boundary conditions will reasonably approximate the coupling to slightly different neighbours.

4. Since $\overline{\overline{S}}^{xx}(x_i, y_j)$ is periodic, the period includes the complete set of all the different cells, and the overall structure will consist in the periodic repetition of the corresponding *super-cell*. Now, simulate this supercell within periodic boundary conditions with the specified incidence angle, and optimize the geometry of the particles so as to maximize energy refraction in the specified direction, i.e., specifically, in the proper diffraction order corresponding to the supercell.

Note that it is practically difficult to realize scattering particles with purely transverse polarizability and hence purely transverse susceptibility. Practical metasurfaces typically always include small non-zero longitudinal susceptibility terms, $\overline{\overline{\chi}}_\perp(x, y)$. Such terms are not excited in 3) above, due to normal incidence, but would play a role in 4) above, given the oblique angle[2]. We shall select a generic particle without longitudinal metallizations, to avoid strong perpendicular electric moments, and without transverse loops, to avoid strong perpendicular magnetic moments. We may therefore expect negligible $\overline{\overline{\chi}}_\perp(x, y)$ and a design essentially correspond to the assumed purely transverse one.

4.4 Design of Scattering Particles

We shall design here two diffraction-free refractive transverse metasurfaces to illustrate the theory of the previous sections: the first metasurface with $(\theta_a, \theta_b) = (20°, -28°)$ at 10 GHz and the second with $(\theta_a, \theta_b) = (0°, -70°)$ at 10.5 GHz. For this purpose, we shall follow the procedure described in Sec. 4.3.3. For experimental simplicity, we assume that the metasurface is entirely surrounded by free space ($k_a = k_b = k_0$, $\eta_a = \eta_b = \eta_0$).

[2]The final design may thus, rigorously, include a small $\overline{\overline{\chi}}_\perp(x, y)$ associated with a slightly modified $\overline{\overline{\chi}}_\parallel(x, y)$. Such a metasurface would strictly correspond to a diffraction-free-refraction design different than the initially purely transverse one. This does not represent any contradiction since the synthesis corresponds to an *inverse problem*, naturally admitting multiple solutions.

As the step 1), we insert the susceptibilities given by (4.12), with $k_a = k_b = k_0$, into (4.13). This yields the scattering parameter functions

$$S_{11}^{xx} = \frac{(-k_0^2 + k_{az}k_{bz})\sin[(k_{ax} - k_{bx})x] + jk_0(k_{az} - k_{bz})\cos[(k_{ax} - k_{bx})x]}{(k_0^2 + k_{az}k_{bz})\sin[(k_{ax} - k_b x)x] + jk_0(k_{az} + k_{bz})\cos[(k_{ax} - k_{bx})x]}, \tag{4.14a}$$

$$S_{22}^{xx} = \frac{(-k_0^2 + k_{az}k_{bz})\sin[(k_{ax} - k_{bx})x] - jk_0(k_{az} - k_{bz})\cos[(k_{ax} - k_{bx})x]}{(k_0^2 + k_{az}k_{bz})\sin[(k_{ax} - k_b x)x] + jk_0(k_{az} + k_{bz})\cos[(k_{ax} - k_{bx})x]}, \tag{4.14b}$$

$$S_{12}^{xx} = S_{21}^{xx} = \frac{2jk_0\sqrt{k_{az}k_{bz}}}{(k_0^2 + k_{az}k_{bz})\sin[(k_{ax} - k_b x)x] + jk_0(k_{az} + k_{bz})\cos[(k_{ax} - k_{bx})x]}. \tag{4.14c}$$

It may a priori seem contradictory with the initial assumption of reflection-less refraction to obtain $S_{11}^{xx} \neq 0$ and $S_{22}^{xx} \neq 0$. However, there is no contradiction if one recalls that Eqs. (4.13) are associated in the *design procedure* with *normal incidence*, both to isolate out transverse susceptibility components and to simulate the cells one by one, whereas the specified incidence angle is generally nonzero. When excited under the specified oblique incidence angle, the metasurface realized by this design methodology will naturally be reflection-less. Note that the metasurface asymmetry predicted in Sec 4.2.5.2 is still clearly apparent from the fact that $S_{11}^{xx} \neq S_{22}^{xx}$, since asymmetry for normal incidence implies asymmetry.

As step 2), we discretize each of the two metasurfaces in 6 different unit cells of size 6×6 mm ($\sim \lambda_0/5$) for the metasurface with $(\theta_a, \theta_b) = (20°, -28°)$ and 5.1×5.1 mm ($\sim \lambda_0/5.6$) for the metasurface with $(\theta_a, \theta_b) = (0°, -70°)$.

As step 3), we choose scattering particles made of three dog-bone shaped metallic layers separated by 1.52 mm-thick ($\sim \lambda_0/20 = \lambda_d/11.55$) Rogers 3003 ($\epsilon_r = 3$, $\tan\delta = 0.0013$) dielectric slabs[3].

The generic dog-bone metallization is shown in Fig. 4.4 (a), while Fig. 4.4 (b) shows the corresponding three-layer unit cell. Each unit cell is then optimized with periodic conditions using a commercial software (CST Studio 2014), which provides a reasonable initial guess for the geometry of the dog-bone patterns.

[3]The reason for the choice of three metallic layers is as follows. The metasurface, as specified by (4.14), is a reciprocal and lossless two-port network for each unit cell. Such a network may be easily shown to support 3 independent parameters, specifically one magnitude and two phases in its characteristic (e.g. scattering) parameters [220]. In order to realize the metasurface, we therefore need 3 independent degrees of freedom, which may be provided by three cascaded admittances, and hence three metal layers.

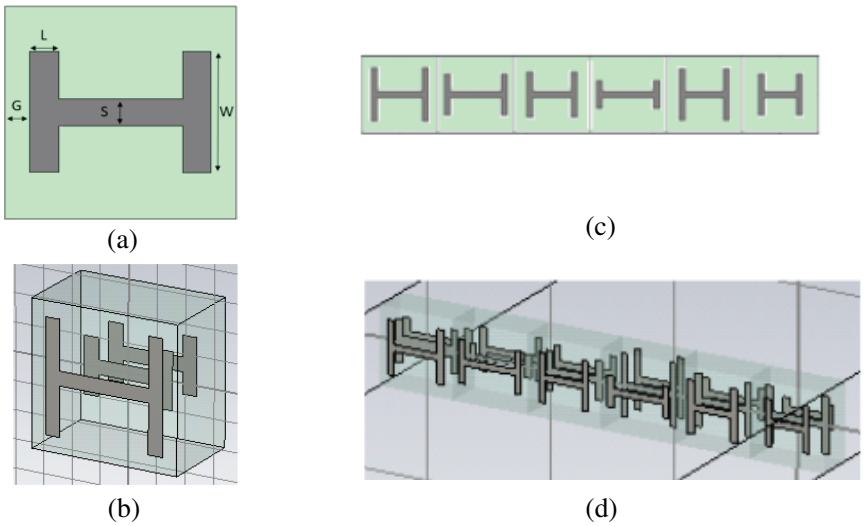

Figure 4.4 Metasurface scattering particles (a) Unit cell front view with dog-bone shaped metallic particle (b) Unit cell perspective view with dielectric substrates made transparent for visualisation (c) Supercell composed of 6 unit cells, front view (d) Supercell perspective view

As step 4), we combine the six different unit cells into a supercell, which is periodically repeated to form the whole metasurface. Figure 4.4 (c) and (d) show the generic structure of the supercell. Finally, the supercell, automatically taking into account the exact (as opposed to periodic) coupling between adjacent unit cells, is optimized. Specifically, we simulate the Floquet space harmonics of the supercell and adjust the geometrical parameters so as to maximize the energy in the desired mode. Given the high number of degrees of freedom of the supercell (6 unit cells $\times$ 3 layers $\times$ 4 geometry parameters), we proceed as follows: i) we optimize the first unit cell within the periodic supercell simulation setup, ii) we subsequently update the supercell, iii) we move on to the second cell and iteratively repeat i) and ii) until the last unit cell. This supercell optimization is done iteratively until the desired performance is achieved. Moreover, in this process, we change only one parameters (W, L, G, S) in each of the three unit cell layers, in order to minimize the computational effort. The dimensions (in mm) of the metallic structures of the different unit cells are listed in Tabs. 4.1 and 4.2 for the two metasurfaces.

4.5 Simulation and Experiment

The full-wave simulated fields of the two diffraction-free bianisotropic reciprocal refractive metasurfaces are plotted in Fig. 4.5. Being perfectly periodic, the metasurface supports in principle an infinite number of space harmonics, as mentioned in the last item of Sec. 4.2.5.

Table 4.1 Dimensions (in millimeter) of the unit cells for the $(\theta_a, \theta_b) = (20°, -28°)$ metasurface

		W	L	G	S
Cell 1	Layer 1	4.25	0.5	0.75	0.5
	Layer 2	3.125	0.5	0.5	0.875
	Layer 3	2.5	0.5	0.25	0.5
Cell 2	Layer 1	3.25	0.5	0.5	0.5
	Layer 2	1.75	0.5	0.5	0.25
	Layer 3	3.25	0.5	0.5	0.5
Cell 3	Layer 1	3.625	0.5	1	0.5
	Layer 2	3	0.5	0.75	0.5
	Layer 3	2.625	0.5	0.5	0.5
Cell 4	Layer 1	2.25	0.5	0.5	0.5
	Layer 2	4.75	0.5	0.75	0.5
	Layer 3	4.5	0.5	1	0.5
Cell 5	Layer 1	4.25	0.5	1	0.5
	Layer 2	4.25	0.5	3.75	0.5
	Layer 3	2.375	0.5	0.5	0.5
Cell 6	Layer 1	3	0.5	1.25	0.5
	Layer 2	4.125	0.5	0.5	0.5
	Layer 3	1.5	0.5	1	0.5

In both designs, only the space harmonics $m = 0$, $m = -1$ and $m = +1$ are propagating, while the others are evanescent, and the incident and refracted waves correspond to the space harmonics $m = 0$ and $m = -1$, respectively. Ideally, from synthesis, 100% of the scattered power should reside in the $m = -1$ space harmonic. Practically, the harmonics R_0, R_{-1}, R_{+1}, T_0 and T_{+1} are also weakly excited, due to the imperfections of the metasurface associated with discretization and fabrication restrictions (essentially limited resolution of the metallic particles), already taken into account at this simulation stage. At this point, it would be interesting to compare the ideal susceptibility functions plotted in Fig. 4.3 for the $(\theta_a, \theta_b) = (0°, -70°)$ metasurface with the susceptibility function of the realized discretized metasurface. However, access to this realized susceptibility is not trivial, and will therefore be discussed in a future publication with specific emphasis on the modeling problem.

Table 4.2 Dimensions (in millimeter) of the unit cells for the $(\theta_a, \theta_b) = (0°, -70°)$ metasurface

		W	L	G	S
Cell 1	Layer 1	3	0.5	0.375	0.5
	Layer 2	2.5	0.5	0.375	0.5
	Layer 3	4	0.5	0.25	0.5
Cell 2	Layer 1	3.25	0.5	0.25	0.5
	Layer 2	3	0.5	0.5	0.5
	Layer 3	2.5	0.5	0.25	0.5
Cell 3	Layer 1	4	0.5	0.75	0.5
	Layer 2	3.75	0.5	0.75	0.5
	Layer 3	2.5	0.5	0.5	0.5
Cell 4	Layer 1	3.25	0.5	0.625	0.5
	Layer 2	1.5	0.5	1	0.5
	Layer 3	2	0.5	0.875	0.5
Cell 5	Layer 1	4.5	0.5	0.75	0.5
	Layer 2	4.5	0.5	0.625	0.5
	Layer 3	4.25	0.5	1	0.5
Cell 6	Layer 1	3.25	0.5	0.875	0.5
	Layer 2	4.25	0.5	0.5	0.5
	Layer 3	4	0.5	1	0.5

The corresponding scattering parameter simulations are shown in Fig. 4.6 and Fig. 4.7 for the $(\theta_a, \theta_b) = (20°, -28°)$ metasurface and the $(\theta_a, \theta_b) = (0°, -70°)$ metasurface, respectively. As expected from synthesis, most of the incident power, except for small conducting and dielectric dissipation loss and negligible coupling to undesired space harmonics, is refracted to the specified direction. The T_{-1} space harmonic is -0.6185 dB at 9.94 GHz for the $(\theta_a, \theta_b) = (20°, -28°)$ metasurface and -0.7978 dB at 10.64 GHz for the $(\theta_a, \theta_b) = (0°, -70°)$ metasurface with reflection lower than -15 dB. In comparison, the simulation result *before* the supercell optimization process (Sec. 4.4) yielded a T_{-1} space harmonic of -1.5045 dB for the $(\theta_a, \theta_b) = (20°, -28°)$ metasurface and of -1.6518 for the $(\theta_a, \theta_b) = (0°, -70°)$ metasurface, which is 0.886 dB and 0.854 dB worse, respectively.

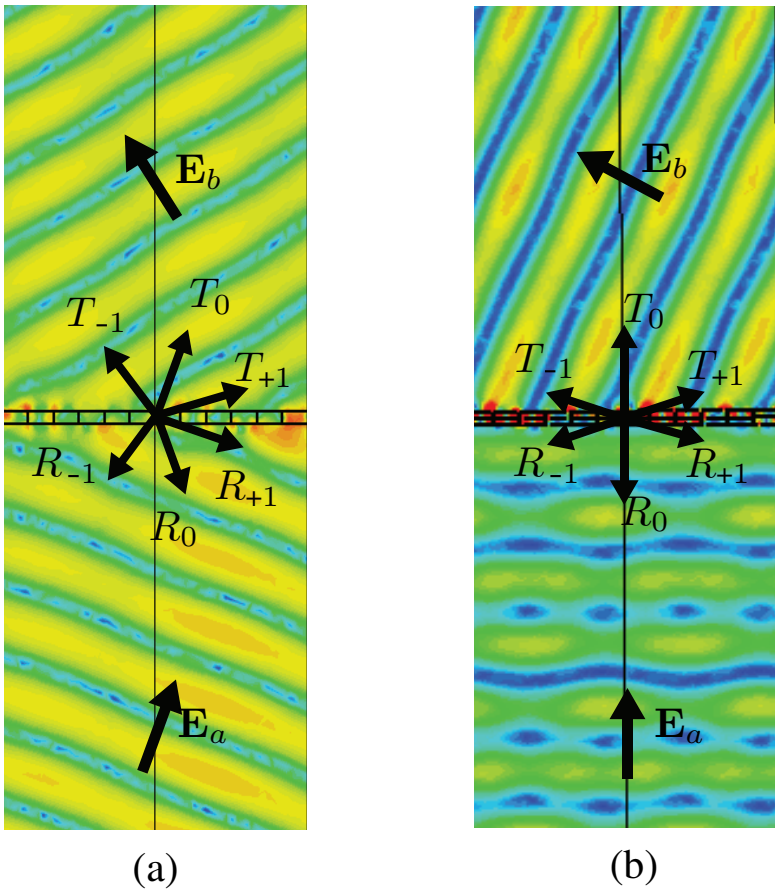

Figure 4.5 Full-wave simulated electric field magnitude for the two diffraction-free bianisotropic reciprocal refractive metasurfaces (a) Metasurface with $(\theta_a, \theta_b) = (20°, -28°)$ at 10 GHz (b) Metasurface with $(\theta_a, \theta_b) = (0°, -70°)$ at 10.5 GHz

The two metasurfaces were fabricated and measured. Figure 4.8 shows a photograph of them and Fig. 4.9 shows the experimental setup used for the measurements. In the measurement, we used a horn antenna placed $\sim$ 400 mm from the metasurface and a near-field probe scanning over a plane parallel to the metasurface in the transmission region. We then applied a near-field to far-field transformation [221] to evaluate the transmission response of the metasurface. The measurement results are shown, superimposed with the simulations, in Figs. 4.10 and 4.11 for the $(\theta_a, \theta_b) = (20°, -28°)$ metasurface and the $(\theta_a, \theta_b) = (0°, -70°)$ metasurface, respectively.

Tables 4.3 and 4.4 compare the simulation and experimental results at the optimal frequency. The slight discrepancy of the experimental frequency compared to the simulated one (3.7% and 1.4% for the $(\theta_a, \theta_b) = (20°, -28°)$ and $(\theta_a, \theta_b) = (0°, -70°)$ metasurfaces, respectively) is explained by the small air gaps existing between the two substrate layers in the metasurface

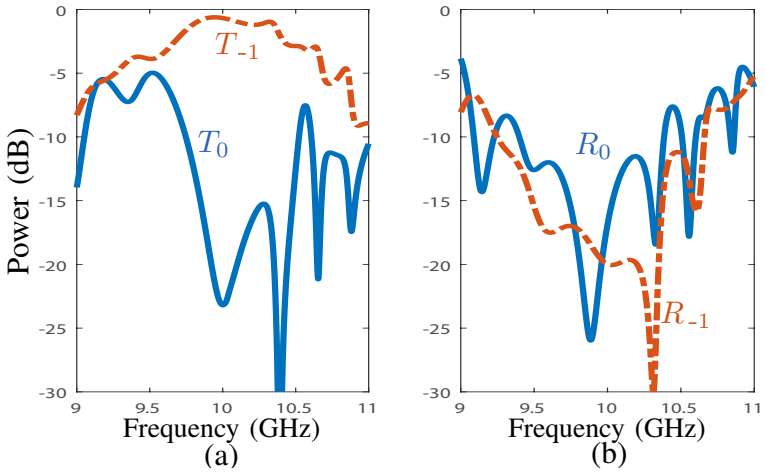

Figure 4.6 Simulated scattering parameters of the $(\theta_a, \theta_b) = (20°, -28°)$ 10 GHz metasurface (a) Transmitted propagating space harmonics. (b) Reflected propagating space harmonics

assembly. The lower efficiency of the T_{-1} harmonic in the experiment compared to the simulation is mostly due to more power diffracted into the T_0 harmonic. While our experiment did not directly measure reflections, the combined reflected and dissipated powers (reflection + loss) from the simulation and experiment are in fairly good agreement. The observed discrepancies between simulation and measurement may be attributed to different factors, including fabrication tolerance, horn antenna excitation (instead of ideal plane wave) and probe antenna imperfection (spurious edge diffraction).

In [10], the authors established a theoretical limit in efficiency for a lossless monoanisotropic metasurface, which is found to be $\sim 75\%$ for $(\theta_a, \theta_b) = (0°, -70°)$. Our bianisotropic metasurface exceeds this lossless monoanisotropic limit by around 4% despite the natural presence of loss. This result suggests that bianisotropic metasurfaces can indeed realize refraction with higher efficiencies than conventional designs. We believe this is the first experimental demonstration of overcoming the fundamental efficiency limit for anomalous refraction using bianisotropic metasurface. In comparison, the experimental work in [148], for a similar wide-angle refraction, had an overall efficiency lower to the efficiency limit of conventional (monoanisotropic) designs due to higher scattering into other diffraction orders and higher absorbtion compared to our metasurface. Note that the experimental efficiency of the $(\theta_a, \theta_b) = (20°, -28°)$ metasurface is lower than the theoritical efficiency of a lossless monoanisotropic metasurface. This is mostly due to dissipation loss in the metal scatterers and in the dielectric. Possible avenues for future work that may reduce the losses and lead to higher efficiencies are to either use similar scattering particles but with less lossy materials or to implement a fully dielectric bianisotropic metasurface.

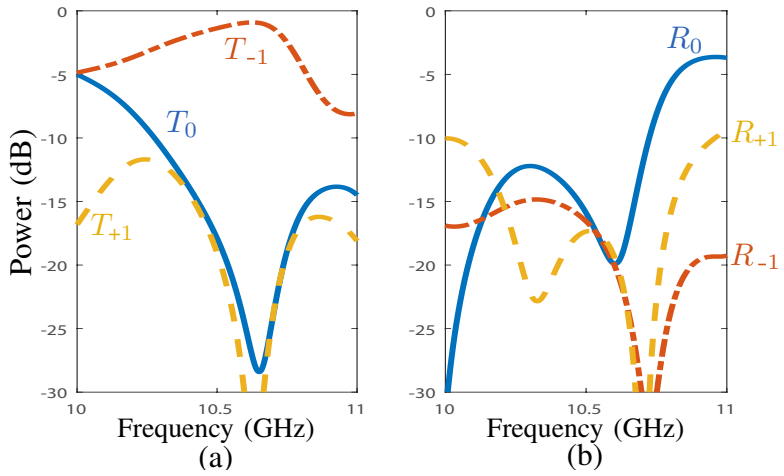

Figure 4.7 Simulated scattering parameters of the $(\theta_a, \theta_b) = (0°, -70°)$ 10.5 GHz metasurface (a) Transmitted propagating space harmonics (b) Reflected propagating space harmonics

Table 4.3 Simulation and experiment result at the optimal frequency $(\theta_a, \theta_b) = (20°, -28°)$ metasurface

	Frequency (GHz)	T_{-1} (dB)	T_0 (dB)	T_{+1} (dB)	Reflections + Losses (dB)
Simulation	9.94	-0.6185	-21.12	< -80	-8.5243
Experiment	10.32	-1.44	-8.476	< -80	-8.5335

4.6 Conclusion

We have derived the conditions for diffraction-free refraction in a metasurface using a medium-based approach based on Generalized Sheet Transition Conditions (GSTCs) and surface susceptibility tensors, and experimentally demonstrated two diffraction-free metasurfaces that are essentially lossless, passive, bianisotropic and reciprocal.

Following [11], we have considered refractive metasurfaces possessing only *transverse* susceptibility components. However, diffraction-less refraction might also be achieved by metasurfaces including *normal* polarizabilities, which would lead to other possibilities than the three reported in [11]. However, solving the synthesis problem for metasurfaces with nonzero normal susceptibility components is not trivial since the corresponding GSTCs relations form a set of *differential* equations instead of just algebraic equations. At this stage, the design of such structures remains an open avenue for further investigation.

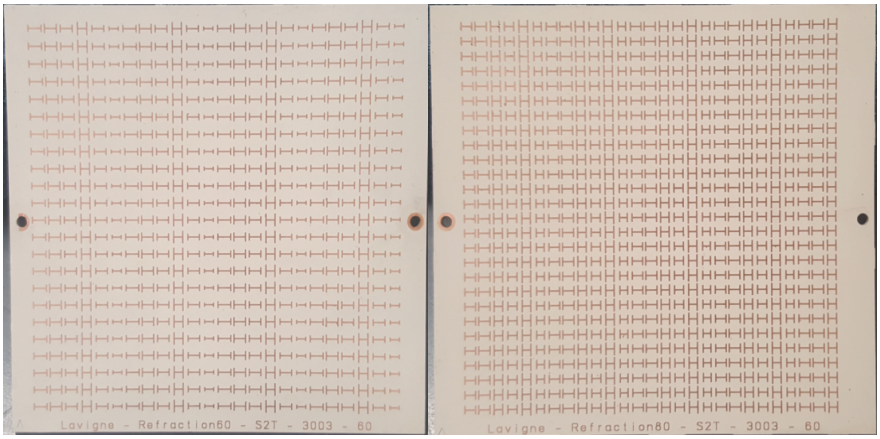

Figure 4.8 Photographs of the two fabricated metasurfaces (a) $(\theta_a, \theta_b) = (20°, -28°)$ metasurface (b) $(\theta_a, \theta_b) = (0°, -70°)$ metasurface

Table 4.4 Simulation and experiment result at the optimal frequency $(\theta_a, \theta_b) = (0°, -70°)$ metasurface

	Frequency (GHz)	T_{-1} (dB)	T_0 (dB)	T_{+1} (dB)	Reflections + Losses (dB)
Simulation	10.64	-0.7978	-24.27	-32.02	-7.8663
Experiment	10.8	-1.0004	-14.28	-22.76	-7.8574

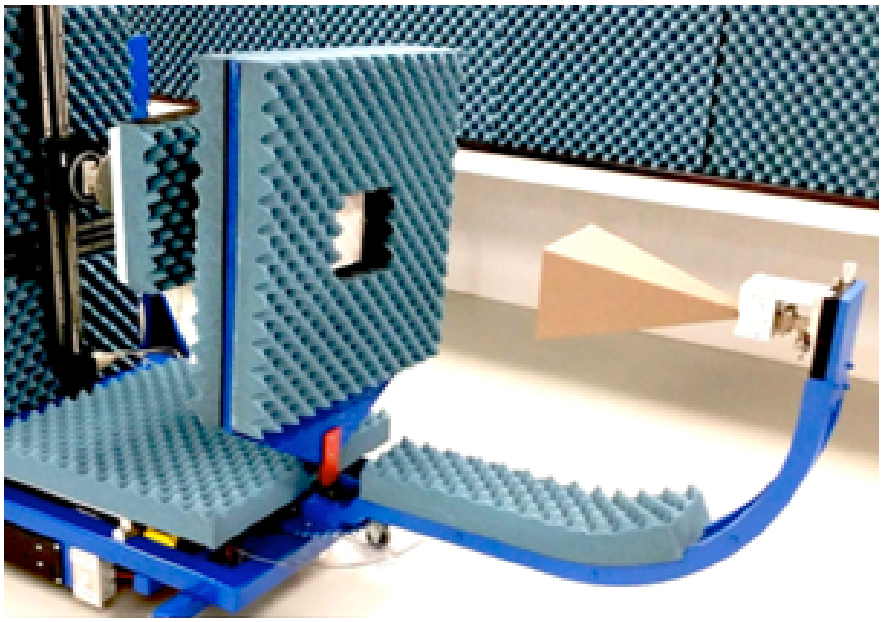

Figure 4.9 Photograph of the experimental setup with the horn antenna on the right and the metasurface being measured in the center surrounded by absorbers

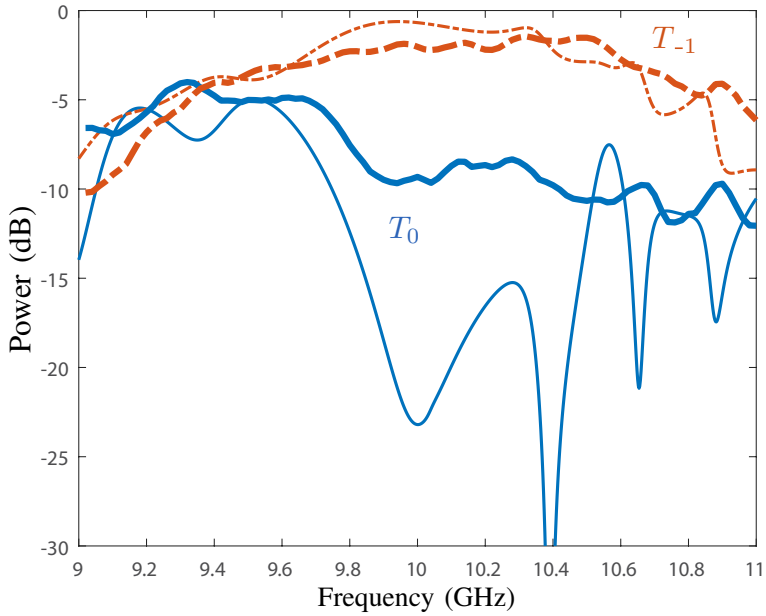

Figure 4.10 Measured (thick lines) and simulated (thin lines) scattering parameters in transmission of the $(\theta_a, \theta_b) = (20°, -28°)$ metasurface.

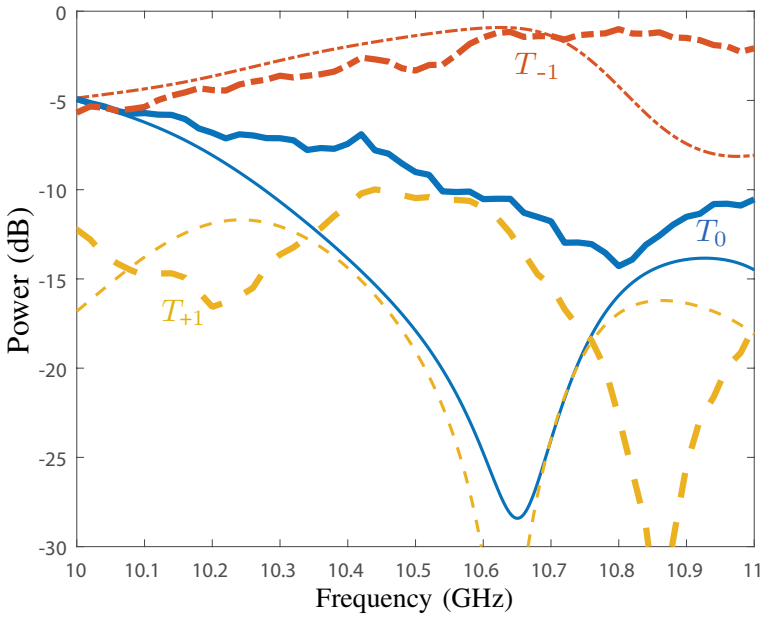

Figure 4.11 Measured (thick lines) and simulated (thin lines) scattering parameters in transmission of the $(\theta_a, \theta_b) = (0°, -70°)$ metasurface

CHAPTER 5 ARTICLE 2: GENERALIZED BREWSTER EFFECT USING BIANISOTROPIC METASURFACES

Authors: Guillaume Lavigne and Christophe Caloz

This work was published in Optics Express, Volume 29, Issue 7, pages 11361-11370, on March 29 2021.

Abstract

We show that a properly designed bianisotropic metasurface placed at the interface between two arbitrary different media, or coating a dielectric medium exposed to the air, provides Brewster (reflectionless) transmission at arbitrary angles and for both the TM and TE polarizations. We present a rigorous derivation of the corresponding surface susceptibility tensors based on the generalized sheet transition conditions, and demonstrate by full-wave simulations the system with planar microwave metasurfaces designed for polarization-independent and azimuth-independent operations. The proposed bianisotropic metasurfaces provide deeply subwavelength matching solutions for initially mismatched media. The reported generalized Brewster effect represents a fundamental advance in optical technology, where it may both improve the performance of conventional components and enable the development of novel devices.

5.1 Introduction

The Brewster effect, which consists in the vanishment of the reflection of TM-polarized waves at the interface between two dielectric media at a specific incidence angle [169], has a history of more than 200 years. In 1808, Malus observed that unpolarized light becomes polarized upon reflection under a particular angle at the surface of water [170]. Seven years later, Brewster experimentally showed that this angle was equal to the inverse tangent of the ratio the refractives indices of the two media [171]. Another six years later, in 1821, Fresnel completed the understanding of the phenomenon using a mechanical model of the interface system and derived the eponymic reflection and transmission coefficients [172], which embed the Brewster effect. Finally, these formulas were generalized to magneto-electric materials, which support either TM-polarization or TE-polarization Brewster transmission, with both possible only for normal incidence, by Giles and Wild [173].

The recent advent of metasurfaces has created novel opportunities to extend the Brewster effect. Metasurfaces allow indeed unprecedented manipulations of electromagnetic waves [21, 25]; specifically, bianisotropic metasurfaces [12] may produce full polarization transformation [7], anomalous reflection [122] and diffractionless generalized refraction [149, 222]. They have recently been shown to support Brewster-like, i.e., reflection-less, transmission when surrounded at both sides by air in planar optical silicon nanodisk configuration [174], high-refractive-index nanorod metasurfaces [175], non-planar microwave split-ring resonator configuration [176, 177] and all-angle Brewster transmission in a terahertz metasurface [178]. Moreover, they have been demonstrated to allow general Brewster transmission, i.e., between two different media, in the particular case of normal incidence in a non-planar bianisotropic loop-dipole configuration [152].
Here, following our initial suggestion in [223], we present a generalization of the Brewster effect between two arbitrary different media, for arbitrary incidence angle and arbitrary polarization, using a planar bianisotropic metasurface. We derive synthesis formulas of the corresponding metasurface susceptibility tensors and demonstrate the generalized Brewster angle by full-wave electromagnetic simulation.

5.2 Generalized Brewster Effect

Figure 5.1 shows the proposed metasurface-based generalized Brewster effect. Figure 5.1(a) illustrates the suppression of reflection for arbitrary wave incidence angle and arbitrary polarization, Fig. 5.1(b) defines the corresponding problem in the plane of scattering, and Fig. 5.1(c) depicts the metaparticule used in the paper as a proof of concept in the microwave regime. The metasurface is assumed to suppress reflection without altering the direction of refraction prescribed by the Snell law for the initial pair of media and without inducing any gyrotropy (polarization rotation), while being passive, lossless and reciprocal. The preservation of the Snell law for the transmitted wave implies a uniform (without phase gradient) metasurface, and hence a uniformly periodic metastructure.

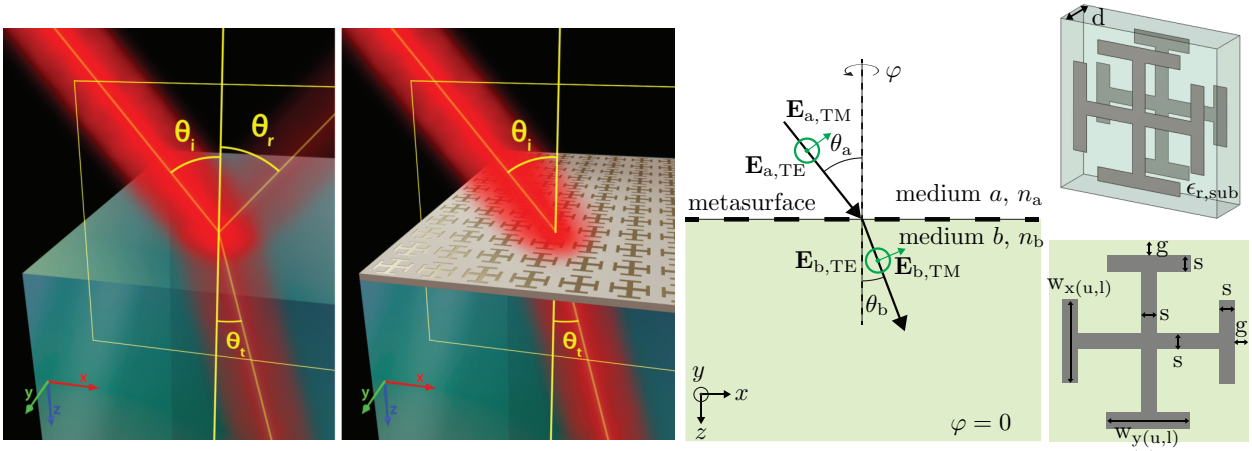

(a) (b) (c)

Figure 5.1 Metasurface-based generalized Brewster refraction between two media (a) Scattering of a wave impinging on the interface under an arbitrary angle (θ_a), with conventional Fresnel transmission and reflection for the case of the bare interface (left) and with reflectionless (Brewster) transmission when a properly designed metasurface is placed at the interface (right) (b) Brewster metasurface problem, for TE and TM polarizations, in the xz-plane scattering plane (c) Proposed 2-layer conducting cross-potent metaparticle for a microwave proof of concept

5.3 Susceptibility Tensor Derivation

5.3.1 Field Specifications

We consider the metasurface problem depicted in Fig. 5.1 (b), where a wave incident from the medium a in the $xz-$plane at an arbitrary angle θ_a is fully transmitted, without reflection ($R = 0$), into the medium b, at the Snell angle $\theta_\mathrm{b} = \arcsin(\frac{n_\mathrm{a}}{n_\mathrm{b}} \sin\theta_\mathrm{a})$. We assume the time-harmonic complex convention $\exp(-i\omega t)$ through the paper, and we shall apply the metasurface synthesis technique described in [124,128] to determine the susceptibility tensors of the metasurface.

The first step in the synthesis is to define the desired tangential fields at both sides of the metasurface in the plane $z = 0$. For a TM-polarized wave, these fields read

$$\mathbf{E}_{\|a,\mathrm{TM}} = \cos\theta_\mathrm{a} e^{-ik_x x}\hat{x}, \tag{5.1a}$$

$$\mathbf{H}_{\|a,\mathrm{TM}} = \frac{e^{-ik_x x}}{\eta_\mathrm{a}}\hat{y}, \tag{5.1b}$$

$$\mathbf{E}_{\|b,\mathrm{TM}} = T\cos\theta_\mathrm{b} e^{-ik_x x} e^{i\phi_\mathrm{TM}}\hat{x}, \tag{5.1c}$$

$$\mathbf{H}_{\|b,\mathrm{TM}} = T\frac{e^{-ik_x x}}{\eta_\mathrm{b}} e^{i\phi_\mathrm{TM}}\hat{y}, \tag{5.1d}$$

while for a TE-polarized wave, they read

$$\mathbf{E}_{\|a,\mathrm{TE}} = -e^{-ik_x x}\hat{y}, \tag{5.2a}$$

$$\mathbf{H}_{\|a,\mathrm{TE}} = \cos\theta_\mathrm{a}\frac{e^{-ik_x x}}{\eta_\mathrm{a}}\hat{x}, \tag{5.2b}$$

$$\mathbf{E}_{\|b,\mathrm{TE}} = -Te^{-ik_x x}e^{i\phi_\mathrm{TE}}\hat{y} \tag{5.2c}$$

$$\mathbf{H}_{\|b,\mathrm{TE}} = T\cos\theta_\mathrm{b}\frac{e^{-ik_x x}}{\eta_\mathrm{b}}e^{i\phi_\mathrm{TE}}\hat{x}, \tag{5.2d}$$

where k_x is the (continuous) tangential wavenumber, $\eta_{(a,b)}$ is the wave impedance in medium (a,b), and T is the transmission coefficient between the two media. The phase terms $e^{i\phi_{\mathrm{TM,TE}}}$ in the transmitted fields are introduced here to account for the typical phase shifts imparted to the wave by a pratical metasurface and to provide degrees of freedom that may be advantageous in the design of the unit-cell metaparticle. In these relations, T must be properly chosen to provide total transmission across the metasurface. It is obtained by enforcing power conservation across the metasurface (passivity and losslessness assumptions), i.e., by enforcing the continuity of the normal component of the Poynting vector at $z = 0$ [128]. This leads, using the fields in (5.1) and (5.2), to

$$T = \sqrt{\frac{\eta_\mathrm{b}\cos\theta_\mathrm{a}}{\eta_\mathrm{a}\cos\theta_\mathrm{b}}}, \tag{5.3}$$

which is identical for the TE and TM polarizations.

5.3.2 Transition Conditions

The boundary conditions in the plane of the metasurface ($z = 0$) are the generalized sheet transition conditions [25, 124, 128]

$$\hat{z}\times\Delta\mathbf{H} = i\omega\epsilon\overline{\overline{\chi}}_\mathrm{ee}\mathbf{E}_\mathrm{av} + i\omega\overline{\overline{\chi}}_\mathrm{em}\sqrt{\mu\epsilon}\mathbf{H}_\mathrm{av}, \tag{5.4a}$$

$$\Delta\mathbf{E}\times\hat{z} = i\omega\mu\overline{\overline{\chi}}_\mathrm{me}\sqrt{\frac{\epsilon}{\mu}}\mathbf{E}_\mathrm{av} + i\omega\mu\overline{\overline{\chi}}_\mathrm{mm}\mathbf{H}_\mathrm{av}, \tag{5.4b}$$

where the symbol Δ and the subscript 'av' represent the differences and averages of the tangential fields at both sides of the metasurface, i.e.,

$$\Delta\mathbf{\Phi} = \mathbf{\Phi}_b - \mathbf{\Phi}_a, \tag{5.5}$$

$$\mathbf{\Phi}_\mathrm{av} = (\mathbf{\Phi}_a + \mathbf{\Phi}_b)/2, \tag{5.6}$$

where $\mathbf{\Phi} = \mathbf{E}, \mathbf{H}$, and $\overline{\overline{\chi}}_{\rm ee}$, $\overline{\overline{\chi}}_{\rm em}$, $\overline{\overline{\chi}}_{\rm me}$ and $\overline{\overline{\chi}}_{\rm mm}$ are the bianisotropic surface susceptibility tensors describing the metasurface. In this paper, we shall restrict our attention to purely tangential susceptibility metasurfaces, corresponding to 2×2 tensors and hence 16 susceptibility parameters in Equation (6.5), although metasurfaces involving normal susceptibility components may offer further possibilities [128], as will be discussed later.

5.3.3 Homoanisotropic Metasurface

We heuristically start our quest for the design described in connection with Fig. 5.1 by considering the simplest type of metasurface, namely an homoanisotropic metasurface, which is defined as a metasurface whose only nonzero susceptibility tensors are $\overline{\overline{\chi}}_{\rm ee}$ and $\overline{\overline{\chi}}_{\rm mm}$. The nongyrotropy condition implies then $\chi_{\rm ee}^{xy} = \chi_{\rm ee}^{yx} = \chi_{\rm mm}^{xy} = \chi_{\rm mm}^{yx} = 0$ [128], which decouples the two polarizations with $\chi_{\rm ee}^{xx}$ and $\chi_{\rm mm}^{yy}$ for TM and $\chi_{\rm ee}^{yy}$ and $\chi_{\rm mm}^{xx}$ for TE (see Fig. 5.1(b)). Inserting the specifications (5.1) and (5.2) into the field differences and averages (5.5) and (5.6), substituting the resulting expressions into into (6.5), and solving for the four nonzero susceptibility components yields

$$\chi_{\rm ee}^{xx} = \frac{2i\eta_{\rm a} T e^{i\phi_{\rm TM}} - 2i\eta_{\rm b}}{\eta_{\rm a}\eta_{\rm b}\omega\epsilon_0 \cos\theta_{\rm a} + \eta_{\rm a}\eta_{\rm b} T\omega\epsilon_0 e^{i\phi_{\rm TM}} \cos\theta_{\rm b}}, \tag{5.7a}$$

$$\chi_{\rm mm}^{yy} = -\frac{2i\eta_{\rm a}\eta_{\rm b}\left(\cos\theta_{\rm a} - T e^{i\phi_{\rm TM}} \cos\theta_{\rm b}\right)}{\mu_0\omega\left(\eta_{\rm b} + \eta_{\rm a} T e^{i\phi_{\rm TM}}\right)}. \tag{5.7b}$$

$$\chi_{\rm ee}^{yy} = \frac{2i\eta_{\rm a} T e^{i\phi_{\rm TE}} \cos\theta_{\rm b} - 2i\eta_{\rm b} \cos\theta_{\rm a}}{\eta_{\rm a}\eta_{\rm b}\omega\epsilon_0 + \eta_{\rm a}\eta_{\rm b} T\omega\epsilon_0 e^{i\phi_{\rm TE}}}, \tag{5.8a}$$

$$\chi_{\rm mm}^{xx} = \frac{i\eta_{\rm a}\eta_{\rm b}\left(-1 + T e^{i\phi_{\rm TE}}\right)}{-\eta_{\rm b}\mu_0\omega\cos\theta_{\rm a} + \eta_{\rm a}\mu_0 T\omega e^{i\phi_{\rm TE}} \cos\theta_{\rm b}}. \tag{5.8b}$$

The complex nature of these susceptibilities indicates the presence of loss or gain, whereas we are searching for a lossless and gainless metasurface. This attempt is therefore unsuccessful, but it demonstrates the necessity for a really bianisotropic metasurface, as will be shown next.

5.3.4 Bianisotropic Metasurface

At this point, we can still hope that adding heteroanisotropy, corresponding to the susceptibilitity tensors $\overline{\overline{\chi}}_{\rm em}$ and $\overline{\overline{\chi}}_{\rm me}$, may allow to remove the loss-gain constraint of the previous design via the resulting extra degrees of freedom. Let us thus add the two heterotropic allowed pairs of nongyrotropic components, namely $\chi_{\rm em}^{xy}$ and $\chi_{\rm me}^{yx}$ for TM and $\chi_{\rm em}^{yx}$ and $\chi_{\rm me}^{xy}$ for TE. This increases the number of parameters to eight, and implies therefore the specification

of an additional wave transformation for each polarization in order to make the system of equations (6.5) full-rank and hence the synthesis problem exactly determined. Since some forms of bianisotropy can lead to nonreciprocity [14], which is here prohibited, we shall enforce reciprocity by specifying a second wave transformation corresponding to the time-reversed version of the fields in (5.1) and (5.2) [224]. The resulting system of equations can be compactly written as

$$\begin{bmatrix}\Delta H_{y1} & \Delta H_{y2} \\ \Delta E_{x1} & \Delta E_{x2}\end{bmatrix} = \begin{bmatrix}-i\omega\epsilon_0\chi_{\mathrm{ee}}^{xx} & -ik_0\chi_{\mathrm{em}}^{xy} \\ -ik_0\chi_{\mathrm{me}}^{yx} & -i\omega\mu_0\chi_{\mathrm{mm}}^{yy}\end{bmatrix} \begin{bmatrix}E_{x1,\mathrm{av}} & E_{x2,\mathrm{av}} \\ H_{y1,\mathrm{av}} & H_{y2,\mathrm{av}}\end{bmatrix}, \tag{5.9}$$

for the TM polarization, and as

$$\begin{bmatrix}\Delta H_{x1} & \Delta H_{x2} \\ \Delta E_{y1} & \Delta E_{y2}\end{bmatrix} = \begin{bmatrix}-i\omega\epsilon_0\chi_{\mathrm{ee}}^{yy} & -ik_0\chi_{\mathrm{em}}^{yx} \\ -ik_0\chi_{\mathrm{me}}^{xy} & -i\omega\mu_0\chi_{\mathrm{mm}}^{xx}\end{bmatrix} \begin{bmatrix}E_{y1,\mathrm{av}} & E_{y2,\mathrm{av}} \\ H_{x1,\mathrm{av}} & H_{x2,\mathrm{av}}\end{bmatrix}, \tag{5.10}$$

for the TE polarization, where the subscript 1 corresponds to the fields in (5.1) and (5.2), and the subscript 2 corresponds to their time-reversed counterpart. Solving this system for the eight susceptibility components yields

$$\chi_{\mathrm{ee}}^{xx} = -\frac{8T\sin\phi_{\mathrm{TM}}}{\omega\epsilon\left(T\alpha(\eta_{\mathrm{b}}\cos\phi_{\mathrm{TM}}+\eta_{\mathrm{a}}T)+2\cos\theta_{\mathrm{a}}(\eta_{\mathrm{b}}+\eta_{\mathrm{a}}T\cos\phi_{\mathrm{TM}})\right)}, \tag{5.11a}$$

$$\chi_{\mathrm{em}}^{xy} = -\chi_{\mathrm{me}}^{yx} = \frac{-2i\left(T\alpha(\eta_{\mathrm{b}}\cos\phi_{\mathrm{TM}}-\eta_{\mathrm{a}}T)+2\cos\theta_{\mathrm{a}}(\eta_{\mathrm{b}}-\eta_{\mathrm{a}}T\cos\phi_{\mathrm{TM}})\right)}{k\left(T\alpha(\eta_{\mathrm{b}}\cos\phi_{\mathrm{TM}}+\eta_{\mathrm{a}}T)+2\cos\theta_{\mathrm{a}}(\eta_{\mathrm{b}}+\eta_{\mathrm{a}}T\cos\phi_{\mathrm{TM}})\right)}, \tag{5.11b}$$

$$\chi_{\mathrm{mm}}^{yy} = -\frac{8\eta_{\mathrm{a}}\eta_{\mathrm{b}}T\cos\theta_{\mathrm{a}}\sin\phi_{\mathrm{TM}}\cos\theta_{\mathrm{b}}}{u\omega\left(T\alpha(\eta_{\mathrm{b}}\cos\phi_{\mathrm{TM}}+\eta_{\mathrm{a}}T)+2\cos\theta_{\mathrm{a}}(\eta_{\mathrm{b}}+\eta_{\mathrm{a}}T\cos\phi_{\mathrm{TM}})\right)} \tag{5.11c}$$

for the TM polarization and

$$\chi_{\mathrm{ee}}^{yy} = \frac{8T\cos\theta_{\mathrm{a}}\sin\phi_{\mathrm{TE}}\cos\theta_{\mathrm{b}}}{\omega\epsilon\left(\eta_{\mathrm{a}}T(T+\cos\phi_{\mathrm{TE}})\alpha+2\eta_{\mathrm{b}}\cos\theta_{\mathrm{a}}(T\cos\phi_{\mathrm{TE}}+1)\right)}, \tag{5.12a}$$

$$\chi_{\mathrm{em}}^{yx} = -\chi_{\mathrm{me}}^{xy} = -\frac{2i\left(\eta_{\mathrm{a}}T(T-\cos\phi_{\mathrm{TE}})\alpha+2\eta_{\mathrm{b}}\cos\theta_{\mathrm{a}}(T\cos\phi_{\mathrm{TE}}-1)\right)}{k\left(\eta_{\mathrm{a}}T(T+\cos\phi_{\mathrm{TE}})\alpha+2\eta_{\mathrm{b}}\cos\theta_{\mathrm{a}}(T\cos\phi_{\mathrm{TE}}+1)\right)}, \tag{5.12b}$$

$$\chi_{\mathrm{mm}}^{xx} = \frac{8\eta_{\mathrm{a}}\eta_{\mathrm{b}}T\sin\phi_{\mathrm{TE}}}{u\omega\eta_{\mathrm{a}}T(T+\cos\phi_{\mathrm{TE}})\alpha+2\eta_{\mathrm{b}}\cos\theta_{\mathrm{a}}(T\cos\phi_{\mathrm{TE}}+1)} \tag{5.12c}$$

for the TE polarization, with $\alpha = \sqrt{\frac{2n_{\mathrm{a}}^2\cos(2\theta_{\mathrm{a}})}{n_{\mathrm{b}}^2}-\frac{2n_{\mathrm{a}}^2}{n_{\mathrm{b}}^2}+4}$. [128]. The direct responses – χ_{ee}^{xx}, χ_{ee}^{yy}, χ_{mm}^{xx} and χ_{mm}^{yy} – are purely real and the cross responses – χ_{em}^{xy}, χ_{em}^{yx}, χ_{me}^{xy} and χ_{me}^{yx} – are purely imaginary, which indicates that the metasurface is lossless and gainless [128]. Thus, this design satisfies all the chosen requirements: it provides Brewster ($R = 0$) transmission for arbitrary incidence and polarization while being lossless and gainless, nongyrotropic

and reciprocal. Hence, inserting a metasurface having the surface susceptibilities of (5.11) and (5.12) between two different media will achieve full transmission for the specified angle of incidence for the TM and TE polarizations, respectively. The realized Brewster transmission may be explained in terms of the metaparticles operating as Huygens' sources, with electric and magnetic dipole resonances that mutually couple so as to act as an impedance transformer. [152].

5.4 Metaparticle Design

We now need to determine the shape of a metaparticle that realizes the susceptibilities in (11) and (12). This shape can be devised upon the basis of a simple pair of conducting wires, typically folded in a dog-bone shape for higher homogeneity, as shown in Fig. 5.2. The notation p_{me}^{yx} represents the y component of the magnetic dipole response due to the x component of the electric field excitation, and so on. The direct responses, χ_{ee}^{xx} and χ_{mm}^{yy}, can be realized with identical wires, as shown in Fig. 5.2 (a). However, such a symmetric structure does not support cross responses. Such responses, specifically the required components χ_{me}^{yx} and χ_{em}^{xy}, can be obtained by breaking the symmetry of the wire-pair, as shown in Fig. 5.2 (b). The exact values of these parameters can be obtained by tuning the level of asymmetry of the structure. Repeating this reasoning for the perpendicular polarization leads to a double dog-bone structure having the form of a cross potent, also often called Jerusalem cross in the literature on metamaterials, which provides independent tuning [126] of the four other susceptibility components – χ_{ee}^{yy}, χ_{mm}^{yy}, χ_{me}^{xy} and χ_{em}^{yx}.
The metaparticle obtained in this fashion will naturally induce some transmission phase, depending on the amounts of asymmetry, and coupling between the two layers. In the present application (Brewster transmission), this phase is not critical, and the design is therefore fully satisfactory as such. If one would wish, for some reason, to add control over the phase, an extra degree of freedom would need to be introduced in the structure. This can be typically accomplished by inserting a third conducting layer – a three-layer structure has been shown to provide full phase coverage with matching [128, 149, 222] – which can be designed from scattering parametric mapping [25, 128, 222] or using a transmission-line admittance model [149, 158].

5.5 Results

As proofs of concept, we designed a series of two-layered metasurfaces composed of cross-potent resonators, as shown in Fig. 5.1(c). The metasurfaces were designed and simulated using CST Studio 2019 with periodic boundary conditions with the general param-

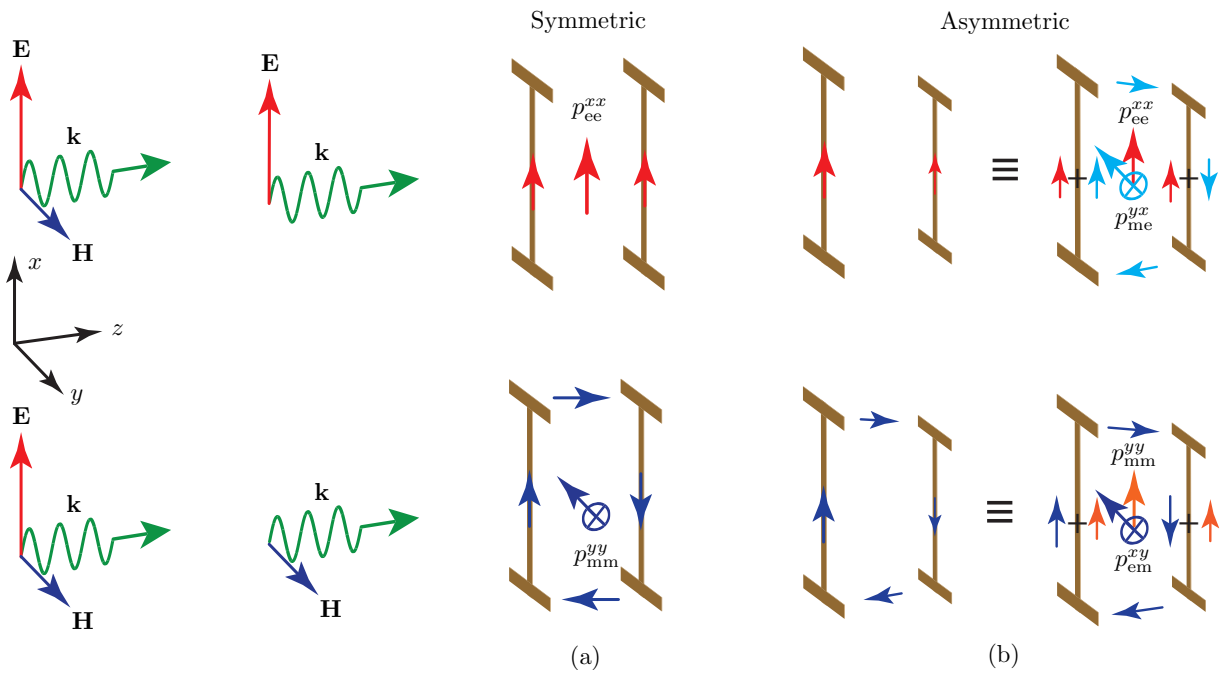

Figure 5.2 Folded wire-pair metaparticle (half of the complete cross-potent metaparticle) (a) Symmetric structure, supporting only the susceptibility components, χ_{ee}^{xx} and χ_{mm}^{yy} (b) Asymmetric structure providing the four susceptibility components required in (5.11)

eters $(\epsilon_{\mathrm{r,a}}, \epsilon_{\mathrm{r,b}}) = (1, 3)$ (bare-interface Brewster angle for the TM polarization at 60°), $\epsilon_{\mathrm{r,subs}} = 3$, $d = 1.52$ mm, $s = 0.5$ mm and $g = 0.5$ mm. Fig. 5.3 presents the results for the metasurface design with the susceptibilities (5.11) and (5.12), which correspond to polarization-independent (TE and TM) Brewster transmission in the xz-plane. Fig. 5.3 (a) presents a Brewster angle at $\theta_{\mathrm{a}} = 0$ (normal incidence) with $w_{y\mathrm{u}} = w_{x\mathrm{u}} = 3.9$ mm and $w_{y\mathrm{l}} = w_{x\mathrm{l}} = 2.75$ mm, Fig. 5.3 (b) present a Brewster angle at $\theta_{\mathrm{a}} = 30°$ with $w_{y\mathrm{u}} = 3.2$ mm, $w_{x\mathrm{u}} = 3.3$ mm, $w_{y\mathrm{l}} = 2.2$ mm and $w_{x\mathrm{l}} = 2.2$ mm and Fig. 5.3 (c) presents a Brewster angle at $\theta_{\mathrm{a}} = 75°$ with $w_{y\mathrm{u}} = 3.35$ mm, $w_{x\mathrm{u}} = 3.9$ mm, $w_{y\mathrm{l}} = 2.65$ mm and $w_{x\mathrm{l}} = 2.45$ mm. These results show that the specifications are perfectly realized by the designed metasurfaces for the chosen Brewster angles (θ_{a} of 0°, 30° and 75°) in the X-band frequency range and also show the angular response of the metasurface system at the operating frequency of the metasurface.

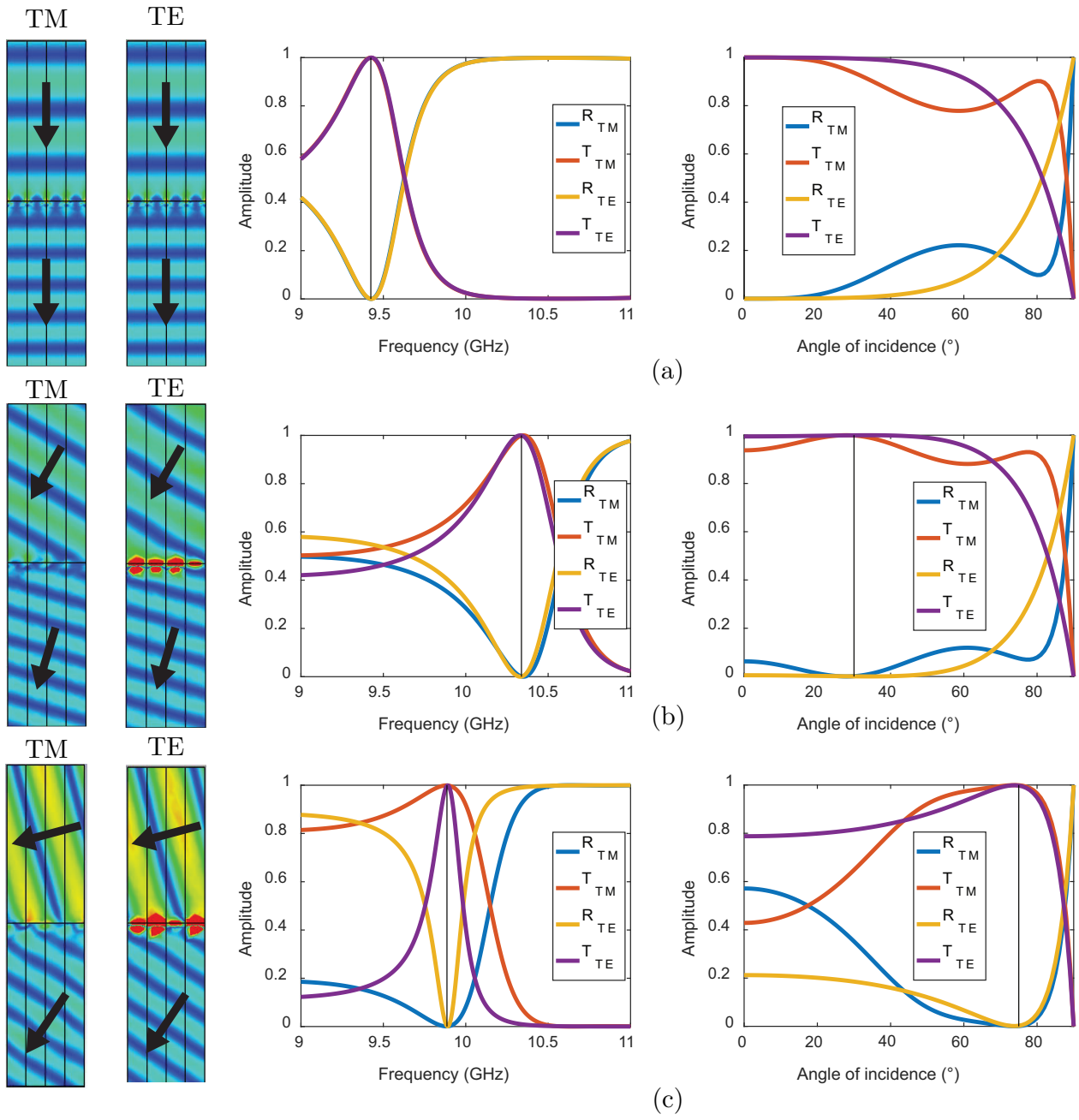

Figure 5.3 Full-wave simulated electric field amplitude distribution, frequency response and angular response of the reflectance and transmittance for polarization-independent xz-plane ($\varphi = 0$) Brewster metasurfaces (a) Brewster angle at $\theta_a = 0$ (normal incidence) (b) Brewster angle at $\theta_a = 30°$ (c) Brewster angle at $\theta_a = 75°$

The design of Fig. 5.3, with coinciding TM and TE Brewster angles, provides full reflection suppression for unpolarized light. However, this response is restricted to scattering in the xz ($\phi = 0$) plane. Indeed, according to Equations (5.11) and (5.12), we have $\chi_{\rm ee}^{yy} \neq \chi_{\rm ee}^{xx}$, $\chi_{\rm mm}^{xx} \neq \chi_{\rm mm}^{yy}$, $\chi_{\rm em}^{xy} \neq \chi_{\rm em}^{yx}$ and $\chi_{\rm me}^{xy} \neq \chi_{\rm me}^{yx}$, and therefore the metasurface structure is anisotropic since the rotation $(x, y) \to (y, -x)$ implies different susceptibilities and different susceptibility cannot lead to the same scattering response.

This single scattering plane restriction can be lifted with the same set of (eight) susceptibility parameters for one of the two polarizations (TM or TE) by combining the selected (TM or TE) xz-plane equations in (5.11) and (5.12) with the corresponding yz-plane equations obtained via the permutations $(x, y) \to (y, -x)$, which is in fact equivalent to making the structure isotropic ($\chi_{\rm ee}^{yy} = \chi_{\rm ee}^{xx}$, $\chi_{\rm mm}^{xx} = \chi_{\rm mm}^{yy}$, $\chi_{\rm em}^{xy} = \chi_{\rm em}^{yx}$ and $\chi_{\rm me}^{xy} = \chi_{\rm me}^{yx}$) since the same Brewster response is expected in the two planes for the selected polarization. The results for corresponding metasurfaces are presented in Fig. 5.4. Fig. 5.4 (a) presents a TM-Brewster angle at $\theta_{\rm a} = 30°$, Fig. 5.4 (b) presents a TE-Brewster angle at $\theta_{\rm a} = 30°$ Fig. 5.4 (c) presents a TM-Brewster angle at $\theta_{\rm a} = 75°$ and Fig. 5.4 (d) presents a TE-Brewster angle at $\theta_{\rm a} = 75°$ with $w_{y\rm u} = w_{x\rm u} = 3.55$ mm and $w_{y\rm l} = w_{x\rm l} = 2.85$ mm. They further confirm the accuracy of the proposed design.

5.6 Discussion

Although the eight-parameter metasurfaces considered here are restricted to either single-plane or single-polarization Brewster transmission, bianisotropic metasurfaces involving a greater number of susceptibility parameters might be able to provide universal Brewster transmission. Since the possibilities of transverse (x and y) susceptibilities have been exhausted, such metasurfaces would require resorting to normal z susceptibilities. Although the related design is in principle still analytically tractable thanks to the uniformity of the metasurface [128], it is considerably more involved and will therefore be deferred to a later study.

Equations (5.11) and (5.12) do not only provide the sought after Brewster transmission design. They point to an extra fundamental capability of an interfacing bianisotropic metasuface that occurs when $\phi_{\rm TM} = \phi_{\rm TE} = 0$, which can be achieved by phase compensation or adjustment. In this case, we have $\chi_{\rm ee}^{xx} = \chi_{\rm mm}^{yy} = \chi_{\rm ee}^{yy} = \chi_{\rm mm}^{xx} = 0$, which leads to the heteroanisotropic generalized sheet transition conditions

$$\hat{z} \times \Delta\mathbf{H} = jk\overline{\overline{\chi}}_{\rm em}\mathbf{H}_{\rm av}, \tag{5.13a}$$

$$\Delta\mathbf{E} \times \hat{z} = jk\overline{\overline{\chi}}_{\rm me}\mathbf{E}_{\rm av}, \tag{5.13b}$$

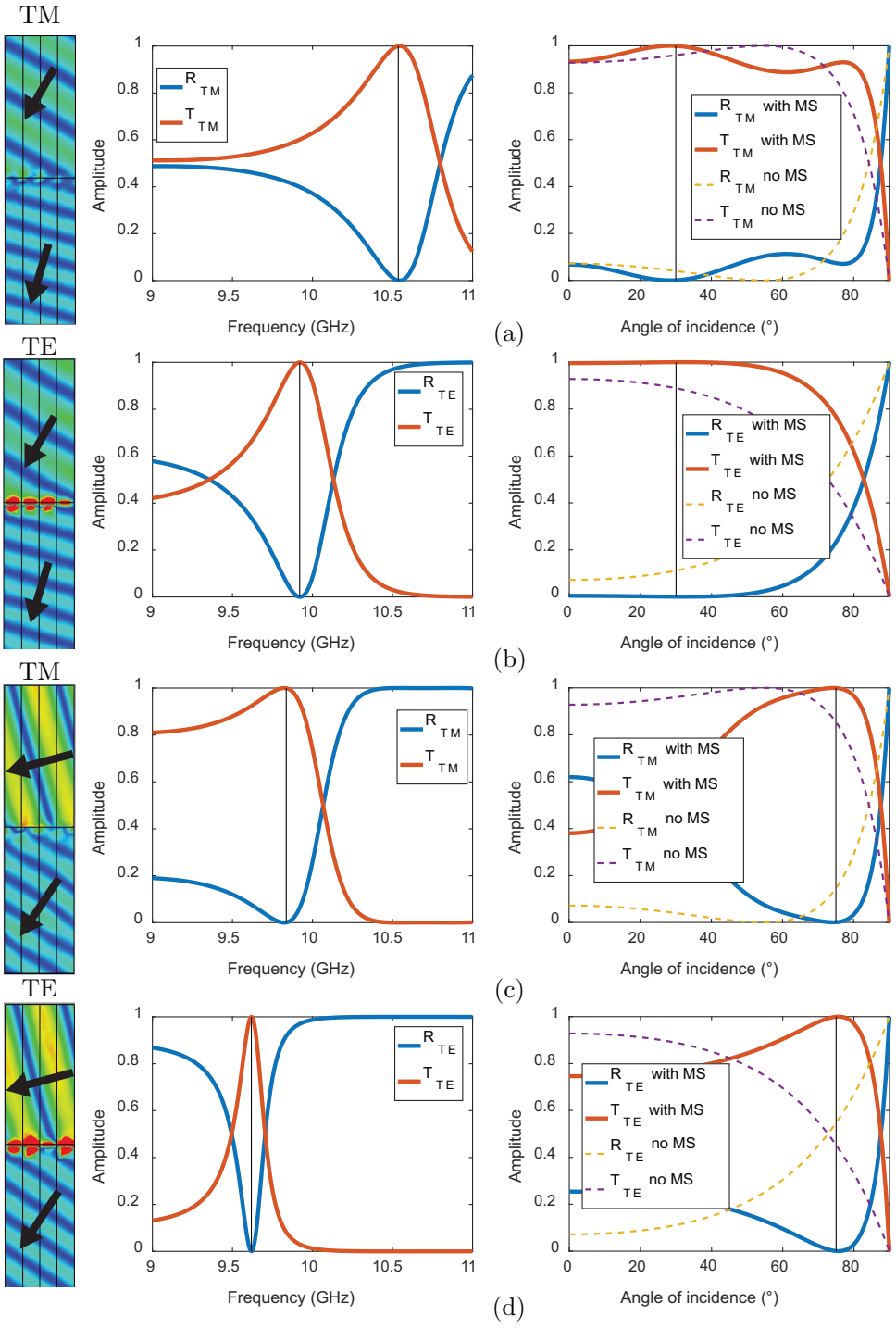

Figure 5.4 Full-wave simulated electric field amplitude distribution, frequency response and angular response of the reflectance and transmittance for azimuth-independent ($\forall\varphi$) single-polarization (TM or TE) Brewster metasurfaces (a) TM-Brewster angle at $\theta_a = 30°$ (b) TE-Brewster angle at $\theta_a = 30°$ (c) TM-Brewster angle at $\theta_a = 75°$ (d) TE-Brewster angle at $\theta_a = 75°$

with $\overline{\overline{\chi}}_{\mathrm{em}} = -\overline{\overline{\chi}}_{\mathrm{em}}^{\mathrm{T}}$ for reciprocity [14]. The corresponding reflection coefficients can easily be computed from general field expressions [128]. They read

$$r_{\mathrm{TM}} = \frac{\eta_1 \cos\theta_1 - \eta_{2,\mathrm{TM,eff}} \cos\theta_2}{\eta_1 \cos\theta_1 + \eta_{2,\mathrm{TM,eff}} \cos\theta_2}, \tag{5.14a}$$

$$r_{\mathrm{TE}} = \frac{\eta_{2,\mathrm{TE,eff}} \cos\theta_1 - \eta_1 \cos\theta_2}{\eta_{2,\mathrm{TE,eff}} \cos\theta_1 + \eta_1 \cos\theta_2}, \tag{5.14b}$$

where

$$\eta_{2,\mathrm{TM,eff}} = \eta_2 \frac{(2i - k\chi_{\mathrm{em}}^{xy})^2}{(2i + k\chi_{\mathrm{em}}^{xy})^2}, \tag{5.15a}$$

$$\eta_{2,\mathrm{TE,eff}} = \eta_2 \frac{(2i - k\chi_{\mathrm{em}}^{yx})^2}{(2i + k\chi_{\mathrm{em}}^{yx})^2}. \tag{5.15b}$$

The relations (5.14) have the same mathematical form as the conventional Fresnel reflection coefficients [169]. This reveals that the proposed [medium – bianisotropic metasurface – medium] system is equivalent to a [medium – *effective medium*] system, with the effective medium having the impedances given by Equations (5.15). Thus, inserting such a bianisotropic metasurface at the interface between two media or coating a dielectric medium exposed to free space with it can change the effective bulk impedance of the transmission medium, which enriches the design possibilities of existing materials.

Although the proof of concept systems in Figures 5.3 and 5.4 pertain to the microwave regime, where bianisotropic metasurfaces (surrounded by air) have been well documented, bianisotropic metasurfaces have also been recently demonstrated in all-dielectric configuration [225, 226]. Therefore, the proposed concepts of metasurface-based generalized Brewster effective refractive medium can be readily extended to the optical regime, where they may be particularly beneficial in terms of reducing the insertion loss associated to impedance mismatch in many common components.

5.7 Conclusion

In summary, we have shown that a properly designed bianisotropic metasurface placed at the interface between two dielectric media or coating a dielectric medium exposed to the air provides Brewster transmission at arbitrary angles and for both the TM and TE polarizations. We have presented a rigorous derivation of the corresponding surface susceptibility tensors and demonstrated the system by microwave proof-of-concept designs. Moreover, we have noted that such a system leads to the concept of effective refractive media with tailorable impedances. The proposed bianisotropic metasurfaces offer deeply subwavelength matching solutions for initially mismatched media, and alternatively lead to the possibility

of on-demand manipulation of the conventional Fresnel coefficients. They represent thus a fundamental advance in optical science and posses a considerable potential for novel technological developments.

CHAPTER 6 ARTICLE 3: MAGNETLESS REFLECTIVE GYROTROPIC SPATIAL ISOLATOR METASURFACE

Authors: Guillaume Lavigne and Christophe Caloz

This work was published in the New Journal of Physics, Volume 23, Issue 7, 075006, on July 21 2021.

Abstract

We present the concept of a magnetless Reflective Gyrotropic Spatial Isolator (RGSI) metasurface. This is a birefringent metasurface that reflects vertically polarized incident waves into a horizontally polarized waves, and absorbs horizontally polarized incident waves, hence providing isolation between the two orthogonal polarization. We first synthesize the metasurface using surface susceptibility-based Generalized Sheet Transition Conditions (GSTCs). We then propose a mirror-backed metaparticle implementation of this metasurface, where transistor-loaded resonators provide the desired magnetless nonreciprocal response. Finally, we demonstrate the metasurface by full-wave simulation results. The proposed RGSI metasurface may be used in various electromagnetic applications, and may also serve as a step towards more sophisticated magnetless nonreciprocal metasurface systems.

6.1 Introduction

Nonreciprocity is a fundamental concept in science and technology [14, 180]. It allows special operations, such as isolation, circulation, nonreciprocal phase shifting and nonreciprocal gyrotropy, that are crucial in a great variety of applications. In electromagnetics, nonreciprocity is conventionally obtained through the use magnetized materials, such as ferrites [15] or terbium garnet crystals [181]. However, magnetized materials have severe drawbacks, such as incompatibility with integrated circuit technologies and bulkiness due to the required biasing magnets. Recently, the concept of magnetless nonreciprocity has arisen as a potential solution to these issues [16], with the transistor-loaded structures [151, 194–203] and spacetime-modulated systems [186–191, 193] being the main practical[1] approaches.

Advances in magnetless nonreciprocity have recently been extended to metasurfaces, where magnetized material technologies would be inapplicable. Metasurfaces have experience spectacular developments over the past decade [21,25]. They have been shown to provide unprece-

[1]Magnetless nonreciprocity can also be obtained by nonlinearity combined by structural asymmetry [16, 185, 227]. However, the related systems are generally unpractical for engineering devices, due major issues such as single excitation at a time, poor transmission and isolation performance, and intensity dependence.

dented control over the fundamental properties of electromagnetic waves, such of polarization, reflection, refraction, spin and orbital angular momentum. However, most of the studies on metasurfaces reported so far have focused on reciprocal structures. Introducing nonreciprocity in metasurfaces has the potential to extend conventional nonreciprocal operations such as isolation and circulation, usually applied to guided waves, to spatial wave manipulations, and to lead to novel metasurface-based wave transformations. As in other platforms, the transistor-loaded route for nonreciprocity, compared spacetime-varying systems, has the advantage in metasurfaces to produce no spurious harmonic and intermodulation frequencies while using the simplest form of biasing, namely a simple DC battery. Transistor-loaded nonreciprocal metasurfaces have been demonstrated realizing nonreciprocal polarization rotators in reflection [197] and in transmission [198], transmissive isolation using an antenna-circuit-antenna approach [151], bianisotropic nonreciprocity [201] and meta-grating reflective circulators [203].

The most fundamental and primary application of nonreciprocity in metasurfaces is probably spatial isolation. Here, we introduce the concept of a reflective isolator metasurface, with a pair of orthogonally-polarized ports coupled by reflective gyrotropy, and demonstrate a corresponding magnetless Reflective Gyrotropic Spatial Isolator (RGSI).

6.2 Operation Principle

Figure 6.1 depicts the operation principle of the proposed RGSI metasurface. The metasurface includes reciprocity-breaking elements, and is designed in such a manner that, using birefringence, it specularly[2] reflects vertically-polarized incident waves into horizontally-polarized waves, as shown in Fig. 6.1(a), and absorbs horizontally-polarized incident waves, as shown in Fig. 6.1(b).

The resulting RGSI device is de facto a two-port reflective spatial isolator, with ports that we denote here P1 and P2, as indicated in the figure. Its electromagnetic response may therefore be described by the following scattering matrix:

$$\mathbf{S}_{\text{spec}}^{\text{RGSI}} = \begin{bmatrix} S_{11}^{\text{RGSI}} & S_{12}^{\text{RGSI}} \\ S_{21}^{\text{RGSI}} & S_{22}^{\text{RGSI}} \end{bmatrix} = \begin{bmatrix} 0 & 0 \\ Ae^{i\phi} & 0 \end{bmatrix}, \tag{6.1}$$

where A and ϕ are the amplitude and the phase, respectively, imparted by the metasurface

[2]"Specular," from the Greek word "speculum" that means "mirror," refers to reflection that occurs under the same angle as the incidence angle, according to Snell law of reflection. We restrict here our attention to specular reflection, as implicitly assumed from the equal incidence and reflection angles (θ) in Fig. 6.1(a). However, the concept of reflective gyrotropic spatial isolator could naturally be extended to non-specular reflection, with reflection angle differing from the incidence angle, by using metasurface gradient and bianisotropy [222].

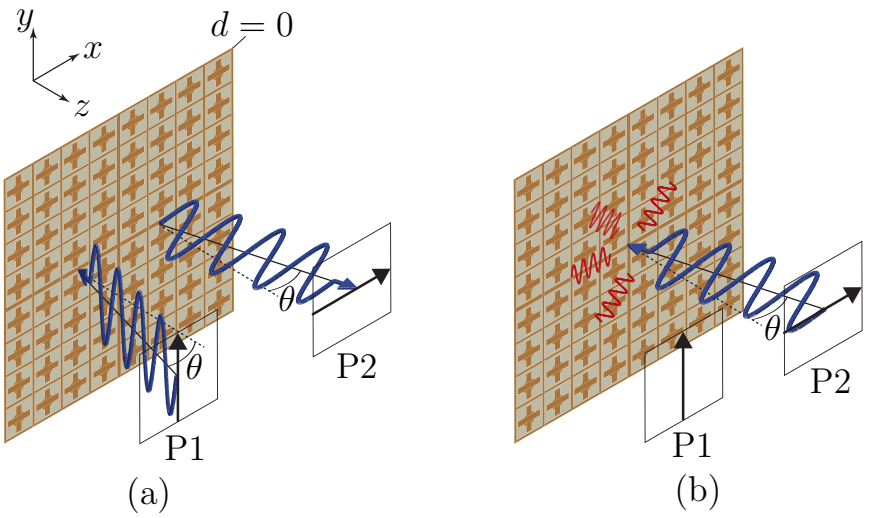

Figure 6.1 Operation principle of the proposed Reflective Gyrotropic Spatial Isolator (RGSI) metasurface (a) A y-polarized incident wave, from port P1, is reflected with x-polarization, to port P2 (b) An x-polarized incident wave, from port P2, is absorbed by the metasurface

to the rotated reflected-transmitted field. For the polarizations assumed in Fig. 6.1, the metasurface may be alternatively described by the reflection matrix

$$\mathbf{R}_{\text{spec}}^{\text{RGSI}} = \begin{bmatrix} R_{xx}^{\text{RGSI}} & R_{xy}^{\text{RGSI}} \\ R_{yx}^{\text{RGSI}} & R_{yy}^{\text{RGSI}} \end{bmatrix} = \begin{bmatrix} 0 & Ae^{i\phi} \\ 0 & 0 \end{bmatrix}, \tag{6.2}$$

so that $\mathbf{R}_{\text{spec}}^{\text{RGSI}} = (\mathbf{S}_{\text{spec}}^{\text{RGSI}})^{\text{T}}$.

6.3 Metasurface Design

6.3.1 GSTC Equations

Metasurfaces may be modeled as zero-thickness discontinuities of space via Generalized Sheet Transition Conditions (GSTCs) and bianisotropic surface susceptibility tensors [25, 124, 128]. The GSTCs, assuming the harmonic time convention $e^{+i\omega t}$, read

$$\hat{z} \times \Delta\mathbf{H} = i\omega\mathbf{P} - \hat{z} \times \nabla M_z, \tag{6.3a}$$

$$\hat{z} \times \Delta\mathbf{E} = -i\omega\mathbf{M} - \frac{1}{\epsilon}\hat{z} \times \nabla P_z, \tag{6.3b}$$

where $\Delta\mathbf{H}$ and $\Delta\mathbf{E}$ are the differences of the magnetic or electric fields at both sides of the metasurface, and where $\mathbf{P}$ and $\mathbf{M}$ are the induced electric and magnetic surface polarization densities on the metasurface. The latter may be expressed in terms of surface susceptibility

tensors as

$$\mathbf{P} = \epsilon\overline{\overline{\chi}}_{\mathrm{ee}}\mathbf{E}_{\mathrm{av}} + k\overline{\overline{\chi}}_{\mathrm{em}}\mathbf{H}_{\mathrm{av}}, \tag{6.4a}$$

$$\mathbf{M} = k\overline{\overline{\chi}}_{\mathrm{me}}\mathbf{E}_{\mathrm{av}} + \mu\overline{\overline{\chi}}_{\mathrm{mm}}\mathbf{H}_{\mathrm{av}}, \tag{6.4b}$$

where $\mathbf{E}_{\mathrm{av}}$ and $\mathbf{H}_{\mathrm{av}}$ are the averages of the electric or magnetic fields at both sides of the metasurface, and $\overline{\overline{\chi}}_{\mathrm{ee}}$, $\overline{\overline{\chi}}_{\mathrm{mm}}$, $\overline{\overline{\chi}}_{\mathrm{em}}$, $\overline{\overline{\chi}}_{\mathrm{me}}$ are the 3×3 bianisotropic susceptibility tensors characterizing the metasurface. In this paper, we shall assume a purely tangential metasurface, i.e., a metasurface with $M_z = P_z = 0$, for which the bianisotropic GSTCs simplify to

$$\hat{z} \times \Delta\mathbf{H} = i\omega\epsilon\overline{\overline{\chi}}_{\mathrm{ee}}\mathbf{E}_{\mathrm{av}} + ik\overline{\overline{\chi}}_{\mathrm{em}}\mathbf{H}_{\mathrm{av}}, \tag{6.5a}$$

$$\Delta\mathbf{E} \times \hat{z} = ik\overline{\overline{\chi}}_{\mathrm{me}}\mathbf{E}_{\mathrm{av}} + i\omega\mu\overline{\overline{\chi}}_{\mathrm{mm}}\mathbf{H}_{\mathrm{av}}, \tag{6.5b}$$

where $\overline{\overline{\chi}}_{\mathrm{ee}}$, $\overline{\overline{\chi}}_{\mathrm{mm}}$, $\overline{\overline{\chi}}_{\mathrm{em}}$, $\overline{\overline{\chi}}_{\mathrm{me}}$ are now 2×2 tensors [228]. In these relations, the differences and averages of the fields are explicitly given by

$$\Delta\mathbf{\Phi} = \mathbf{\Phi}_{\mathrm{t}} - (\mathbf{\Phi}_{\mathrm{i}} + \mathbf{\Phi}_{\mathrm{r}}), \tag{6.6a}$$

$$\mathbf{\Phi}_{\mathrm{av}} = (\mathbf{\Phi}_{\mathrm{t}} + \mathbf{\Phi}_{\mathrm{i}} + \mathbf{\Phi}_{\mathrm{r}})/2, \tag{6.6b}$$

where $\mathbf{\Phi} = \mathbf{E}, \mathbf{H}$, where the subscript t, i and r denote the transmitted, incident and reflected fields, respectively.

6.3.2 Susceptibility Synthesis

The metasurface can be designed using the susceptibility synthesis procedure described in [128]: 1) specify the desired field transformations, 2) compute the corresponding field differences and averages, 3) insert the expressions for these differences and averages into the susceptibility-GSTC equations, and 4) solve the resulting equations for the surface susceptibility tensors.

The GSTCs assumed here, given by (6.5), form a linear system of 4 scalar equations in the 16 susceptibility components containing the 4 susceptibility tensors $\overline{\overline{\chi}}_{\mathrm{ee}}$, $\overline{\overline{\chi}}_{\mathrm{mm}}$, $\overline{\overline{\chi}}_{\mathrm{em}}$, and $\overline{\overline{\chi}}_{\mathrm{me}}$ of dimensions 2×2. The isolator operation in Fig. 6.1 involves 2 non-trivial[3] transformations, specular gyrotropic reflection-transmission from P1 to P2, and absorption by the metasurface from P2, which implies $2 \times 4 = 8$ scalar equations in the 16 susceptibility parameters. This represents an undetermined system, requiring extra specifications for full-rank solvability. Such specifications largely depend from the specific nature of the required transformations.

[3]By "non-trivial" transformations, we mean here transformations that would not be performed by the simplest metasurfaces, i.e., passive, reciprocal and nongyrotropic metasurfaces.

The transformations in Fig. 6.1 obviously involve *gyrotropy* and *nonreciprocity*. Nonreciprocity implies $\overline{\overline{\chi}}_{\rm ee} \neq \overline{\overline{\chi}}_{\rm ee}^{T}$ or $\overline{\overline{\chi}}_{\rm mm} \neq \overline{\overline{\chi}}_{\rm mm}^{T}$ or $\overline{\overline{\chi}}_{\rm em} \neq -\overline{\overline{\chi}}_{\rm me}^{T}$ [128], where the superscript "T" denotes the transpose operation, while gyrotropy implies either off-diagonal components of $\overline{\overline{\chi}}_{\rm ee}$ and $\overline{\overline{\chi}}_{\rm mm}$ or diagonal components of $\overline{\overline{\chi}}_{\rm em}$ and $\overline{\overline{\chi}}_{\rm me}$ [128]. This leaves us with several possibilities to eliminate 8 of the 16 susceptibility parameters for fully-specified resolution. We choose here, and subsequently implement, a *homoanisotropic design*, characterized by the parameters $\overline{\overline{\chi}}_{\rm ee}$ and $\overline{\overline{\chi}}_{\rm mm}$ with $\overline{\overline{\chi}}_{\rm em} = \overline{\overline{\chi}}_{\rm me} = 0$, and discuss in Sec. 6.7.7 an alternative *bianisotropic design*[4]. We are then left with the 8 parameters, with the gyrotropy condition $\chi_{\rm ee}^{yx}, \chi_{\rm ee}^{xy} \neq 0$ or/and $\chi_{\rm mm}^{yx}, \chi_{\rm mm}^{xy} \neq 0$ and the nonreciprocal condition $\chi_{\rm ee}^{yx} \neq \chi_{\rm ee}^{xy}$ or/and $\chi_{\rm mm}^{yx} \neq \chi_{\rm mm}^{xy}$, which leads to a full-rank GSTC-susceptibility system.

Considering s-polarization (the p-polarization problem can be treated analogously) and assuming that the metasurface positioned in the plane $z = 0$, the 2 operations in Fig. 6.1 correspond to the following tangential field specifications:

$$\mathbf{E}_i = e^{-ik_0 \sin\theta x}\hat{y}, \quad \mathbf{H}_i = e^{-ik_0 \sin\theta x}\cos\theta/\eta\hat{x}, \tag{6.7a}$$

$$\mathbf{E}_r = Ae^{-ik_0 \sin\theta x}\cos\theta e^{i\phi}\hat{x}, \quad \mathbf{H}_r = Ae^{-ik_0 \sin\theta x}e^{i\phi}/\eta\hat{y}, \tag{6.7b}$$

$$\mathbf{E}_t = 0, \quad \mathbf{H}_t = 0, \tag{6.7c}$$

where θ is the angle of incidence and reflection, for the specular gyrotropic reflection-transmission from P1 to P2, and

$$\mathbf{E}_i = \cos(-\theta)e^{-ik_0 \sin(-\theta)x}\hat{x}, \quad \mathbf{H}_i = -e^{-ik_0 \sin(-\theta)x}/\eta\hat{y}, \tag{6.8a}$$

$$\mathbf{E}_r = 0, \quad \mathbf{H}_r = 0, \tag{6.8b}$$

$$\mathbf{E}_t = 0, \quad \mathbf{H}_t = 0. \tag{6.8c}$$

and for the absorption by the metasurface from P2.

[4]We follow here the convenient Greek prefix terminology used in [128], where *homo-* involves only the parameters ee and mm, *hetero-* involves only the parameters em and me, and *bi-*, introduced by Kong [229], involves both homo and hetero parameters.

Substituting the field specifications (6.7) and (6.8) into (6.6), inserting the resulting expressions into (6.5), and solving for the susceptibility tensors yields the sought-after susceptibility synthesis result

$$\overline{\overline{\chi}}_{\rm ee} = \begin{bmatrix} \chi_{\rm ee}^{xx} & \chi_{\rm ee}^{xy} \\ \chi_{\rm ee}^{yx} & \chi_{\rm ee}^{yy} \end{bmatrix} = \begin{bmatrix} \frac{-2i\sec\theta}{k} & \frac{4iAe^{i\phi}}{k} \\ 0 & \frac{-2i\cos\theta}{k} \end{bmatrix} \tag{6.9a}$$

$$\overline{\overline{\chi}}_{\rm mm} = \begin{bmatrix} \chi_{\rm mm}^{xx} & \chi_{\rm mm}^{xy} \\ \chi_{\rm mm}^{yx} & \chi_{\rm mm}^{yy} \end{bmatrix} = \begin{bmatrix} \frac{-2i\sec\theta}{k} & 0 \\ \frac{4iAe^{i\phi}}{k} & \frac{-2i\cos\theta}{k} \end{bmatrix}, \tag{6.9b}$$

where all the components are independent from the spatial variables x and y, as might have been expected from the fact that the specified reflection is specular and hence momentum conservative.

6.4 Metastructure Implementation

6.4.1 Metaparticle Configuration

The next step of the metasurface design is naturally to implement the synthesized susceptiblities (6.9) in a real metasurface structure, with fully defined metaparticle material and shape, and with specific nonreciprocal elements. For the latter, we shall use here *transistors*, for their advantages of spectral purity (single-frequency operation), symmetry-breaking low-cost source (DC battery) and biasing simplicity (DC circuit). Moreover, we shall consider a normal-incidence ($\theta = 0$) design, for simplicity, but the proposed procedure and structure are easily extensible to the case of oblique incidence.

We propose the 2-layer metaparticle implementation shown in Fig. 6.2 to realize the responses (6.9). The metaparticle structure is composed of two identical L-shaped metal resonators, each loaded by a unilateral[5] transistor chip at the corner of the L. The transistors are biased in the non-amplifying regime where they exhibit the ideal-isolator scattering response $\mathbf{S}_{\rm tran} = [0, 0; 1, 0]$, and they are oriented so that they pass currents flowing from the vertical section to the horizontal section and block currents flowing in the opposite direction.

Figure 6.2(a) depicts the response of the metaparticle to an x-polarized wave. The x-direct incident electric field induces an electric dipole moment along the x direction ($\chi_{\rm ee}^{xx}$), without inducing any response along the y direction due to transistor blocking ($\chi_{\rm ee}^{yx} = 0$), while the y-directed incident magnetic field induces a magnetic dipole moment along the y direction ($\chi_{\rm mm}^{yy}$) without response along the x direction ($\chi_{\rm mm}^{xy} = 0$). Figure 6.2(b) depicts the response of the metaparticle to a y-polarized wave. In this case, the y-directed incident electric field

[5]In the case of a Field-Effect Transistor (FET), such a unilateral operation implies a common-source configuration, as typically used in RF amplifiers [230], whereas the common-gate configuration, typically used in logic electronics, is bilateral.

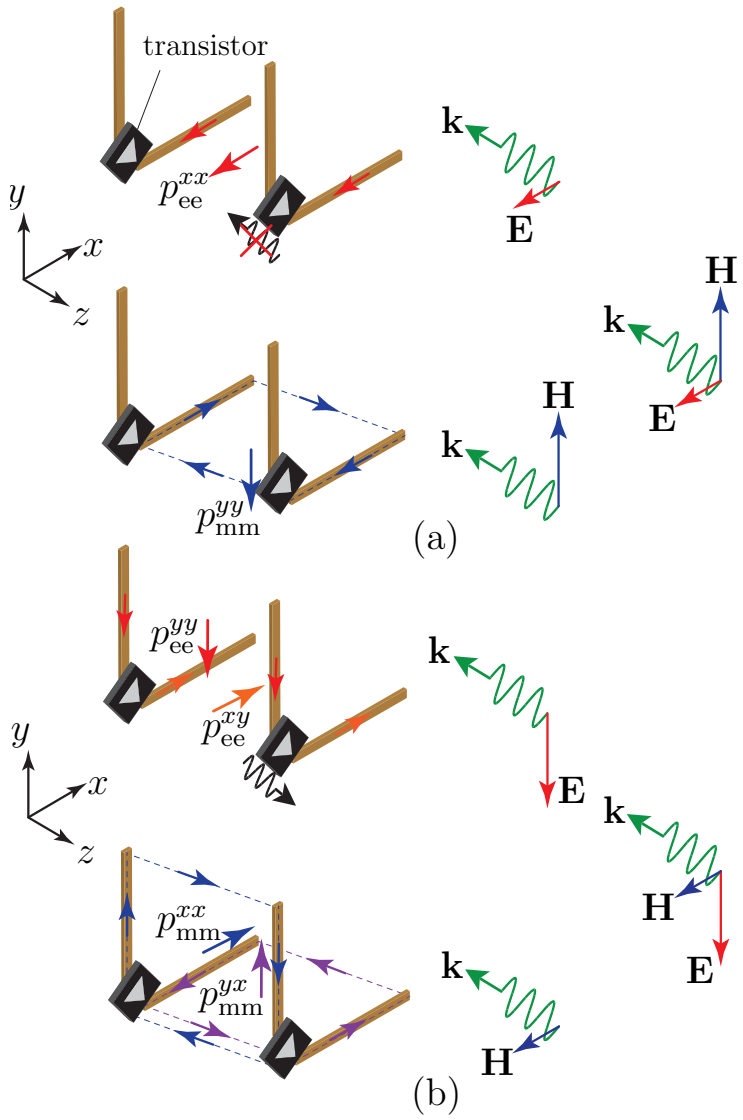

Figure 6.2 Proposed 2-layer transistor-loaded metaparticle to realize the susceptibilities in Eqs. (6.9) for the operation in Fig. 6.1 (a) x-polarization excitation (b) y-polarization excitation

induces electric dipole moments along both the y *and* x directions (χ^{yy}_{ee} and χ^{xy}_{ee}) via the current passing across the transistor and, similarly, the x-directed incident magnetic field induces magnetic dipole moments along both the x *and* y directions (χ^{xx}_{mm} and χ^{yx}_{mm}). Hence, this configuration precisely provides the required non-zero and zero susceptibility components in (6.9).

By symmetry, the metastructure in Fig. 6.2 is in fact equivalent, on the reflection side of the metasurface, to the simpler structure where the back resonator is suppressed and replaced by a mirror placed halfway between the two initial layers, as shown in Fig. 6.3. Indeed, the

latter structure, according to the image equivalence principle, exhibits the same scattering response as the former one. Given its greater simplicity, involving only one structured layer and only half the number of transistors, we shall adopt here this configuration.

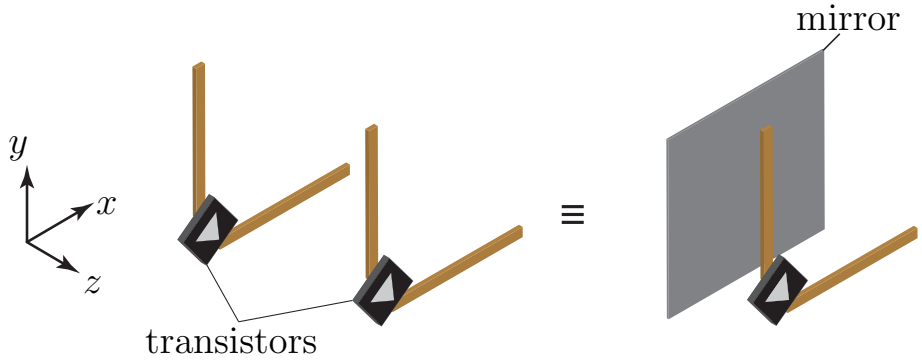

Figure 6.3 Equivalence in the $z > 0$ (reflection) half-plane, according to image theory, between the initial metaparticle in Fig. 6.2, with structure recalled at the left, and the simpler mirror-backed structure, shown at the right

6.4.2 Metaparticle Design

In the selected back-mirror metaparticle (right side in Fig. 6.3), the design task reduces to determining the layer at top of the mirror. This layer represents a metasurface per se, which is different from the overall effective metasurface that it forms with the mirror, and this layer will therefore be subsequently considered as an independent metasurface, on top of a mirror-backed substrate.

In order to account for the multiple scattering occurring between the top metasurface and the mirror, we shall use the transmission-line model [7] shown in Fig. 6.4. The metasurface and the mirror are modelled by the admittance matrices $\mathbf{Y}'$ and $\mathbf{Y}_\mathrm{c}$, respectively, and are separated by a substrate of wave impedance η_d and thickness d. The admittance matrix of the metasurface, whose parameters are to be determined, may be written as

$$\mathbf{Y}' = \begin{bmatrix} Y^{xx\prime} & Y^{yx\prime} \\ Y^{yx\prime} & Y^{yy\prime} \end{bmatrix}, \tag{6.10}$$

while the admittance of the mirror, which will be realized by a simple conducting copper plate, is given by

$$\mathbf{Y}_\mathrm{c} = i\sigma\mathbf{I}, \tag{6.11}$$

where σ is the conductivity of the mirror, with $\sigma = 5 \times 10^7\ 1/\Omega$.

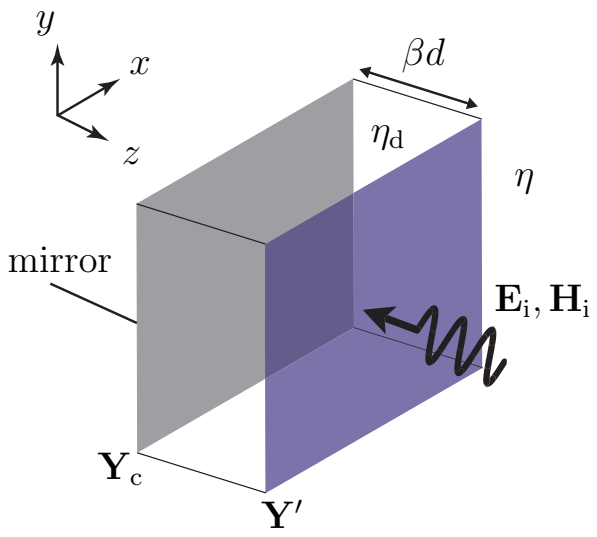

Figure 6.4 Admittance model for the mirror-backed structure in Fig. 6.3

The transmission or ABCD matrix of the overall structure in Fig. 6.4 is then easily found by as

$$\begin{bmatrix} \mathbf{A} & \mathbf{B} \\ \mathbf{C} & \mathbf{D} \end{bmatrix} = \begin{bmatrix} \mathbf{I} & 0 \\ \mathbf{n}\mathbf{Y}' & \mathbf{I} \end{bmatrix} \begin{bmatrix} \mathbf{I}\cos\beta d & -\mathbf{n}i\eta_d \sin\beta d \\ \mathbf{n}\frac{i\sin\beta d}{\eta_d} & \mathbf{I}\cos\beta d \end{bmatrix} \begin{bmatrix} \mathbf{I} & 0 \\ \mathbf{n}\mathbf{Y}_\mathrm{c} & \mathbf{I} \end{bmatrix}, \tag{6.12}$$

where

$$\mathbf{I} = \begin{bmatrix} 1 & 0 \\ 0 & 1 \end{bmatrix} \quad \text{and} \quad \mathbf{n} = \begin{bmatrix} 0 & -1 \\ 1 & 0 \end{bmatrix} \tag{6.13}$$

are the identity matrix and the 90°-rotation matrix, respectively. The transmission matrix (6.12) can then be converted into its scattering matrix counterpart as [230]

$$\mathbf{S} = \begin{bmatrix} \mathbf{S}_{11} & \mathbf{S}_{12} \\ \mathbf{S}_{21} & \mathbf{S}_{22} \end{bmatrix} = \begin{bmatrix} -\mathbf{I} & \frac{\mathbf{B}\mathbf{n}}{\eta} + \mathbf{A} \\ \frac{\mathbf{n}}{\eta} & \frac{\mathbf{D}\mathbf{n}}{\eta} + \mathbf{C} \end{bmatrix}^{-1} \begin{bmatrix} \mathbf{I} & \frac{\mathbf{B}\mathbf{n}}{\eta} - \mathbf{A} \\ \frac{\mathbf{n}}{\eta} & \frac{\mathbf{D}\mathbf{n}}{\eta} - \mathbf{C} \end{bmatrix}, \tag{6.14}$$

whose $\mathbf{Y}'$ (unknown) and other structural dependencies are naturally available from (6.12). For the mirror-backed metasurface structure to realize the operation in Fig. 6.1, its reflection block, $\mathbf{S}_{11}$ in (6.14), must equal the reflection matrix $\mathbf{R}_\mathrm{spec}^\mathrm{RGSI}$ in (6.2), and hence $(\mathbf{S}_\mathrm{spec}^\mathrm{RGSI})^\mathrm{T}$ in (6.2). Enforcing this equality and solving for $\mathbf{Y}'$ yields

$$Y^{xx\prime} = Y^{yy\prime} = \frac{\eta^2 \sin(\beta d) - \eta_\mathrm{d}^2 \sin(\beta d) + i\eta\eta_\mathrm{d}\sigma\cos(\beta d)}{\eta_\mathrm{d}^2\sigma \sin(\beta d) - \eta_\mathrm{d}^2 \sin(\beta d) + i\eta\eta_\mathrm{d}\cos(\beta d)}, \tag{6.15a}$$

$$Y^{xy\prime} = 2Ae^{i\phi}, \tag{6.15b}$$

$$Y^{yx\prime} = 0. \tag{6.15c}$$

To translate this admittance matrix into metasurface susceptibilities, we write the ABCD matrix corresponding to $\mathbf{Y}'$ as

$$\begin{bmatrix} \mathbf{A}' & \mathbf{B}' \\ \mathbf{C}' & \mathbf{D}' \end{bmatrix} = \begin{bmatrix} \mathbf{I} & 0 \\ \mathbf{nY}' & \mathbf{I} \end{bmatrix}. \tag{6.16}$$

convert this matrix to its scattering counterpart by reusing the formula (6.14), and map this matrix, which we shall call $\mathbf{S}' = [\mathbf{S}'_{11}, \mathbf{S}'_{12}; \mathbf{S}'_{21}, \mathbf{S}'_{22}]$, to the surface susceptibility matrix according to the procedure that is described in [25, 128], and that leads to the following equation:

$$\overline{\overline{\Delta}} = \overline{\overline{\tilde{\chi}}}' \cdot \overline{\overline{A}}_{\mathrm{v}}, \tag{6.17a}$$

where

$$\overline{\overline{\Delta}} = \begin{bmatrix} -\mathbf{m}/\eta + \mathbf{mS}'_{11}/\eta + \mathbf{mS}'_{21}/\eta & -\mathbf{m}/\eta + \mathbf{mS}'_{12}/\eta + \mathbf{mS}'_{22}/\eta \\ -\mathbf{nm} - \mathbf{nmS}'_{11} + \mathbf{nmS}'_{21} & \mathbf{nm} - \mathbf{nmS}'_{12} + \mathbf{nmS}'_{22} \end{bmatrix}, \tag{6.17b}$$

$$\overline{\overline{A}}_{\mathrm{v}} = \frac{1}{2} \begin{bmatrix} \mathbf{I} + \mathbf{S}'_{11} + \mathbf{S}'_{21} & \mathbf{I} + \mathbf{S}'_{12} + \mathbf{S}'_{22} \\ \mathbf{n}/\eta - \mathbf{nS}_{11}/\eta + \mathbf{nS}'_{21}/\eta & -\mathbf{n}/\eta - \mathbf{nS}'_{12}/\eta + \mathbf{nS}'_{22}/\eta \end{bmatrix} \tag{6.17c}$$

and

$$\overline{\overline{\tilde{\chi}}}' = \begin{bmatrix} -i\omega\epsilon\chi_{\mathrm{ee}}^{xx\prime} & -i\omega\epsilon\chi_{\mathrm{ee}}^{xy\prime} & -ik\chi_{\mathrm{em}}^{xx\prime} & -ik\chi_{\mathrm{eme}}^{xy\prime} \\ i\omega\epsilon\chi_{\mathrm{ee}}^{yx\prime} & i\omega\epsilon\chi_{\mathrm{ee}}^{yy\prime} & ik\chi_{\mathrm{em}}^{yx\prime} & ik\chi_{\mathrm{em}}^{yy\prime} \\ ik\chi_{\mathrm{me}}^{xx\prime} & ik\chi_{\mathrm{me}}^{xy\prime} & i\omega\mu\chi_{\mathrm{mm}}^{xx\prime} & i\omega\mu\chi_{\mathrm{mm}}^{xy\prime} \\ -ik\chi_{\mathrm{me}}^{yx\prime} & -ik\chi_{\mathrm{me}}^{yy\prime} & -i\omega\mu\chi_{\mathrm{mm}}^{yx\prime} & -i\omega\mu\chi_{\mathrm{mm}}^{yy\prime} \end{bmatrix}, \tag{6.17d}$$

with

$$\mathbf{m} = \begin{bmatrix} 1 & 0 \\ 0 & -1 \end{bmatrix}. \tag{6.17e}$$

Substituting $\mathbf{S}'$ into (6.17b) and (6.17c), inserting the resulting expressions into (6.17a), and inverting the resulting system yields the explicit susceptibility solutions, corresponding to (6.17d):

$$\chi_{\mathrm{ee}}^{xx\prime} = \chi_{\mathrm{ee}}^{yy\prime} = \frac{i}{\omega\epsilon} \frac{\eta\alpha i\zeta - \eta_{\mathrm{d}}\gamma(\sigma - 1)\zeta}{\eta_{\mathrm{d}}^3\gamma^2 + \eta_{\mathrm{d}}^3\sigma^2\gamma^2 - 2\eta_{\mathrm{d}}^3\sigma\gamma^2}, \tag{6.18a}$$

$$\chi_{\mathrm{ee}}^{xy\prime} = \frac{i}{\omega\epsilon} 2Ae^{i\phi}, \tag{6.18b}$$

$$\chi_{\mathrm{ee}}^{yx\prime} = 0, \tag{6.18c}$$

where $\alpha = \cos(\beta d)$, $\gamma = \sin(\beta d)$, $\zeta = (\eta^2\gamma - \eta_{\mathrm{d}}^2\gamma + \eta_{\mathrm{d}}^2\sigma\gamma + \eta\eta_{\mathrm{d}}\sigma\alpha i)$ and A is the amplitude

of the cross-polarized reflected wave as defined in (6.1). The other susceptibility tensors, $\overline{\overline{\chi}}_{\mathrm{mm}}$, $\overline{\overline{\chi}}_{\mathrm{em}}$ and $\overline{\overline{\chi}}_{\mathrm{me}}$, are found to zero, which reveals that the effective tensor $\overline{\overline{\chi}}_{\mathrm{mm}}$, required from (6.9b), is automatically provided by xz-loops formed between the top metasurface and the mirror, hence simplifying the former to a purely electrical homoanisotropic metasurface, characterized by the sole $\overline{\overline{\chi}}_{\mathrm{ee}}$ susceptibility tensor.

The last step of the design is to perform geometrical-parameter full-wave simulation mapping, as described in [128]. Figure 6.5 shows the final metaparticle design, where we folded the strips into C-section structure for better subwavelength confinement and hence better homogenizability. Note that the currents in the parallel strips of the C-sections do not fully cancel out due to resonance non-uniformity (zero current at the edges and maximum at the center of the unfolded strip structure), which provides the same responses as those previously described despite the smaller footprint.

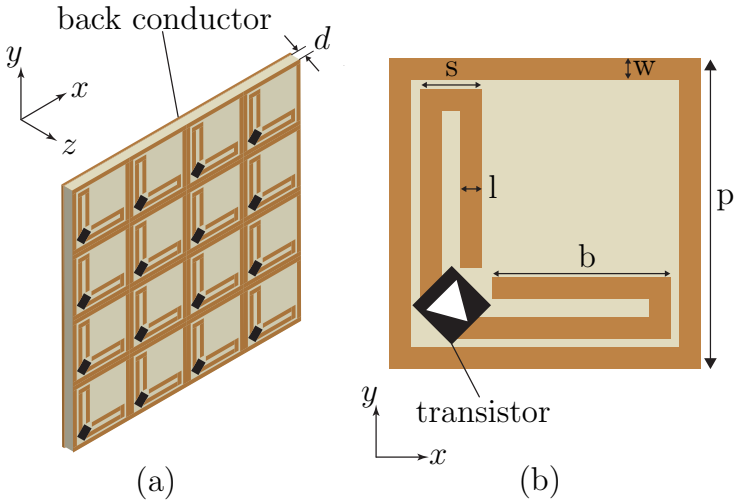

Figure 6.5 Proposed practical implementation of the RGSI metasurface (a) Perspective view (b) Front view of the unit cell

6.5 Results

This section present full-wave simulation results, using the commercial software CST Microwave Studio, for the RGSI metasurface implementation in Fig. 6.5. We shall consider and compare two implementations: one using quasi-ideal unity-gain unilateral transistors, corresponding to a quasi-ideal isolator with scattering matrix $\mathbf{S}_{\mathrm{trans}} = [0, I; 1, 0]$, with $I = -30$ dB, and one using the HMC441LP3E transistor chip from Analog Devices, with (frequency dependent) scattering parameters, including gain, given in the data sheet of the chip provided by the company. The design frequency is set to 7.5 GHz. For both implementations, we shall

plot the simulated scattering parameters versus frequency, and the susceptibilities of the top layer extracted from these scattering parameters for comparison with the ideal susceptibilities given by (6.18)[6].

Figures 6.6 and 6.7 present the results for the RGSI metasurface with the quasi-ideal unity-gain unilateral transistor with a substrate of $\epsilon_r = 6.2$ and for the parameters $l = 0.5$ mm, $d = 3$ mm, $w = 1$ mm, $b = 9$ mm, $s = 1.5$ mm, and $p = 14.8$ mm. The desired RGSI operation (Fig. 6.1) is clearly observed at the design frequency (7.5 GHz) in Fig. 6.6, where the metasurface exhibits and isolation of around 40 dB between the cross-polarized ports S_{11}^{xy} and S_{11}^{yx}, and a matching of -15 dB for both co-polarized reflections. Moreover, the design results $\chi_{ee}^{xx\prime} = \chi_{ee}^{yy\prime}$ of (6.18a), $\chi_{ee}^{xy\prime} \neq 0$ of (6.18b) and $\chi_{ee}^{yx\prime} = 0$ of (6.18c), satisfying the nonreciprocity relation $\chi_{ee}^{yx\prime} \neq \chi_{ee}^{xy\prime}$, are verified in Fig. 6.7.

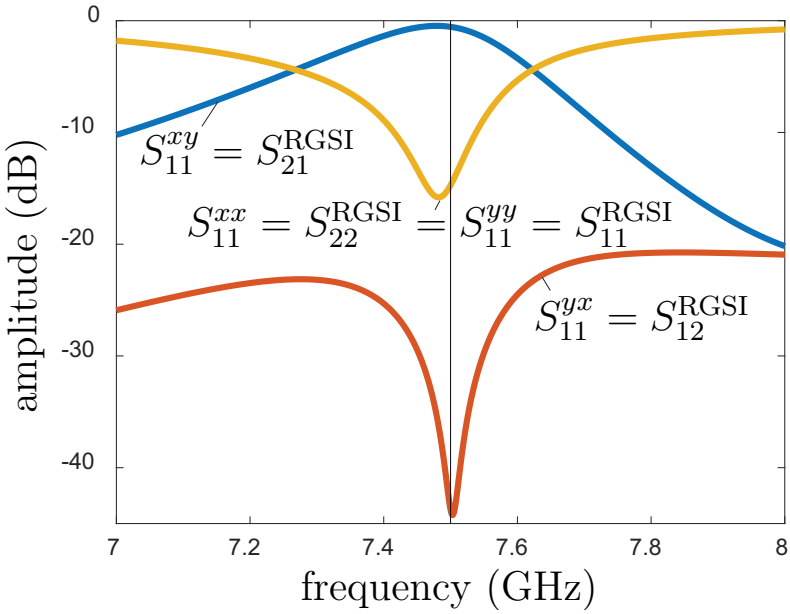

Figure 6.6 Full-wave simulated scattering parameters for the RGSI metasurface in Fig. 6.5 using gain-less unilateral transistor

Figures 6.8 and 6.9 present the results for the RGSI metasurface with the HMC441LP3E transistor chips. The spectrum observed in Fig. 6.8 is slightly different from the design target, due to asymmetries of the chip that were not accounted for in the design; a better operation frequency here could be 7.467 GHz, which features the best trade-off between gain,

[6]This extraction is done, following the method described in Sec. 6.4.2.4.2, as follows: 1) equating the simulated scattering matrix to the scattering matrix (6.14) with (6.12), 2) solving the resulting equations for the admittance matrix $\mathbf{Y}'$, and 3) translating this so-obtained admittance matrix into surface susceptibilities using (6.16) and (6.17a).

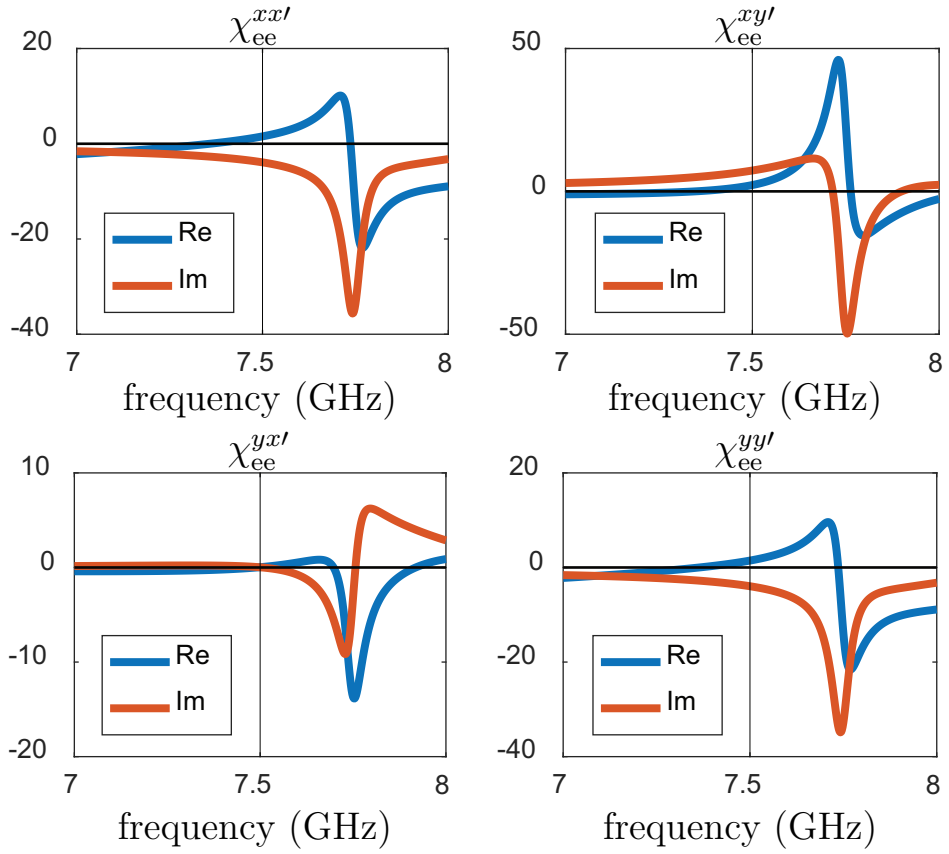

Figure 6.7 Electric susceptibilities for the top metasurface layer in Fig. 6.5, extracted from the scattering parameters in Fig. 6.6

isolation and matching. At this frequency, a good RGSI operation is achieved, with a gain of 13 dB (S_{11}^{xy}), an isolation of over 40 dB (with respect to S_{11}^{yx}) and equal port matching of -12.9 dB (S_{11}^{xx} and S_{11}^{yy}). The extracted susceptibilities in Fig. 6.8, although quite different from those obtained for the uasi-ideal unilateral transistors (in Fig. 6.7), still satisfy $\chi_{ee}^{xy\prime} \neq 0$ of (6.18b) and $\chi_{ee}^{yx\prime} = 0$ of (6.18c), whereas the relation (6.18a) is not satisfied anymore, due the asymmetry of the transistor chip, fortunately without fatal consequence on the RGSI operation of the metasurface, as we saw in Fig. 6.8

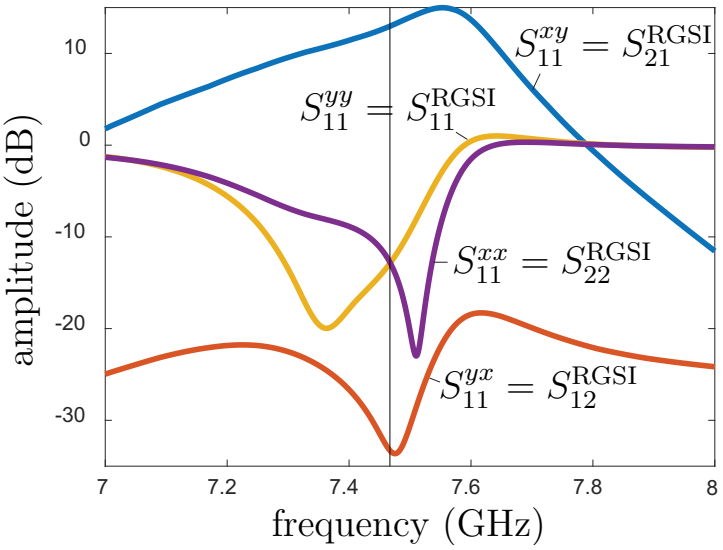

Figure 6.8 Full-wave simulated scattering parameters of the RGSI metasurface of Fig. 6.5 using the HMC441LP3E transistor chips, and for the same substrate and geometric parameters as in Fig. 6.6

6.6 Conclusion

We have presented the concept of a magnetless RGSI metasurface. We have derived the surface susceptibility tensors required to realize this operation, and proposed a transistor-based mirror-backed implementation of a corresponding RGSI metasurface. Finally, we have demonstrated the device by full-wave simulations for both quasi-ideal unity-gain isolators and commercial transistor chips with gain. This RGSI metasurface may be used in various electromagnetic applications and as a step towards more sophisticated magnetless nonreciprocal systems.

6.7 Bianisotropic Design

In Sec. 6.3.2, we made the homoanisotropic choice of the 8 susceptiblity components χ_{ee}^{xx}, χ_{ee}^{xy}, χ_{ee}^{yx}, χ_{ee}^{yy}, χ_{mm}^{xx}, χ_{mm}^{xy}, χ_{mm}^{yx} and χ_{mm}^{yy} to implement the proposed magnetless gyrotropic reflective spatial isolator metasurface, but we could have chosen a different set of eight susceptibility components. Let us consider here the alternative axial bianisotropic set χ_{ee}^{xx}, χ_{ee}^{yy}, χ_{mm}^{xx}, χ_{mm}^{yy}, χ_{em}^{xx}, χ_{em}^{yy}, χ_{me}^{xx}, χ_{me}^{yy}, where the gyrotropic components are now χ_{em}^{xx}, χ_{em}^{yy}, χ_{me}^{xx} and χ_{me}^{yy} instead of χ_{ee}^{xy}, χ_{ee}^{yx}, χ_{mm}^{xy} and χ_{mm}^{yx}. Following the same procedure as in Sec. 6.3.2 for this alternative

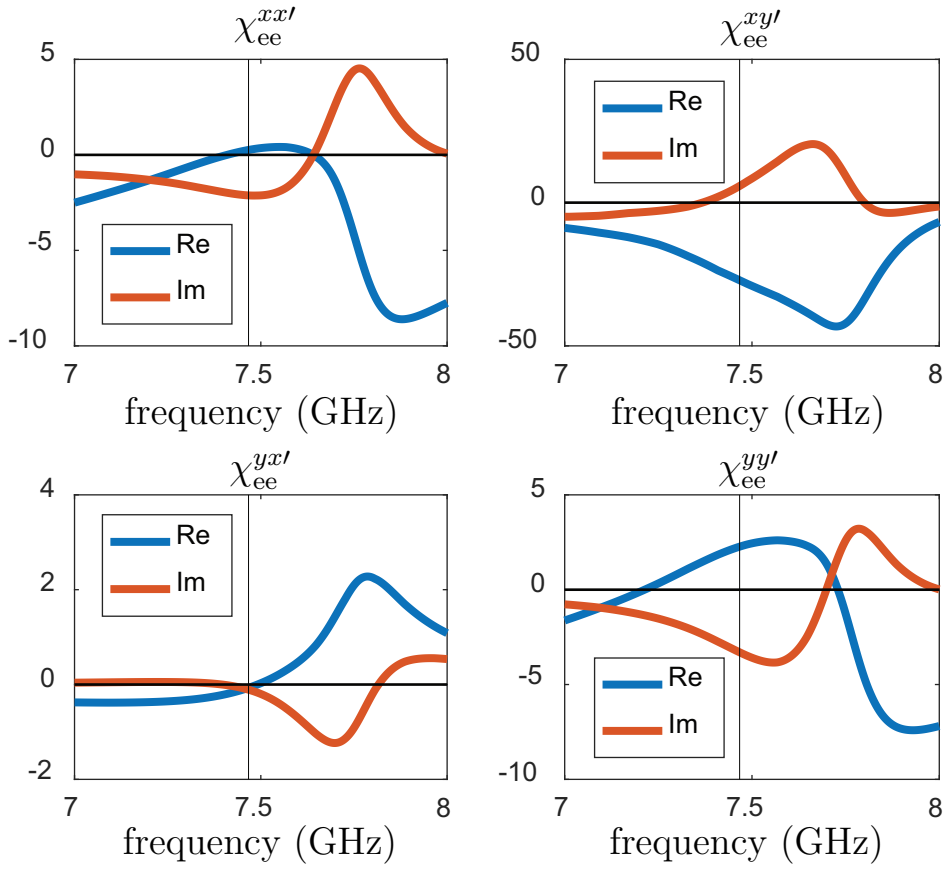

Figure 6.9 Electric susceptibilities for the top layer, extracted from the susceptibilities in Fig. 6.8

set yields

$$\overline{\overline{\chi}}_{\mathrm{ee}} = \begin{bmatrix} \chi_{\mathrm{ee}}^{xx} & \chi_{\mathrm{ee}}^{xy} \\ \chi_{\mathrm{ee}}^{yx} & \chi_{\mathrm{ee}}^{yy} \end{bmatrix} = \begin{bmatrix} \frac{-2i\sec\theta}{k} & 0 \\ 0 & \frac{-2i\cos\theta}{k} \end{bmatrix}, \tag{6.19a}$$

$$\overline{\overline{\chi}}_{\mathrm{mm}} = \begin{bmatrix} \chi_{\mathrm{mm}}^{xx} & \chi_{\mathrm{mm}}^{xy} \\ \chi_{\mathrm{mm}}^{yx} & \chi_{\mathrm{mm}}^{yy} \end{bmatrix} = \begin{bmatrix} \frac{-2i\sec\theta}{k} & 0 \\ 0 & \frac{-2i\cos\theta}{k} \end{bmatrix}, \tag{6.19b}$$

$$\overline{\overline{\chi}}_{\mathrm{em}} = \begin{bmatrix} \chi_{\mathrm{em}}^{xx} & \chi_{\mathrm{em}}^{xy} \\ \chi_{\mathrm{em}}^{yx} & \chi_{\mathrm{em}}^{yy} \end{bmatrix} = \begin{bmatrix} \frac{-4iAe^{i\phi}\sec\theta}{k} & 0 \\ 0 & 0 \end{bmatrix}, \tag{6.19c}$$

$$\overline{\overline{\chi}}_{\mathrm{me}} = \begin{bmatrix} \chi_{\mathrm{me}}^{xx} & \chi_{\mathrm{me}}^{xy} \\ \chi_{\mathrm{me}}^{yx} & \chi_{\mathrm{me}}^{yy} \end{bmatrix} = \begin{bmatrix} 0 & 0 \\ 0 & \frac{-4iAe^{i\phi}\cos\theta}{k} \end{bmatrix}. \tag{6.19d}$$

This alternative solution would naturally lead to different metaparticles than those used in the paper. Particularly, the magnetodielectric coupling terms would imply chiral, z-asymmetric metaparticles [231, 232], which could potentially be implemented by introducing transistors into chiral metaparticles similar to those in [233].

CHAPTER 7 COMPLEMENTARY RESULTS

In this chapter, we present three complementary results relating to nonreciprocal bianisotropic metasurfaces. First, the problem of performing Faraday rotation in transmission with a metasurface is theoretically analyzed. Second, a the concept of a bianisotropic nonreciprocal phase-gradient metasurface is presented. Third, a metasurface specular isolator utilizing normal nonreciprocal susceptibilities is demonstrated.

7.1 Transmissive Faraday Rotation Metasurface

As mentioned in Sec. 2, conventional nonreciprocal systems usually rely on magnetized materials that provide Faraday rotation, in which the polarization of a linearly polarized wave experiences the same rotation independently of the direction of propagation of the wave. Some efforts have been made to realize this type of response using magnetless metamaterial structures. For instance, cross-polarized dipoles properly connected by a transistor-loaded circuit were shown to realize nonreciprocal gyrotropy [198], and transistor-loaded ring resonators were shown to produce a unidirectional rotating magnetic dipole moment that emulates the electron spin precession in magnetized ferrites [197, 199, 200]. The later works focused on reflective structures, but a transmissive structure following the same operation principle, but with an open ground plane to allow transmission was proposed [202, 234]. However, this transmissive structure was mismatched and a large amount of co- and cross-polarized reflection limited the transmission efficiency of the structure. In this section, we analyze the problem of realizing an efficient Faraday rotation metasurface in transmission and derive suitable susceptibilities to realize this operation. We derive two types of nonreciprocal metasurfaces that provides arbitrary-angle Faraday rotation with zero reflection.

We consider a uniform tangential metasurface surrounded by air and placed in the xy plane at $z = 0$. We heuristically begin by assuming a nonbianisotropic metasurface, where $\overline{\overline{\chi}}_{\rm em}$ and $\overline{\overline{\chi}}_{\rm me}$ are zero. Under this assumption, the GSTCs in (3.8) reduce to

$$\hat{z} \times \Delta\mathbf{H} = j\omega\epsilon\overline{\overline{\chi}}_{\rm ee}\mathbf{E}_{\rm av}, \tag{7.1a}$$

$$\hat{z} \times \Delta\mathbf{E} = -j\omega\mu\overline{\overline{\chi}}_{\rm mm}\mathbf{H}_{\rm av}. \tag{7.1b}$$

Equations (7.1) are 2 vectorial equations, whose projection onto the xy-plane yields the four scalar equations

$$-\Delta H_y = j\omega\epsilon\chi_{\rm ee}^{xx}E_{x,\rm av} + j\omega\epsilon\chi_{\rm ee}^{xy}E_{y,\rm av}, \tag{7.2a}$$

$$\Delta H_x = j\omega\epsilon\chi_{\rm ee}^{yx}E_{x,\rm av} + j\omega\epsilon\chi_{\rm ee}^{yy}E_{y,\rm av}, \tag{7.2b}$$

$$\Delta E_y = j\omega\mu\chi_{\rm mm}^{xx}H_{x,\rm av} + j\omega\mu\chi_{\rm mm}^{xy}H_{y,\rm av}, \tag{7.2c}$$

$$-\Delta E_x = j\omega\mu\chi_{\rm mm}^{yx}H_{x,\rm av} + j\omega\mu\chi_{\rm mm}^{yy}H_{y,\rm av}. \tag{7.2d}$$

Equations (7.2) form a system of 4 equations with 8 unknowns, and is hence undetermined. We have thus the degrees of freedom required to specify two arbitrary distinct wave transformations for the metasurface. The system of equations containing the two specified wave transformations can be compactly written in the matrix form

$$\begin{bmatrix} -\Delta H_{y1} & -\Delta H_{y2} \\ \Delta H_{x1} & \Delta H_{x2} \end{bmatrix} = \begin{bmatrix} j\omega\epsilon\chi_{\rm ee}^{xx} & j\omega\epsilon\chi_{\rm ee}^{xy} \\ j\omega\epsilon\chi_{\rm ee}^{yx} & j\omega\epsilon\chi_{\rm ee}^{yy} \end{bmatrix} \begin{bmatrix} E_{x1,\rm av} & E_{x2,\rm av} \\ E_{y1,\rm av} & E_{y2,\rm av} \end{bmatrix}, \tag{7.3}$$

$$\begin{bmatrix} \Delta E_{y1} & \Delta E_{y2} \\ -\Delta E_{x1} & -\Delta E_{x2} \end{bmatrix} = \begin{bmatrix} j\omega\mu\chi_{\rm mm}^{xx} & j\omega\mu\chi_{\rm mm}^{xy} \\ j\omega\mu\chi_{\rm mm}^{yx} & j\omega\mu\chi_{\rm mm}^{yy} \end{bmatrix} \begin{bmatrix} H_{x1,\rm av} & H_{x2,\rm av} \\ H_{y1,\rm av} & H_{y2,\rm av} \end{bmatrix}, \tag{7.4}$$

where the subscripts 1 and 2 represent the first and second specified wave transformations, respectively. Resolving Eqs. (7.3) and (7.3) provides the 8 susceptibility components required to perform the specified transformations.

The concept of a 'perfect' Faraday-rotation metasurface is illustrated in Fig. 7.1. A linearly polarized wave incident on the metasurface in the forward direction is transmitted, without any reflection and any absorption, with an arbitrary polarization rotation angle, θ, and that wave, when sent back in the opposite direction, keeps rotating in the same direction so as to reach the angle of 2θ. The angle accumulation in the return direction is a manifestation of the nonreciprocity associated with the Faraday rotation phenomenon, contrasting with reciprocal chiral polarization rotation.

Figure 7.2 shows the field specifications for the two wave transformations required to realize a perfect Faraday-rotation metasurface. The first transformation rotates without reflection a plane wave polarized along x and propagating along $+z$ by the angle θ. The electric and magnetic fields of this wave transformation read

$$E_{xa1} = 1, \quad H_{ya1} = 1/\eta, \tag{7.5a}$$

$$E_{ya1} = 0, \quad H_{xa1} = 0, \tag{7.5b}$$

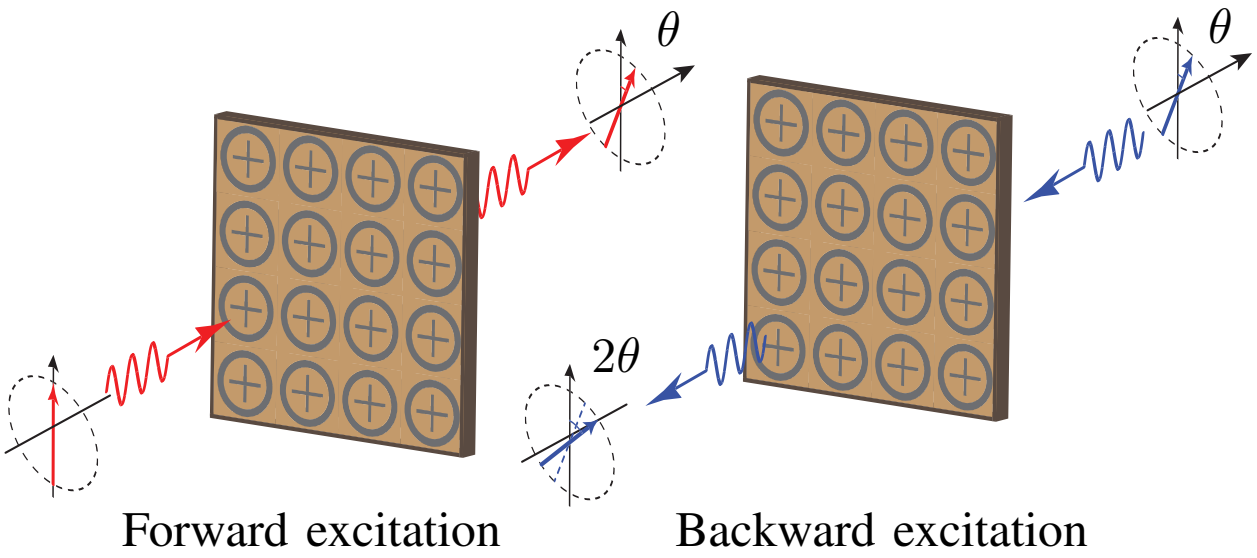

Figure 7.1 Concept of a 'perfect' Faraday-rotation metasurface, corresponding to reflectionless and absorptionless nonreciprocal polarization rotation by an arbitrary angle θ

$$E_{xb1} = Ae^{j\phi_1}\cos\theta, \quad H_{yb1} = Ae^{j\phi_1}\cos\theta/\eta, \tag{7.5c}$$

$$E_{yb1} = Ae^{j\phi_1}\sin\theta, \quad H_{xb1} = -Ae^{j\phi_1}\sin\theta/\eta, \tag{7.5d}$$

where A is the forward transmission coefficient of the metasurface, ϕ_1 is the forward transmission phase, and the subscript a and b correspond to the two sides of the metasurface at $z = 0^-$ and $z = 0^+$ respectively.

The second transformation rotates without reflection a plane wave polarized along the angle θ and propagating along $-z$ by an additional angle θ leading to a final polarization angle of 2θ. The electric and magnetic fields of this wave transformation read

$$E_{xa2} = Be^{j\phi_2}\cos 2\theta, \quad H_{ya2} = -Be^{j\phi_2}\cos 2\theta/\eta \tag{7.6a}$$

$$E_{ya2} = Be^{j\phi_2}\sin 2\theta, H_{xa2} = Be^{j\phi_2}\sin 2\theta/\eta \tag{7.6b}$$

$$E_{xb2} = \cos\theta, \quad H_{yb2} = -\cos\theta/\eta \tag{7.6c}$$

$$E_{yb2} = \sin\theta, \quad H_{xb2} = \sin\theta/\eta \tag{7.6d}$$

where B is the backward transmission coefficient of the metasurface and ϕ_2 is the backward transmission phase of the metasurface.

Inserting the field specifications of Eqs. (7.5) and (7.6) into Eqs. (7.3) and (7.4) yields the desired susceptibility components as a function of the transmission coefficients A and B, of

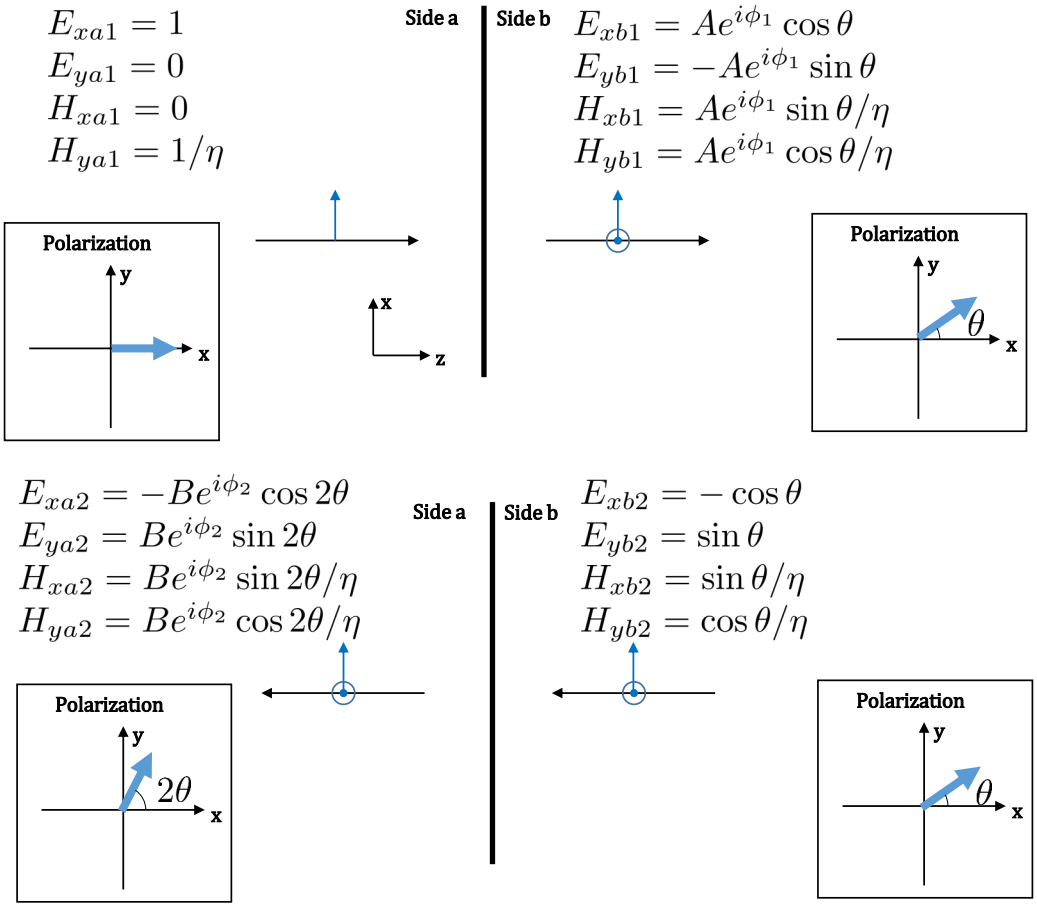

Figure 7.2 Field specifications for the transmission-type Faraday-rotation metasurface for both specified wave transformations

the transmission phases ϕ_1 and ϕ_2, and of the polarization rotation angle θ as follows:

$$\chi_{\mathrm{ee}}^{xx} = \frac{2j\left(Be^{j\phi 2}\left(-2\cos\theta + Ae^{j\phi 1}\right) + 2Ae^{j\phi 1}\cos\theta - 1\right)}{k\left(1 + Be^{j\phi 2}\left(2\cos\theta + Ae^{j\phi 1}\right)\right)}, \tag{7.7a}$$

$$\chi_{\mathrm{ee}}^{yy} = \frac{2j\left(Be^{j\phi 2}\left(2\cos\theta + Ae^{j\phi 1}\right) - 2Ae^{j\phi 1}\cos\theta - 1\right)}{k\left(1 + Be^{j\phi 2}\left(2\cos\theta + Ae^{j\phi 1}\right)\right)}, \tag{7.7b}$$

$$\chi_{\mathrm{ee}}^{xy} = \frac{4j\left(Be^{j\phi 2}\cos(2\theta)\csc\theta - Ae^{j\phi 1}\cos\theta\cot\theta\right)}{k\left(1 + Be^{j\phi 2}\left(2\cos\theta + Ae^{j\phi 1}\right)\right)}, \tag{7.7c}$$

$$\chi_{\mathrm{ee}}^{yx} = \frac{4jAe^{j\phi 1}\sin\theta}{\mu\omega\left(1 + ABe^{j(\phi 1+\phi 2)}\right) + 2Bke^{j\phi 2}\cos\theta}, \tag{7.7d}$$

$$\chi_{\mathrm{mm}}^{xx} = \frac{2j\left(Be^{j\phi 2}\left(2\cos\theta + Ae^{j\phi 1}\right) - 2Ae^{j\phi 1}\cos\theta - 1\right)}{k\left(1 + Be^{j\phi 2}\left(2\cos\theta + Ae^{j\phi 1}\right)\right)}, \tag{7.7e}$$

$$\chi_{\mathrm{mm}}^{yy} = \frac{2j\left(Be^{j\phi 2}\left(-2\cos\theta + Ae^{j\phi 1}\right) + 2Ae^{j\phi 1}\cos\theta - 1\right)}{k\left(1 + Be^{j\phi 2}\left(2\cos\theta + Ae^{j\phi 1}\right)\right)}, \tag{7.7f}$$

$$\chi_{\mathrm{mm}}^{xy} = -\frac{4jAe^{j\phi 1}\sin\theta}{\mu\omega\left(1 + ABe^{j(\phi 1+\phi 2)}\right) + 2Bke^{j\phi 2}\cos\theta}, \tag{7.7g}$$

$$\chi_{\mathrm{mm}}^{yx} = \frac{4j\csc\theta\left(Ae^{j\phi 1}\cos\theta\cot\theta - Be^{j\phi 2}\cos(2\theta)\csc\theta\right)}{k\left(1 + Be^{j\phi 2}\left(2\cos\theta + Ae^{j\phi 1}\right)\right)}. \tag{7.7h}$$

Equations (7.7) indicate that the reciprocity conditions, $\overline{\overline{\chi}}_{\mathrm{ee}} = \overline{\overline{\chi}}_{\mathrm{ee}}^{\mathrm{T}}$ and $\overline{\overline{\chi}}_{\mathrm{mm}} = \overline{\overline{\chi}}_{\mathrm{mm}}^{\mathrm{T}}$, are both broken since $\chi_{\mathrm{ee}}^{xy} \neq \chi_{\mathrm{ee}}^{yx}$ and $\chi_{\mathrm{mm}}^{xy} \neq \chi_{\mathrm{mm}}^{yx}$. This result reveals that one way to obtain a 'perfect' Faraday-rotation metasurface in transmission is to realize a metasurface having *both* nonreciprocal magnetic and electric responses. A possible practical way to realize such a metasurface would be by using properly designed transistor-loaded resonators of the type presented in Fig. 6.2.

Assuming a lossless and gainless design ($A = B = 1$) with identical phases in the two directions ($\phi_1 = \phi_2 = \phi$), simplifies the susceptibilities in Eqs. (7.7) to

$$\chi_{\mathrm{ee}}^{xx} = -\frac{2\sin(\phi)}{k\cos(\theta) + k\cos(\phi)}, \tag{7.8a}$$

$$\chi_{\mathrm{ee}}^{yy} = -\frac{2\sin(\phi)}{k\cos(\theta) + k\cos(\phi)}, \tag{7.8b}$$

$$\chi_{\mathrm{ee}}^{xy} = -\frac{2j\sin(\theta)}{k\cos(\theta) + k\cos(\phi)}, \tag{7.8c}$$

$$\chi_{\mathrm{ee}}^{yx} = \frac{2j\sin(\theta)}{k\cos(\theta) + k\cos(\phi)}, \tag{7.8d}$$

$$\chi_{\mathrm{mm}}^{xx} = -\frac{2\sin(\phi)}{k\cos(\theta) + k\cos(\phi)}, \tag{7.8e}$$

$$\chi_{\mathrm{mm}}^{yy} = -\frac{2\sin(\phi)}{k\cos(\theta) + k\cos(\phi)}, \tag{7.8f}$$

$$\chi_{\mathrm{mm}}^{xy} = -\frac{2j\sin(\theta)}{k\cos(\theta) + k\cos(\phi)}, \tag{7.8g}$$

$$\chi_{\mathrm{mm}}^{yx} = \frac{2j\sin(\theta)}{k\cos(\theta) + k\cos(\phi)}. \tag{7.8h}$$

It appears that $\chi_{\mathrm{mm}}^{xy} = -\chi_{\mathrm{mm}}^{yx}$ and $\chi_{\mathrm{ee}}^{xy} = -\chi_{\mathrm{ee}}^{yx}$ as is the case for lossless magnetized ferrites [220] and magnetized plasma, respectively [235]. Moreover, we verify the lossless condi-

tions $\overline{\overline{\chi}}_{\mathrm{ee}}^{\mathrm{T}} = \overline{\overline{\chi}}_{\mathrm{ee}}^{*}$, and $\overline{\overline{\chi}}_{\mathrm{mm}}^{\mathrm{T}} = \overline{\overline{\chi}}_{\mathrm{mm}}^{*}$, consistent with the specification of $A = B = 1$.

At the start of this section, we heuristically considered a nonbianisotropic metasurface and were able to find a solution using only $\overline{\overline{\chi}}_{\mathrm{ee}}$ and $\overline{\overline{\chi}}_{\mathrm{mm}}$. However, this is not necessarily the unique possible solution. We shall next present an alternative bianisotropic solution providing the same response for the specified incidences, but using the 8 susceptibility components χ_{ee}^{xx}, χ_{ee}^{yy}, χ_{mm}^{xx}, χ_{mm}^{yy}, χ_{em}^{xx}, χ_{em}^{yy}, χ_{me}^{xx} and χ_{me}^{yy}. We replaced the electric and magnetic gyrotropic susceptibility components χ_{ee}^{xy}, χ_{ee}^{yx}, χ_{mm}^{xy} and χ_{mm}^{yx} with the bianisotropic gyrotropic components χ_{em}^{xx}, χ_{em}^{yy}, χ_{me}^{xx} and χ_{me}^{yy}.

Using those 8 susceptibility components, we write the tangential GSTCs as

$$-\Delta H_y = j\omega\epsilon\chi_{\mathrm{ee}}^{xx}E_{x,\mathrm{av}} + jk\chi_{\mathrm{em}}^{xx}H_{x,\mathrm{av}}, \tag{7.9a}$$

$$\Delta H_x = jk\chi_{\mathrm{em}}^{yy}H_{y,\mathrm{av}} + j\omega\epsilon\chi_{\mathrm{ee}}^{yy}E_{y,\mathrm{av}}, \tag{7.9b}$$

$$\Delta E_y = j\omega\mu\chi_{\mathrm{mm}}^{xx}H_{x,\mathrm{av}} + jk\chi_{\mathrm{me}}^{xx}E_{x,\mathrm{av}}, \tag{7.9c}$$

$$-\Delta E_x = jk\chi_{\mathrm{me}}^{yy}E_{y,\mathrm{av}} + j\omega\mu\chi_{\mathrm{mm}}^{yy}H_{y,\mathrm{av}}. \tag{7.9d}$$

Similarly to (7.3), the system of equations containing the two wave transformations of (7.5) and (7.6) can be written in matrix form as

$$\begin{bmatrix} -\Delta H_{y1} & -\Delta H_{y2} \\ \Delta E_{y1} & \Delta E_{y2} \end{bmatrix} = \begin{bmatrix} j\omega\epsilon\chi_{\mathrm{ee}}^{xx} & jk\chi_{\mathrm{em}}^{xx} \\ jk\chi_{\mathrm{me}}^{xx} & j\omega\epsilon\chi_{\mathrm{mm}}^{xx} \end{bmatrix} \begin{bmatrix} E_{x1,\mathrm{av}} & E_{x2,\mathrm{av}} \\ H_{x1,\mathrm{av}} & H_{x2,\mathrm{av}} \end{bmatrix}, \tag{7.10}$$

$$\begin{bmatrix} \Delta H_{x1} & \Delta H_{x2} \\ -\Delta E_{x1} & -\Delta E_{x2} \end{bmatrix} = \begin{bmatrix} j\omega\mu\chi_{\mathrm{mm}}^{xx} & jk\chi_{\mathrm{em}}^{yy} \\ jk\chi_{\mathrm{me}}^{yy} & j\omega\mu\chi_{\mathrm{mm}}^{yy} \end{bmatrix} \begin{bmatrix} E_{y1,\mathrm{av}} & E_{y2,\mathrm{av}} \\ H_{y1,\mathrm{av}} & H_{y2,\mathrm{av}} \end{bmatrix}, \tag{7.11}$$

Inserting the field specifications of Eqs. (7.5) and (7.6) into Eqs. (7.10) and (7.11) with $A = B = 1$ and $\phi_1 = \phi_2 = \phi$ as in (7.8) yields the susceptibility components

$$\chi_{\mathrm{ee}}^{xx} = \frac{2j(e^{2j\phi}(1 + 2\cos(2\theta)) - 2e^{j\phi} - 1)}{k(2 + 6e^{2j\phi}\cos\theta) + k(e^{2j\phi}(2\cos(2\theta) + 1) - 2e^{j\phi} - 1)}, \tag{7.12a}$$

$$\chi_{\mathrm{ee}}^{yy} = \frac{2j(e^{2j\phi}(2\cos(2\theta) + 1) + 2e^{j\phi} - 1)}{k(2 + 2e^{2j\phi}\cos\theta) + k(e^{2j\phi}(2\cos(2\theta) + 1) - 2e^{j\phi}\cos\theta - 1)} \tag{7.12b}$$

$$\chi_{\mathrm{mm}}^{xx} = \frac{2j(e^{2j\phi}(2\cos(2\theta) + 1) + 2e^{j\phi}\cos\theta - 1)}{k(e^{2j\phi}(2\cos(2\theta) + 1) + 4e^{j\phi}\cos\theta - 1)} \tag{7.12c}$$

$$\chi_{\mathrm{mm}}^{yy} = \frac{2j(e^{2j\phi}(1 - 2\cos(2\theta)) + 2e^{j\phi} - 1)}{k(e^{2j\phi}(2\cos(2\theta) + 1) + 4e^{j\phi} - 1)} \tag{7.12d}$$

$$\chi_{\mathrm{em}}^{xx} = -\frac{4je^{j\phi}\sin\theta}{k + 4e^{j\phi}k\cos\theta + ke^{2j\phi}(1 + 2\cos(2\theta))} \tag{7.12e}$$

$$\chi_{\text{em}}^{yy} = \frac{4je^{j\phi}\sin\theta}{k + 4e^{j\phi}k\cos\theta + ke^{2j\phi}(2\cos(2\theta)+1)} \tag{7.12f}$$

$$\chi_{\text{me}}^{xx} = -\frac{4je^{j\phi}\sin\theta}{k + 4e^{j\phi}k\cos\theta + ke^{2j\phi}(2\cos(2\theta)+1)} \tag{7.12g}$$

$$\chi_{\text{me}}^{yy} = \frac{4je^{j\phi}\sin\theta}{k + 4e^{j\phi}k\cos\theta + ke^{2j\phi}(2\cos(2\theta)+1)} \tag{7.12h}$$

We can verify that this is indeed nonreciprocal since $\chi_{\text{em}}^{xx} \neq -\chi_{\text{me}}^{xx}$ and $\chi_{\text{em}}^{yy} \neq -\chi_{\text{me}}^{yy}$, which breaks the reciprocity tensorial relation $\overline{\overline{\chi}}_{\text{em}} = -\overline{\overline{\chi}}_{\text{me}}^{T}$. This nonreciprocal response correspond to Tellegen-type bianisotropic nonreciprocity [236]. However, this solution is not lossless/gainless since it does not follow the conditions $\overline{\overline{\chi}}_{\text{ee}}^{\text{T}} = \overline{\overline{\chi}}_{\text{ee}}^{*}$, $\overline{\overline{\chi}}_{\text{mm}}^{\text{T}} = \overline{\overline{\chi}}_{\text{mm}}^{*}$ and $\overline{\overline{\chi}}_{\text{em}}^{\text{T}} = \overline{\overline{\chi}}_{\text{me}}^{*}$. Hence, equations (7.8) and (7.12) represent two different possible solutions to realize a transmissive Faraday rotation metasurface by using different susceptibility tensors. Each of those solutions would require different scattering particle geometries to be implemented, but would still provide the same response for the specified incident waves. Their angular response, related to other unspecified incidence waves, would also be different.

7.2 Nonreciprocal Phase Gradient Metasurface

In this section, we introduce the concept of nonreciprocal phase gradient metasurfaces that exhibit different phase gradients depending on the direction of propagation of the incident wave. We will show that such a metasurface can be realized by using nonreciprocal bianisotropic phase shifting unit cells that can be arranged into supercells exhibiting different phase gradients for opposite directions of propagation. We will present numerical simulations of two spatial circulators to illustrate the concept and propose a potential antenna-circuit-antenna implementation backed by full-wave simulations.

Figure 7.3 presents the concept of the nonreciprocal phase gradient metasurface. As an example, the metasurface in Fig. 7.3 (a) produces no gradient for a wave propagating in the forward z-direction, but produces a phase gradient for a wave propagating in the backward z-direction, which deflects it. Such a metasurface can be realized by arranging several different nonreciprocal phase-shifting unit cells into supercell as illustrated in Fig. 7.3 (b). For the forward direction (shown in red), all the unit cells produce the same relative phase of 0° and the wave propagation direction is unchanged. For the backward direction, each unit cell produce a different phase, which produces a phase gradient and deflect the wave depending on the period of the supercell. While, the current example provides no gradient in the forward direction, we could in general provide different gradients in both directions. The required unit cell to realize this would be of a general nonreciprocal phase-shifting unit cell, as shown in Fig. 7.3 (c), which can produce a transmission phase ϕ_1 for waves propagating in the

forward z-direction and a transmission phase ϕ_2 for waves propagating in the backward z-direction. We shall next synthesize the susceptibilities of such a nonreciprocal phase-shifting unit cell.

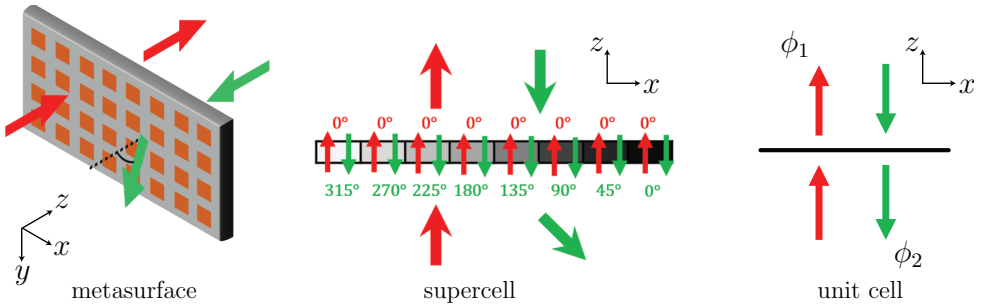

Figure 7.3 Nonreciprocal phase gradient metasurface based on nonreciprocal phase shifting unit cells (a) Illustration of a nonreciprocal phase gradient metasurface (b) Illustration of a nonreciprocal phase gradient metasurface supercell composed of 8 discretized nonreciprocal phase shifters (c) Required unit cell general response

We assume here a purely tangential metasurface and nongyrotropy. We can then synthesize independently the response of the two polarization, with the x-polarized wave having related susceptibility components $\chi_{\rm ee}^{xx}$, $\chi_{\rm em}^{xy}$, $\chi_{\rm me}^{yx}$ and $\chi_{\rm mm}^{yy}$, and the y-polarized having the related susceptibility components $\chi_{\rm ee}^{yy}$, $\chi_{\rm em}^{yx}$, $\chi_{\rm me}^{xy}$ and $\chi_{\rm mm}^{xx}$. The GSTCs in (3.8) then reduce to the scalar equations

$$-\Delta H_y = j\omega\epsilon\chi_{\rm ee}^{xx}E_{x,\rm av} + jk\chi_{\rm em}^{xy}H_{y,\rm av}, \tag{7.13a}$$

$$-\Delta E_x = jk\chi_{\rm me}^{yx}E_{x,\rm av} + j\omega\mu\chi_{\rm mm}^{yy}H_{y,\rm av}, \tag{7.13b}$$

for the x-polarization and to

$$\Delta H_x = jk\chi_{\rm em}^{yx}H_{x,\rm av} + j\omega\epsilon\chi_{\rm ee}^{yy}E_{y,\rm av}, \tag{7.14a}$$

$$\Delta E_y = j\omega\mu\chi_{\rm mm}^{xx}H_{x,\rm av} + jk\chi_{\rm me}^{xy}E_{y,\rm av}, \tag{7.14b}$$

for the y-polarization.

We specify two field transformations for each polarization. First, in the forward z-direction, we specify that a normally incident wave is fully transmitted with a phase ϕ_1. Second, in the backward z-direction, we specify that a normally incident wave is fully transmitted with a different phase ϕ_2. The field specifications are written as

$$E_{xa1} = 1, \quad H_{ya1} = 1/\eta, \tag{7.15a}$$

$$E_{xb1} = 1e^{j\phi_1}, \quad H_{yb1} = 1e^{j\phi_1}/\eta, \tag{7.15b}$$

$$E_{xa2} = -1e^{j\phi_2}, \quad H_{ya2} = 1e^{j\phi_2}/\eta, \tag{7.15c}$$

$$E_{xb2} = -1, \quad H_{yb2} = 1/\eta, \tag{7.15d}$$

for an x-polarized wave and similarly

$$E_{ya1} = 1, \quad H_{xa1} = -1/\eta, \tag{7.16a}$$

$$E_{yb1} = 1e^{j\phi_1}, \quad H_{xb1} = -1e^{j\phi_1}/\eta, \tag{7.16b}$$

$$E_{ya2} = -1e^{j\phi_2}, \quad H_{xa2} = -1e^{j\phi_2}/\eta, \tag{7.16c}$$

$$E_{yb2} = -1, \quad H_{xb2} = -1/\eta, \tag{7.16d}$$

for an y-polarized wave. The subscript a and b correspond to the two sides of the metasurface at $z = 0^-$ and $z = 0^+$ respectively, and the subscript 1 and 2 represent the first and second wave transformations respectively. We can now write the synthesis problem for each polarization in matrix form as

$$\begin{bmatrix} \Delta H_{y1} & \Delta H_{y2} \\ \Delta E_{x1} & \Delta E_{x2} \end{bmatrix} = \begin{bmatrix} -j\omega\epsilon\chi_{\text{ee}}^{xx} & -jk\chi_{\text{em}}^{xy} \\ -jk\chi_{\text{me}}^{yx} & -j\omega\mu\chi_{\text{mm}}^{yy} \end{bmatrix} \begin{bmatrix} E_{x1,\text{av}} & E_{x2,\text{av}} \\ H_{y1,\text{av}} & H_{y2,\text{av}} \end{bmatrix}, \tag{7.17a}$$

for the x-polarization and

$$\begin{bmatrix} \Delta H_{x1} & \Delta H_{x2} \\ \Delta E_{y1} & \Delta E_{y2} \end{bmatrix} = \begin{bmatrix} j\omega\epsilon\chi_{\text{ee}}^{yy} & jk\chi_{\text{em}}^{yx} \\ jk\chi_{\text{me}}^{xy} & j\omega\mu\chi_{\text{mm}}^{xx} \end{bmatrix} \begin{bmatrix} E_{y1,\text{av}} & E_{y2,\text{av}} \\ H_{x1,\text{av}} & H_{x2,\text{av}} \end{bmatrix}, \tag{7.17b}$$

for the y-polarization. Substituting the field definitions of (7.15) and (7.16) into (3.3) to calculate the differences and averages of the fields, inserting those into (7.17) and solving for the required susceptibility components yields

$$\chi_{\text{ee}}^{xx} = \frac{\tan(\phi_1/2) + \tan(\phi_2/2)}{k}, \tag{7.18a}$$

$$\chi_{\text{mm}}^{yy} = \frac{\tan(\phi_1/2) + \tan(\phi_2/2))}{k}, \tag{7.18b}$$

$$\chi_{\text{em}}^{xy} = \frac{\tan(\phi_1/2) - \tan(\phi_2/2)}{k}, \tag{7.18c}$$

$$\chi_{\text{me}}^{yx} = \frac{\tan(\phi_1/2) - \tan(\phi_2/2)}{k}, \tag{7.18d}$$

for the x-polarization and

$$\chi_{\mathrm{ee}}^{yy} = \frac{\tan(\phi_1/2) + \tan(\phi_2/2)}{k}, \tag{7.19a}$$

$$\chi_{\mathrm{mm}}^{xx} = \frac{\tan(\phi_1/2) + \tan(\phi_2/2))}{k}, \tag{7.19b}$$

$$\chi_{\mathrm{em}}^{yx} = \frac{\tan(\phi_2/2) - \tan(\phi_1/2)}{k}, \tag{7.19c}$$

$$\chi_{\mathrm{me}}^{xy} = \frac{\tan(\phi_2/2) - \tan(\phi_1/2)}{k}, \tag{7.19d}$$

for the y-polarization. Those susceptibilities can now be used to design different nonreciprocal phase-shifting unit cells to be assembled into a supercell realizing nonreciprocal phase gradients.

To verify the results, we simulated, using a FDFD simulation code including the susceptibility GSTCs [140], two metasurfaces with nonreciprocal phase gradients for an x-polarized wave. Figure 7.4 presents FDFD simulation results for the first metasurface realizing no gradient in the forward z-direction and a gradient realizing a 45° deflection for the backward z-direction. The metasurface is composed of supercells of period $\sqrt{2}\lambda_0$, corresponding to the phase gradient period for 45° deflection of a normally incident wave. This supercell is discretized in 8 unit cells synthesized following (7.18). In this simulation setup, 6 ports are placed in the directions corresponding to the 6 propagating diffraction orders of the supercell period as illustrated in Fig. 7.4. As can be seen, for propagation in the forward z-direction, the incident wave is transmitted without being deflected and for propagation in the backward direction, the wave is deflected by the phase gradient. Interestingly, this metasurface operates as a 6-port spatial circulator with circulation following the sequence $1 \to 4 \to 3 \to 5 \to 2 \to 6 \to 1$.

The FDFD simulation of a second metasurface realizing phase gradients deflecting waves in opposite directions for propagation in the forward and backward z-direction is shown in Fig. 7.5. The period of the supercell is the same as in Fig. 7.4, deflecting a normally incident wave at 45° towards the $-x$-direction for forward propagation along the z-direction and deflecting a normally incident wave at 45° towards the $+x$-direction for backward propagation along the z-direction. This metasurface realizes two 3-port spatial circulators, with circulation following $1 \to 3 \to 5 \to 1$ and $2 \to 6 \to 4 \to 2$.

The results of Fig. 7.4 and Fig. 7.5 only represent two examples; other devices can be realized by appropriately designing the forward and backward phase gradients. In addition to realizing spatial circulation, such metasurfaces can be used to realize nonreciprocal receive and transmit radiation patterns. For instance, placing an antenna at the port 5 of Fig. 7.5, would

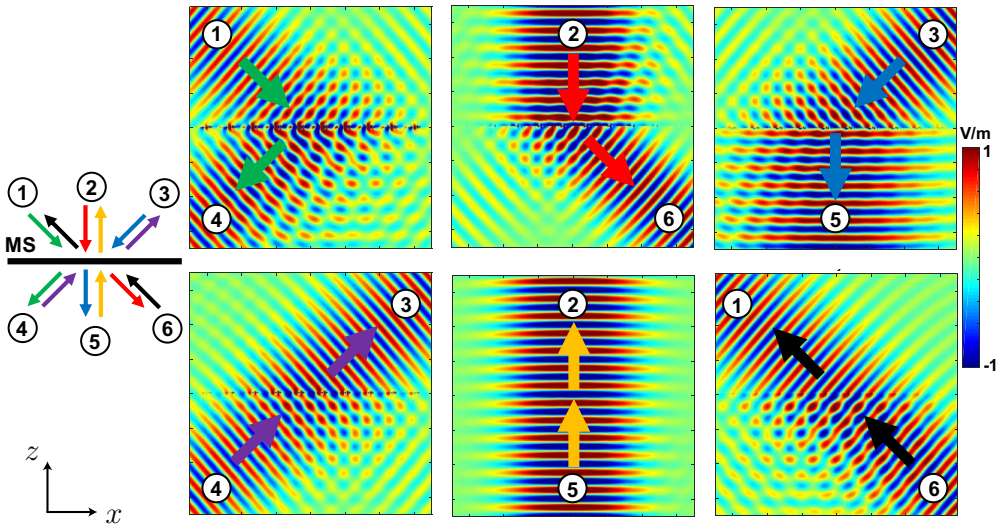

Figure 7.4 FDFD-simulated real part of E_x of a nonreciprocal phase gradient metasurface with no phase gradient for forward propagation along the z-direction and a phase gradient deflecting a normally incident wave by 45° for a backward propagating wave along the z-direction which realizes a spatial 6-port circulator

create a system with a transmit radiation pattern pointing towards port 1 ($-x$-direction) and a receive radiation pattern pointing towards port 3 ($+x$-direction). In general, such a metasurface could be used to realize independently tunable receive and transmit radiation patterns.

We next present a potential implementation of this type of nonreciprocal bianisotropic metasurface using an antenna-circuit-antenna architecture that has been previously used to realize transistor-loaded nonreciprocal metasurfaces [151, 206]. Specifically, the work in [151] presented an isolator metasurface composed of patch antennas and connected through transistor circuits that were shown to be realize a nonreciprocal bianisotropic response. Figure 7.6 presents the nonreciprocal phase-shifting unit cell. Figure 7.6 (a) and (b) show the perspective view and front view of the unit cell respectively. It is composed of two c-shaped dipoles oriented in the x-direction on the outer layers of the structures with a separating ground plane in the middle layer. The two c-shaped dipoles are connected through a nonreciprocal circuit shown in Fig. 7.6 (c). The circuit is composed of two resistive power divider, two isolators and two phase shifter. One phase shifter is used to control the phase of transmission ϕ_1 in the forward direction and the other to control the phase of transmission in the backward direction ϕ_2. This allows independent control of the phase of transmission in both direction of propagation. However, due to the presence of the resistive power dividers and of

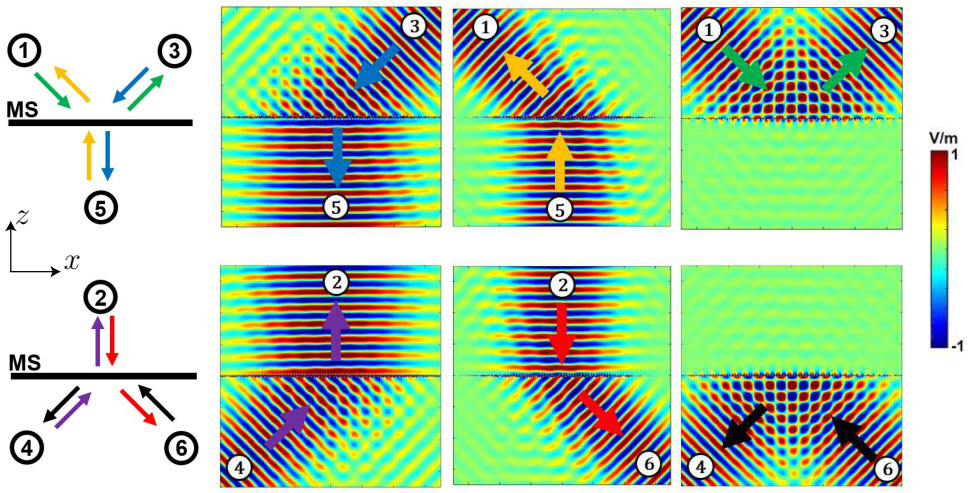

Figure 7.5 FDFD-simulated real part of E_x of a nonreciprocal phase gradient metasurface with the same phase gradient for forward and backward propagation, but with opposite direction which realizes a spatial 3-port circulator

the isolators, the transmission efficiency is limited to −6 dB.

Figure 7.7 presents the simulation of the unit cell of Fig. 7.6 for the forward excitation of an x-polarized wave. Figure 7.7 (a) presents the amplitude of S_{21} and S_{11} for different phase of transmission ϕ_1, while keeping a constant phase ϕ_2 for the backward direction. As can be seen at the operating frequency of 7.1 GHz, the amplitude of transmission is constant at around 0.5 (−6 dB) as the phase of transmission varies for full 360° phase coverage as seen in Fig. 7.7 (b). The same frequency response is also obtained for the backward excitation (S_{12} and S_{22}) with independent control of the phase of transmission ϕ_2.

A supercell composed of 4 of the unit cells of Fig. 7.6 was assembled to realize the nonreciprocal phase gradient metasurface as shown in Fig. 7.8. The period of the supercell is 1.4λ at the operating frequency of 7.1 GHz, which corresponds to a wave deflection of 45.58°. The phases of transmission of each unit cells in the forward and backward were set to realize opposite phase gradients as in Fig. 7.5, which should realize a 3 port circulator. From left to right the forward phases of transmission ϕ_1 are 0°, 90°, 180° and 270°, and the backward phases of transmission ϕ_2 are 270°, 180°, 90° and 0°.

Figure 7.8 (b) present the simulation results of the supercell for excitations at the 3 ports shown in Fig. 7.8 (a). The simulation results for excitations from ports 5 and 1 are in agreement with what we expected for the circulation operation of Fig. 7.5, but with the limited efficiency due to the circuit. However, excitation from port 3 reveals a large coupling

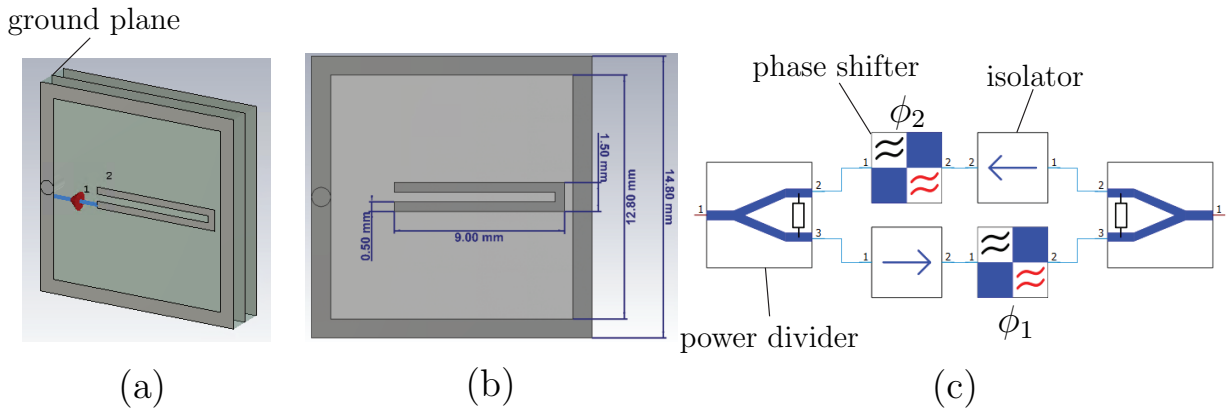

Figure 7.6 Nonreciprocal phase-shifting unit cell based on the antenna-circuit-antenna configuration (a) Perspective view of the unit cell (b) Front view of the unit cell (c) Circuit connecting the two sides of the unit cell composed of power dividers, isolators and phase shifters

S_{13} which completely impedes the structure to act as a 3 port spatial circulator. Further study and optimization of the structure would be required to remove the parasitic S_{13} reflection. Still, the structure did realize a nonreciprocal phase gradient as seen from the response of S_{15} and S_{53} and, hence, could be used to provide nonreciprocal transmission and reception radiation patterns for an antenna placed at port 5.

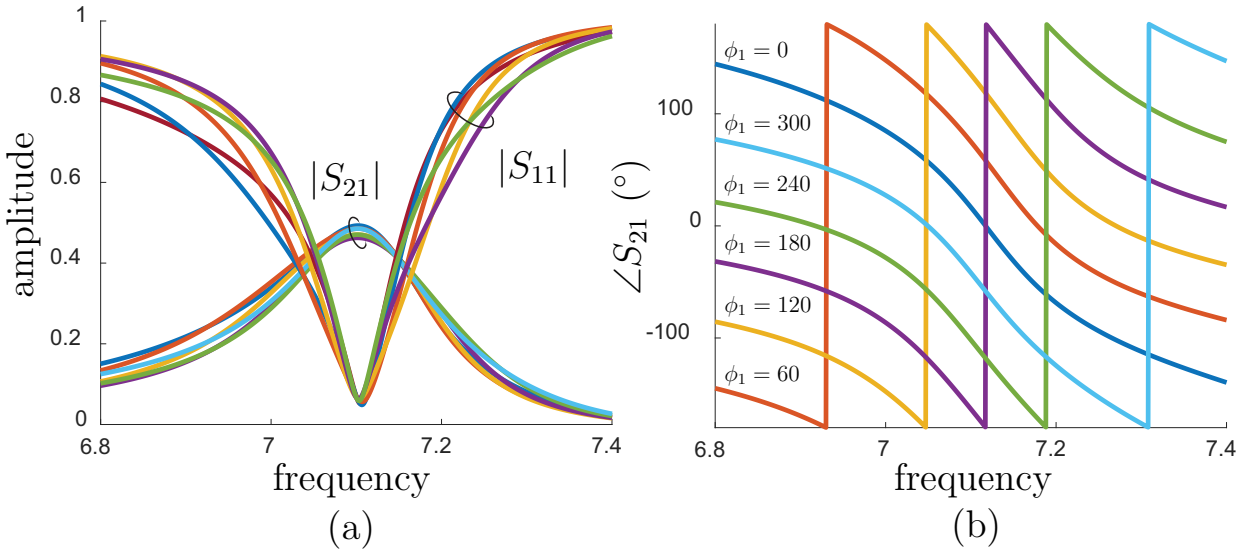

Figure 7.7 Simulation of the unit cell of figure for different phases ϕ_1 (0°, 60°, 120°, 180°, 240° and 300°) versus frequency (a) Amplitude of S_{21} and S_{11} (b) Phase of S_{21}

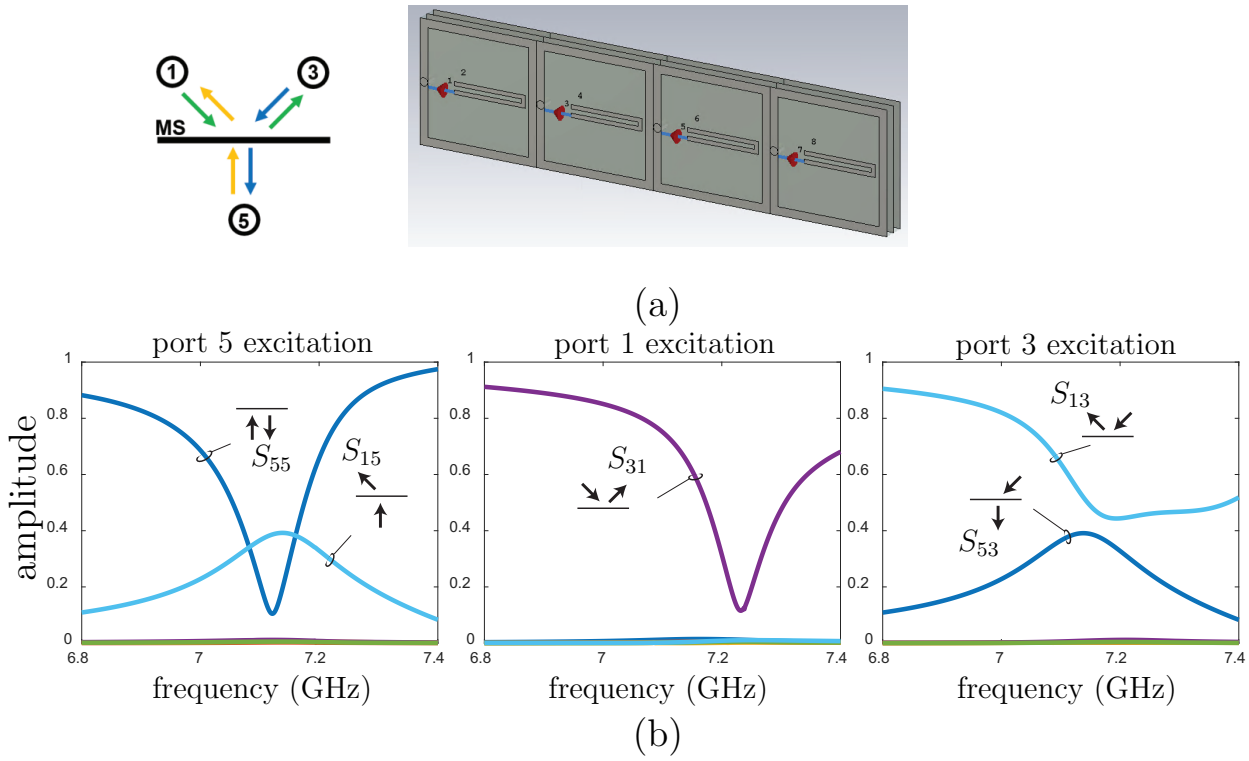

Figure 7.8 Simulation of the supercell realizing opposite gradients for forward and backward directions (a) Supercell composed of 4 unit cells (b) Scattering parameters for excitation from the three ports shown in (a)

7.3 Magnetless Metasurface Specular Isolator

This section reports a transistor-loaded magnetless nonreciprocal metasurface providing specular isolation, i.e. reflecting the wave incident from one direction as a mirror and absorbing the wave incident from the opposite direction. The related asymmetric reflection coefficient is realized by leveraging nonreciprocal normal metasurface susceptibilities [108, 131]. The specular isolation operation is demonstrated by both full-wave simulation and prototype measurement.

Specular Isolator Concept

Figure 7.9 depicts the concept of the proposed metasurface specular isolator. A wave incident in the xz-plane at an angle $\theta_\mathrm{i} = \sin^{-1}(k_{x,\mathrm{i}}/k) = \theta_0$, with $k = \omega/c$, where θ_0 is the operation angle, is specularly reflected, while a wave incident at the angle $\theta_\mathrm{i} = -\theta_0$ is absorbed by the metasurface.

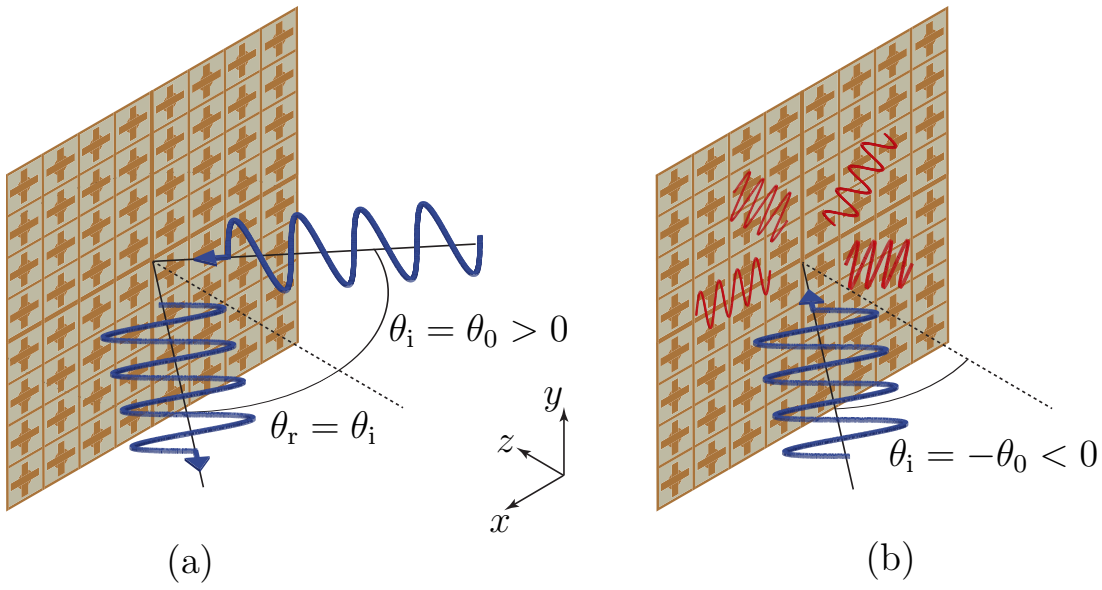

Figure 7.9 Concept of the metasurface specular isolator (a) A wave incident at an angle $\theta_\mathrm{i} = \theta_0$ is specularly reflected (b) A wave incident at an angle $\theta_\mathrm{i} = -\theta_0$ is absorbed by the structure without reflections

This operation implies the following three conditions on the metasurface. First, the specular nature of the reflection ($\theta_\mathrm{r} = \theta_\mathrm{i}$) requires that the metasurface has no phase gradient, which implies that it must be uniform. Second, the fact that there is only one scattered wave, and hence no diffraction orders, implies, assuming a periodic metasurface structure of period d,

that $d < |\lambda/(\sin\theta_\mathrm{i} \pm 1)|$. Third, the spatial asymmetry of the reflection implies breaking Lorentz reciprocity, which means that the metasurface must be nonreciprocal.
In addition, we assume that the metasurface is nongyrotropic, i.e., that it does not rotate the polarization of the incident wave upon reflection. Moreover, we shall consider only the p-polarized problem with incidence in the xz-plane, whose nonzero electromagnetic field components are E_x, E_z and H_y, the s-polarized problem being solvable in an analog fashion.

Required Susceptibility Components

To realize the proposed specular isolator, the susceptibility components should be independent on x and y to satisfy the metasurface uniformity condition. Moreover, the required nonreciprocity implies the global condition [14, 128]

$$\overline{\overline{\chi}}_\mathrm{ee} \neq \overline{\overline{\chi}}_\mathrm{ee}^T, \quad \overline{\overline{\chi}}_\mathrm{mm} \neq \overline{\overline{\chi}}_\mathrm{mm}^T \quad \text{or} \quad \overline{\overline{\chi}}_\mathrm{em} \neq -\overline{\overline{\chi}}_\mathrm{me}^T. \tag{7.20}$$

The nongyrotropy and p-polarized incidence assumptions eliminate 24 out of the 36 susceptibility components, simplifying the bianisotropic susceptibility tensors to

$$\overline{\overline{\chi}}_\mathrm{ee} = \begin{bmatrix} \chi_\mathrm{ee}^{xx} & 0 & \chi_\mathrm{ee}^{xz} \\ 0 & 0 & 0 \\ \chi_\mathrm{ee}^{zx} & 0 & \chi_\mathrm{ee}^{zz} \end{bmatrix}, \quad \overline{\overline{\chi}}_\mathrm{em} = \begin{bmatrix} 0 & \chi_\mathrm{em}^{xy} & 0 \\ 0 & 0 & 0 \\ 0 & \chi_\mathrm{em}^{zy} & 0 \end{bmatrix}, \tag{7.21a}$$

$$\overline{\overline{\chi}}_\mathrm{me} = \begin{bmatrix} 0 & 0 & 0 \\ \chi_\mathrm{me}^{yx} & 0 & \chi_\mathrm{me}^{yz} \\ 0 & 0 & 0 \end{bmatrix}, \quad \overline{\overline{\chi}}_\mathrm{mm} = \begin{bmatrix} 0 & 0 & 0 \\ 0 & \chi_\mathrm{mm}^{yy} & 0 \\ 0 & 0 & 0 \end{bmatrix}, \tag{7.21b}$$

which include overall 9 parameters, where the nonreciprocity condition (7.20) translate into

$$\chi_\mathrm{ee}^{xz} \neq \chi_\mathrm{ee}^{zx}, \quad \chi_\mathrm{em}^{xy} \neq -\chi_\mathrm{me}^{yx} \quad \text{or} \quad \chi_\mathrm{em}^{zy} \neq -\chi_\mathrm{me}^{yz}. \tag{7.22}$$

The corresponding metasurface for the s-polarization would involve the dual susceptibility components χ_mm^{xx}, χ_mm^{xz}, χ_mm^{zx}, χ_mm^{zz}, χ_em^{yx}, χ_em^{yz}, χ_me^{xy}, χ_me^{zy} and χ_ee^{yy}, with the nonreciprocity condition $\chi_\mathrm{mm}^{xz} \neq \chi_\mathrm{mm}^{zx}$, $\chi_\mathrm{em}^{yx} \neq -\chi_\mathrm{me}^{xy}$ or $\chi_\mathrm{em}^{yz} \neq -\chi_\mathrm{me}^{zy}$.
Inserting (3.2) into (3.1) with (7.21) leads the following explicit scalar GSTC equations

$$\Delta H_y = -j\omega\epsilon\chi_\mathrm{ee}^{xx} E_{\mathrm{av},x} - j\omega\epsilon\chi_\mathrm{ee}^{xz} E_{\mathrm{av},z} - jk\chi_\mathrm{em}^{xy} H_{\mathrm{av},y}, \tag{7.23a}$$

$$\begin{aligned} \Delta E_x = &- j\omega\mu\chi_\mathrm{mm}^{yy} H_{\mathrm{av},y} - jk\chi_\mathrm{me}^{yx} E_{\mathrm{av},x} - jk\chi_\mathrm{me}^{yz} E_{\mathrm{av},z} \\ &- \chi_\mathrm{ee}^{xz}\partial_x E_{\mathrm{av},z} - \chi_\mathrm{ee}^{zz}\partial_x E_{\mathrm{av},z} - \eta\chi_\mathrm{em}^{zy}\partial_x H_{\mathrm{av},y}, \end{aligned} \tag{7.23b}$$

where ∂_x denotes the spatial derivative versus x. Assuming plane wave incidence, which allows the substitution $\partial_x \to -jk_x$, where $k_x = k\sin\theta$, reduces then (7.23) to

$$\Delta H_y = -j\omega\epsilon\chi_{\rm ee}^{xx}E_{{\rm av},x} - j\omega\epsilon\chi_{\rm ee}^{xz}E_{{\rm av},z} - jk\chi_{\rm em}^{xy}H_{{\rm av},y}, \tag{7.24a}$$

$$\begin{aligned}\Delta E_x = &- j\omega\mu\chi_{\rm mm}^{yy}H_{{\rm av},y} - jk\chi_{\rm me}^{yx}E_{{\rm av},x} - jk\chi_{\rm me}^{yz}E_{{\rm av},z}\\ &+ jk_x\chi_{\rm ee}^{xz}E_{{\rm av},z} + jk_x\chi_{\rm ee}^{zz}E_{{\rm av},z} + jk_x\eta\chi_{\rm em}^{zy}H_{{\rm av},y},\end{aligned} \tag{7.24b}$$

which are the final GSTCs equations for the problem at hand.
In these relations, the field differences and averages are found from (3.3) in terms of the reflection and transmission coefficients, R and T. Assuming incidence in the $+z$ direction, theses quantities read

$$\Delta E_x = \frac{k_z}{k}(T-1-R), \tag{7.25a}$$

$$\Delta H_y = (-1+R+T)/\eta, \tag{7.25b}$$

$$E_{{\rm av},x} = \frac{k_z}{2k}(1+R+T), \tag{7.25c}$$

$$E_{{\rm av},z} = \frac{k_x}{2k}(1+T-R), \tag{7.25d}$$

$$H_{{\rm av},y} = (1+T-R)/2\eta, \tag{7.25e}$$

where $k_z = k\cos\theta$. Substituting (7.25) into (7.24), and solving for R gives [131]

$$\begin{aligned}R =&\frac{2}{C}\{k_x^2\chi_{\rm ee}^{zz} - k_z^2\chi_{\rm ee}^{xx} - k_z[k_x(\chi_{\rm ee}^{xz}-\chi_{\rm ee}^{zx}) - k(\chi_{\rm em}^{xy}-\chi_{\rm me}^{yx})]\\ &- kk_x(\chi_{\rm em}^{zy}+\chi_{\rm me}^{yz}) + k^2\chi_{\rm mm}^{yy}\},\end{aligned} \tag{7.26a}$$

where

$$\begin{aligned}C =&2[k_z^2\chi_{\rm ee}^{xx} + k_x^2\chi_{\rm ee}^{zz} - kk_x(\chi_{\rm em}^{zy}+\chi_{\rm me}^{yz}) + k^2\chi_{\rm mm}^{yy}]\\ &+ k^2(\chi_{\rm ee}^{xx}\chi_{\rm mm}^{yy} - \chi_{\rm em}^{xy}\chi_{\rm me}^{yx}) - jk_z\{k_x^2(\chi_{\rm ee}^{xz}\chi_{\rm ee}^{zx} - \chi_{\rm ee}^{xx}\chi_{\rm ee}^{zz})\\ &+ 4 - kk_x[\chi_{\rm ee}^{zx}\chi_{\rm em}^{xy} + \chi_{\rm ee}^{xz}\chi_{\rm me}^{yx} - \chi_{\rm ee}^{xx}(\chi_{\rm em}^{zy}+\chi_{\rm me}^{yz})]\}.\end{aligned} \tag{7.26b}$$

Realizing the specular isolation operation (see Fig. 7.9) requires breaking the symmetry of the reflection coefficient with respect to x or, equivalently, with respect to k_x. In other words, the reflection coefficient (7.26) must be a non-even function of k_x, i.e.,

$$R(k_x) \neq R(-k_x). \tag{7.27}$$

Inspecting (7.26) reveals that this condition requires

$$\chi_{\mathrm{ee}}^{xz} \neq \chi_{\mathrm{ee}}^{zx} \quad \text{or} \quad \chi_{\mathrm{em}}^{zy} \neq -\chi_{\mathrm{me}}^{yz}, \tag{7.28}$$

which correspond to the first and third relations in (7.22), respectively. Thus, breaking reciprocity in reflection can be accomplished only via *normal* susceptibilities (under the prevailing nongyrotropy assumption). It can be shown that the second relation in (7.22), involving tangential susceptibilities, breaks reciprocity in the z-direction [131], which is useful for transmission-type nonreciprocity like in Sec. 7.2.

Metasurface Design

Susceptibility Derivation

We shall specify two field transformations related to the desired operation in Fig. 7.9. The first field transformation is the specular reflection of the wave incident in the $+z$-direction at the operation angle θ_0 [Fig. 7.9 (a)]. The related fields are

$$\mathbf{E}_{1,\mathrm{i}} = \cos\theta_0 e^{-jk_x x}\hat{x} - \sin\theta_0 e^{-jk_x x}\hat{z}, \quad \mathbf{H}_{1,\mathrm{i}} = (e^{-jk_x x}/\eta)\hat{y}, \tag{7.29a}$$

$$\mathbf{E}_{1,\mathrm{r}} = -\cos\theta_0 e^{j\phi} e^{-jk_x x}\hat{x} - \sin\theta_0 e^{j\phi} e^{-jk_x x}\hat{z}, \quad \mathbf{H}_{1,\mathrm{r}} = (e^{j\phi} e^{-jk_x x}/\eta)\hat{y}, \tag{7.29b}$$

where ϕ is the reflection phase induced by the metasurface. The second transformation is the absorption of the wave incident at the angle $-\theta_0$ [Fig. 7.9 (b)]. The related fields are

$$\mathbf{E}_{2,\mathrm{i}} = \cos\theta_0 e^{-jk_x x}\hat{x} + \sin\theta_0 e^{-jk_x x}\hat{z}, \quad \mathbf{H}_{2,\mathrm{i}} = (e^{-jk_x x}/\eta)\hat{y}, \tag{7.30a}$$

$$\mathbf{E}_{2,\mathrm{r}} = 0, \quad \mathbf{H}_{2,\mathrm{r}} = 0. \tag{7.30b}$$

Successively substituting both (7.29) and (7.30) into (3.3) and inserting the resulting expressions into (7.24) leads a system of $2 \times 2 = 4$ scalar equations with 9 unknowns. This is an underdetermined system with an infinite number of possible sets of susceptibilities. Since the operation of the metasurface has been completely determined at θ_0, these sets correspond to different responses at other (unspecified) angles of incidence, and represent therefore degrees of freedom, which may be generally leveraged in the design of the metaparticle. Among these degrees of freedom, the parameters χ_{em}^{xy} and χ_{me}^{yx} correspond to structural asymmetry along the z-direction [131], which would imply considerable complexity in the metaparticle design. Therefore, we heuristically set these parameters to zero ($\chi_{\mathrm{em}}^{xy} = \chi_{\mathrm{me}}^{yx} = 0$). This reduces the number of unknowns to 7, which we shall maintain as degrees of freedom at this point. The

resulting system of equations leads to the 2 explicit susceptibility solutions

$$\chi_{\text{ee}}^{xx} = \frac{-2j(1+e^{j\phi})\sec\theta_0}{k}, \tag{7.31a}$$

$$\chi_{\text{ee}}^{xz} = \frac{2je^{j\phi}\csc\theta_0}{k}, \tag{7.31b}$$

and to the 2 constraint relations

$$\chi_{\text{mm}}^{yy} = -\frac{2j\cos\theta_0 + k\chi_{\text{ee}}^{zz}\sin^2\theta_0 + e^{j\phi}k\sin\theta_0(\chi_{\text{ee}}^{zx}\cos\theta_0 + \chi_{\text{ee}}^{zz}\sin\theta_0)}{(1+e^{j\phi})k}, \tag{7.31c}$$

$$\chi_{\text{em}}^{zy} = -\frac{k\chi_{\text{me}}^{yz} + k\chi_{\text{ee}}^{zx}\cos\theta_0 + e^{j\phi}(k\chi_{\text{me}}^{yz} + 2j\cot\theta_0)}{(1+e^{j\phi})k}, \tag{7.31d}$$

between the remaining 5 susceptibilities.

Transistor-loaded Metaparticle

The metaparticle structure satisfying the condition (7.28) (nonreciprocity along the x-direction for p-polarization) and the relations (7.31) (reflection and absorption at $\pm\theta_0$) may be devised as follows. Let us start by enforcing the first nonreciprocity condition in (7.28), namely $\chi_{\text{ee}}^{xz} \neq \chi_{\text{ee}}^{zx}$. This condition implies the existence of nonreciprocally related electric dipole responses along x and z, which immediately suggests an L-shape conducting structure loaded by a transistor in the xz-plane; this configuration is incidentally consistent with (7.31a) and (7.31b). Such a structure implies in particular a χ_{ee}^{zz} response, which generally implies in turn a χ_{mm}^{yy} response according to (7.31c). The latter corresponds to a y-directed magnetic dipole moment, which prompts us to close the L-shape into a loop in the xz-plane. We shall leave the loop open, as is customarily done for compactness in ring resonators, and we shall terminate the opened ends of the resulting U-shaped loop by T-shaped strips to reduce the size of the metaparticle.

All these considerations lead to the metaparticle structure represented in Fig. 7.10, which is composed of conducting strips in the three directions of space, with the spacing between the two xy-plane metallization planes being much smaller than the wavelength ($v \ll l < \lambda$, figure not to scale). We shall next analyze this metaparticle in details to verify that it indeed satisfies all the required conditions and to fully characterize it. Figure 7.10 decomposes the excitations (incident fields) and responses (dipole moments) in order to determine how the metaparticle realizes the sought after nonreciprocal susceptibility components, although all of the excitations and responses naturally occur simultaneously. Using this approach, we shall

next examine the polarizability responses of the isolated metaparticle, which are directly related to the susceptibilities of the metasurface formed by its periodic repetition [128].

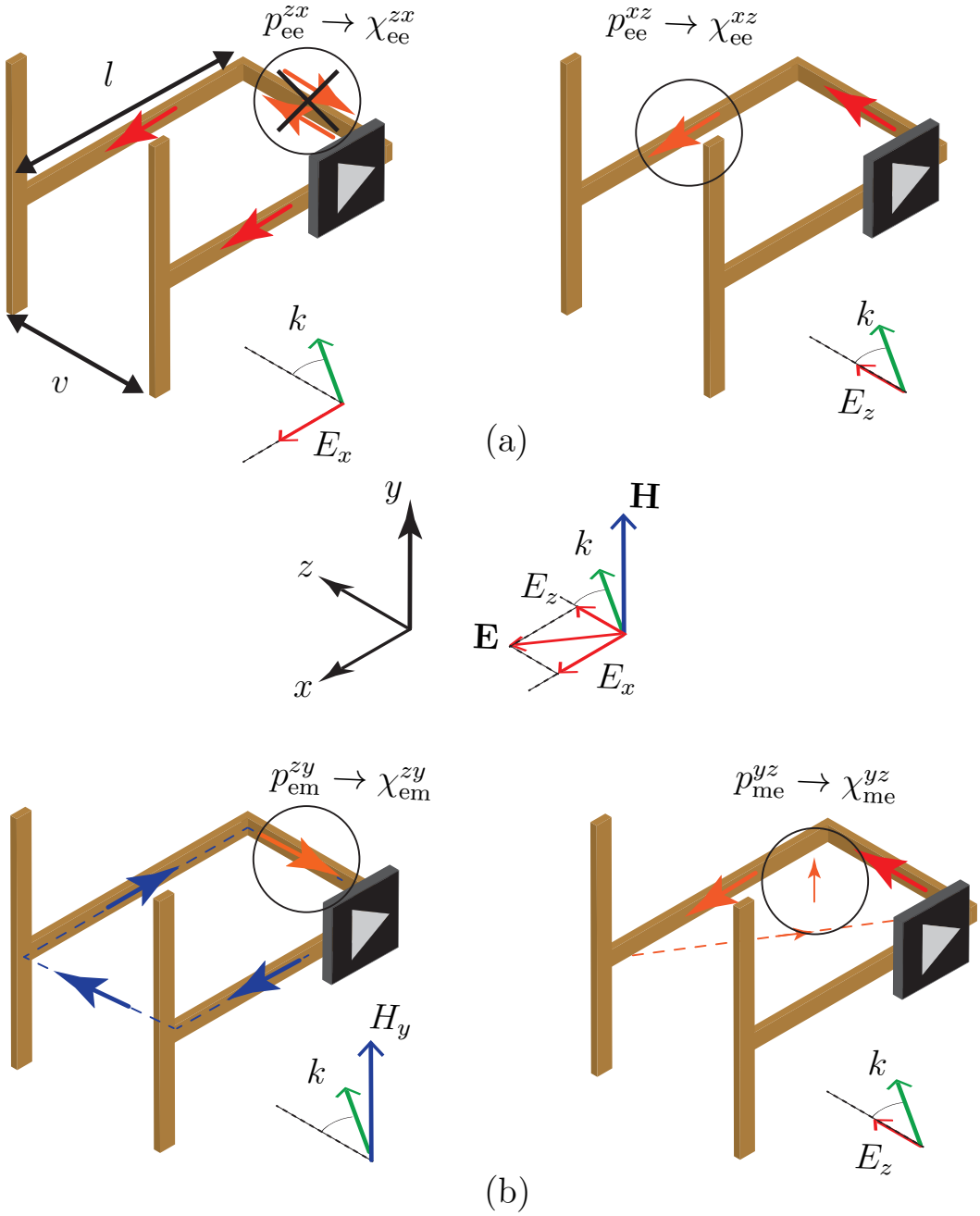

Figure 7.10 Operation principle of the transistor-loaded metaparticle, with orientation corresponding to Fig. 7.9 (a) Excitation E_x (left) and E_z (right), showing that $\chi_{ee}^{zx} \neq \chi_{ee}^{xz}$ (b) Excitation from H_y (left) and E_z (right), showing that $\chi_{em}^{zy} \neq -\chi_{me}^{yz}$

Figure 7.10 (a)[1] depicts the operation principle of the metaparticle realizing a response of the type $\chi_{\rm ee}^{xz} \neq \chi_{\rm ee}^{zx}$. On the left, the x-directed incident electric field induces in-phase ($v \ll \lambda$) currents in the two x-directed strips. When they reach the z-directed strip, these currents cancel out, which implies that the electric response along z to the electric excitation along x is zero ($p_{\rm ee}^{zx} = 0 \rightarrow \chi_{\rm ee}^{zx} = 0$). On the right, the z-directed incident electric field induces a current in the z-directed strip. This induces a current only in one of the x-directed strips, given the orientation of the transistor, which implies that the electric response along x to the electric field along z is nonzero ($p_{\rm ee}^{xz} \neq 0 \rightarrow \chi_{\rm ee}^{xz} \neq 0$). Thus, the metaparticle corresponds to a specific set of solutions of (7.31c) and (7.31d) that is characterized by $\chi_{\rm ee}^{zx} = 0$, which simplifies these constraint equations to

$$\chi_{\rm mm}^{yy} = -\frac{2j\cos\theta_0 + (1+e^{j\phi})k\chi_{\rm ee}^{zz}\sin^2\theta_0}{(1+e^{j\phi})k}, \tag{7.32a}$$

and

$$\chi_{\rm em}^{zy} = -\chi_{\rm me}^{yz} - \frac{2je^{j\phi}\cot\theta_0}{(1+e^{j\phi})k}. \tag{7.32b}$$

Equation (7.32b) reveals that the metaparticle must also satisfy the second nonreciprocity condition in (7.28). Let us see whether this is indeed the case with the help of Fig. 7.10 (b). On the left, the y-directed incident magnetic field induces a current in the metaparticle loop. The current flowing in the z-directed strip implies an electric response along z due to the magnetic excitation along y ($p_{\rm em}^{zy} \rightarrow \chi_{\rm em}^{zy}$). On the right, the z-directed incident electric field induces a current in z-directed strip. This can induce a current only in one of the two x-directed strips given the to the orientation of the transistor, which produces only a weak magnetic loop along y ($p_{\rm me}^{yz} \rightarrow \chi_{\rm me}^{yz}$). This implies that $\chi_{\rm em}^{zy} \neq -\chi_{\rm me}^{yz}$, which is consistent with the requirement of (7.32b).

We have thus found that the metasurface constituted of the heuristic metaparticle shown in Fig. 7.10 breaks reciprocity in two distinct fashions, through $\chi_{\rm ee}^{zx} \neq \chi_{\rm ee}^{xz}$ and $\chi_{\rm me}^{yz} \neq \chi_{\rm em}^{zy}$. These two types of nonreciprocity represent, both in isolation and in combination, novel metasurface nonreciprocal responses. Moreover, these responses, involving normal susceptibility components, were deemed particularly difficult to realize in practice [131]. The asymmetry of the electric susceptibility tensor, $\overline{\overline{\chi}}_{\rm ee} \neq \overline{\overline{\chi}}_{\rm ee}^{\rm T}$, also appears in magnetized plasmas, but conjunctly with gyrotropy, while the non-antisymmetry between the magneto-electric susceptibility tensors, $\overline{\overline{\chi}}_{\rm em} \neq -\overline{\overline{\chi}}_{\rm me}^{\rm T}$, also appears in the transmissive nonreciprocal metasurface in [151], but in terms of tangential nonreciprocal components.

Figure 7.11 shows the metasurface unit cell of our experimental prototype. This unit cell

[1]The drawing is not to scale: in reality, $v \ll l$. The notation $p_{\rm em}^{zy}$ represents the z component of the electric dipole response due to the y component of the magnetic field excitation, and so on.

corresponds to the metaparticle in Fig. 7.10, except for the additional supporting substrate, backing ground plane and conducting front frame, where the ground plane ensures impenetrability of the structure for all angles of incidence (extra specification) and the front frame isolates the unit cells from each other (hence ensuring direct correspondence between the polarizabilities and the susceptibilities). The parameters of the unit cell were optimized to satisfy (7.31a) and (7.31b) and one of the possible solutions of (7.32).

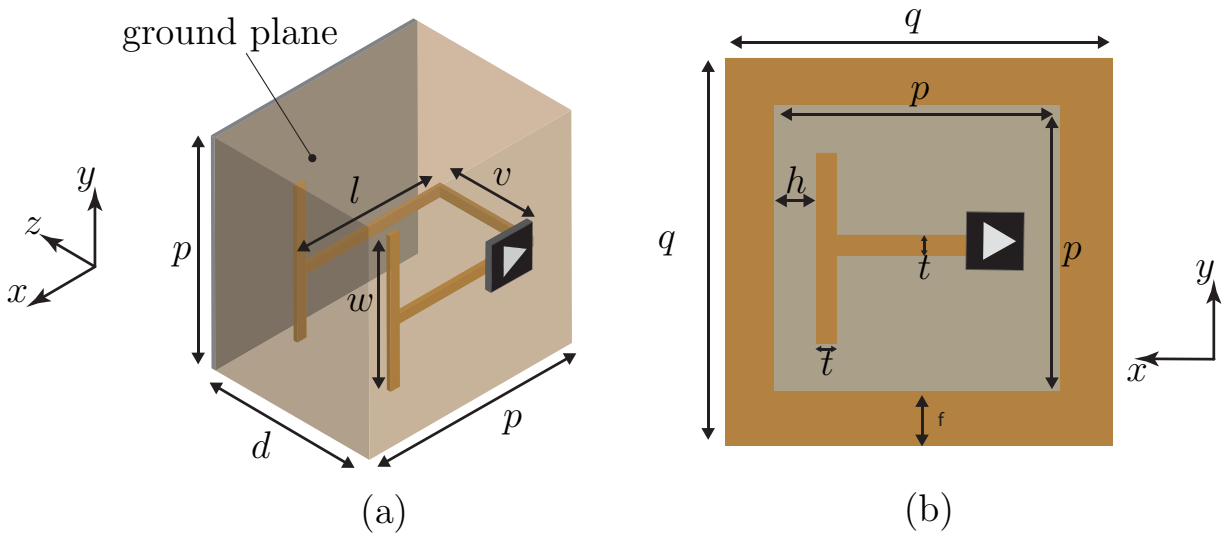

Figure 7.11 Unit cell corresponding to the metaparticle in Fig. 7.10, within a substrate of relative permittivity $\epsilon_{\mathrm{r}} = 4.5$, backed by a ground plane and with a front conducting frame (a) Perspective view (without the front frame, for visibility) (b) Top view

Simulation and Experiment

The transistor-loaded unit cell in Fig. 7.11 was simulated with periodic boundary conditions using a full-wave electromagnetic simulator (CST Microwave Studio) and the unilateral transistor circuit was modelled as an ideal isolator with a phase shifter. An FR4 slab with $\epsilon_r = 4.5$ was used as the substrate and the geometrical parameters of the metasurface were optimized to realize the specular isolation operation. The metasurface was designed to provide specular isolation between the angles $\pm 18^\circ$ at the frequency of $f_0^{\mathrm{sim}} = 6.56$ GHz for p-polarization. Figure 7.12 presents the simulation results. Figure 7.12(a) shows the isolation response versus frequency, with the isolation $R(-18^\circ)/R(+18^\circ)$ (see Fig. 7.9) reaching 41.75 dB at f_0^{sim}. Figure 7.12(b) shows the angular response of the reflection coefficient at the operating frequency of f_0^{sim}, whose strong asymmetry with respect to broadside ($\theta_{\mathrm{i}} = 0$) is the expected signature of the device.

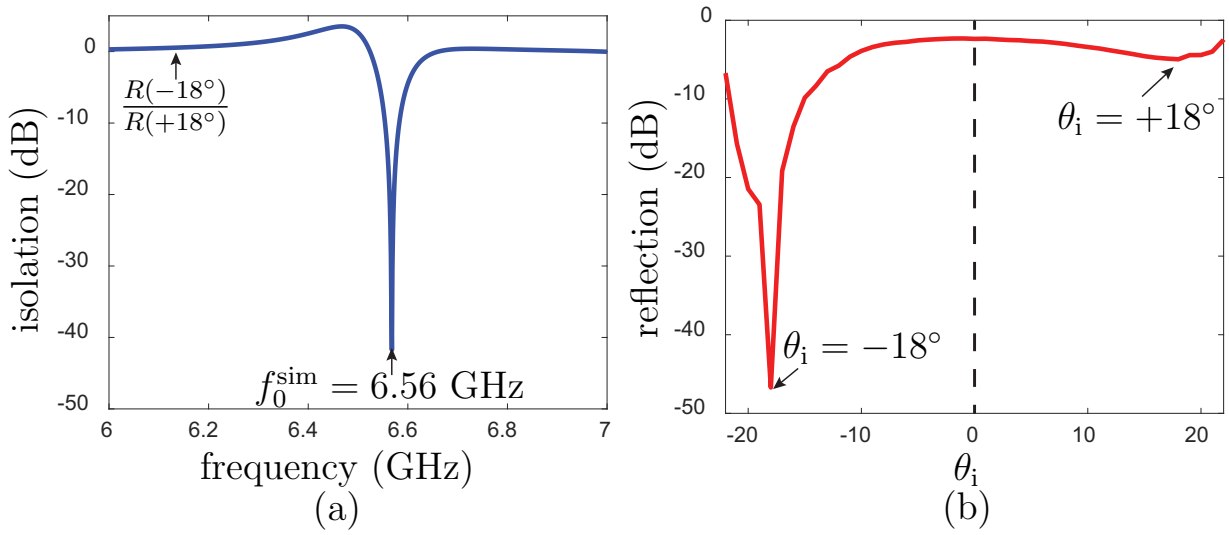

Figure 7.12 Full-wave simulation of the specular isolator with the unit cell in Fig. 7.11 and parameters $p = 22.5$ mm, $w = 14$ mm, $l = 20$ mm, $v = 1.6$ mm, $d = 3.2$ mm, $q = 32.5$ mm, $h = 1$ mm and $t = 2$ mm (a) Isolation versus frequency for incidence at $\theta_{\text{i}} = \pm 18°$ (design angle of isolation) (b) Specular reflection coefficient versus incidence angle (θ_{i}) at the operating frequency $f_0^{\text{sim}} = 6.58$ GHz

Figure 7.13 presents the experimental results[2]. Figure 7.13(a) shows the prototype, composed of 2×3 unit cells. It includes two FR4 substrates of thickness 1.6 mm glued together. The device was measured by a bistatic measurement system with two horn antennas symmetrically aiming (under the same angle with respect to the normal of the metasurface) at the metasurface. The reflection coefficient was measured for angles sweeping the sector extending $-22°$ to $22°$. Figure 7.13(b) shows the measured isolation ($|S_{12}|/|S_{21}|$) versus frequency for the incidence angle of $\theta_{\text{i}} = \pm 20°$. An isolation of more than 38 dB is observed at the frequency of $f_0^{\text{exp}} = 6.797$ GHz, whose discrepancy (0.217 GHz, i.e., 3.3%) may be explained by the small gap between the two substrates that was not taken into account in the simulation and by the difference between the actual transistor circuit response and the ideal isolator model used in simulation. Figure 7.13(c) shows the measured angular reflection coefficient at the operating frequency of f_0^{exp}. Here, the discrepancy translates into an angular difference ($2°$).

[2]The fabrication of the prototype and the measurements were performed by Toshiro Kodera in Meisei University, Japan.

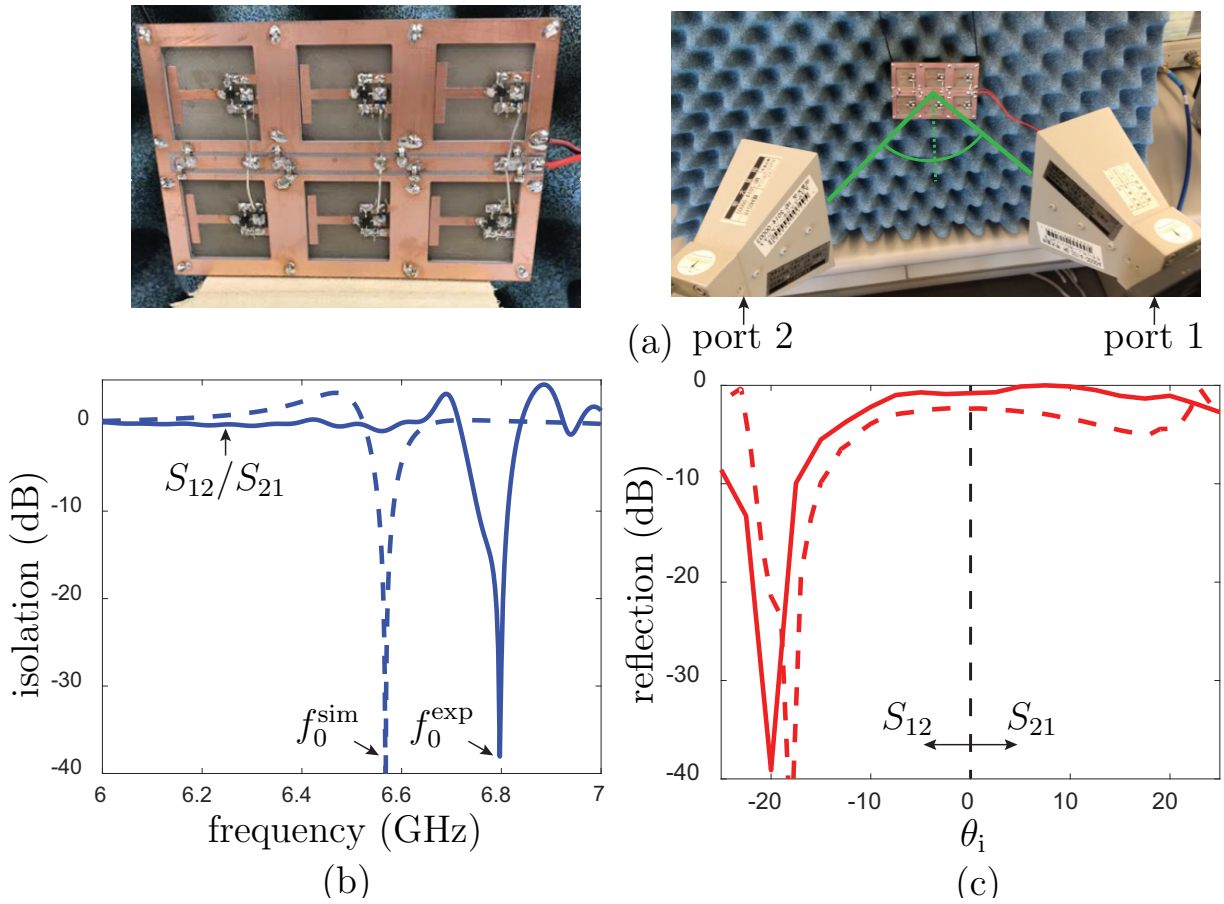

Figure 7.13 Experiment (a) Fabricated prototype (left) and experimental setup (right) (b) Isolation versus frequency for incidence at $\theta_{\text{i}} = \pm 20^{\circ}$ (maximal isolation angle) (c) Specular reflection coefficient versus incidence angle (θ_{i}) the operating frequency of $f_0^{\text{exp}} = 6.797$ GHz with the dashed lines corresponding to the simulation results of Fig. 7.12

CHAPTER 8 GENERAL DISCUSSION

This section will present a short general discussion, which will relate the contributions presented in the thesis with other works in the literature and discuss the main limitations. We shall separate the discussion in two parts. First, we will discuss the passive and reciprocal bianisotropic metasurfaces related to chapter 4 and chapter 5. Second, we will discuss the nonreciprocal bianisotropic metasurfaces related to chapter 6 and chapter 7.

Passive and Reciprocal Metasurfaces

The experimental demonstration of the bianisotropic refracting metasurfaces without spurious diffraction in chapter 4 was the conclusion of a decade of works by several researchers. The generalized law of refraction and reflection conceptualized in [49] sparked a large interest in metasurfaces for manipulating electromagnetic waves with phase gradients. However, it was soon realized that such simple symmetric structures had limited efficiency due to reflections and the excitations of undesired diffraction orders [10]. An initial attempt to get rid of the undesired diffraction orders was to include resistors in the metasurface design to realize a lossy structure at the cost of limited refraction efficiency [163]. It was then theoretically demonstrated that bianisotropic metasurfaces, which are asymmetric structures [12], could provide lossless, passive and reciprocal refraction with optimal efficiency [11, 147]. Hence, the main contributions of the work in chapter 4 was being the first experimental demonstration confirming the pertinency of bianisotropic metasurfaces for large-angle refraction and presenting a complete bianisotropic metasurface design method based on susceptibility tensors. While, chapter 4 only presented the case of the p-polarization, the solution for the s-polarization was given, by duality, in [127].

An alternative method to realize large-angle refraction is through the use of metagratings [164–168]. Those structures are typically composed of a single large scatterer that is properly designed to radiate only in the desired diffraction order. Hence, compared to bianisotropic metasurfaces that require multiple subwavelength unit cells to be realized, the metagratings have the benefit of simplicity and easier fabrication due to their fewer components. Metagratings are especially interesting for optical frequencies, where purely dielectric scatterers, which are generally bigger than their metallic counterparts, are preferred to avoid high plasmonic losses and for easier fabrication.

Nevertheless, bianisotropic metasurfaces of the type presented in chapters 4 and 5 have the advantage to be able to realize more sophisticated wave operations that go beyond wave deflection. As previously mentioned, any wave transformation that respects local power conservation can straightforwardly be realized by a single, passive, lossless and reciprocal bianisotropic metasurface [13]. Furthermore, the local power conservation condition can be lifted by either specifying additional auxiliary evanescent waves [115] or by using a pair of bianisotropic metasurfaces allowing multiple reflections between them [152, 153].
The generalization of the Brewster effect presented in chapter 5 is an example of a wave transformation that would not be properly implemented with metagratings since it requires a uniform structure with no diffraction orders composed of subwavelength scattering particles. Note that the susceptibilities presented in chapter 5 to realize the generalized Brewster effect is a particular solution of the generalized refraction susceptibilities of chapter 4 where the angle of refraction in the single medium is specified to follows Snell's law ($k_{ax} = k_{bx}$).
One of the main limitations of the passive and reciprocal bianisotropic metasurface is their bandwidth. Metasurfaces rely on resonant particles, which generally prevent the implementation of broadband devices. Furthermore, resonant metallic particles composing the metasurface, even when folded to reduce their sizes like in the metasurfaces of chapters 4 and 5, are still on the order of the wavelength of the operating frequency. For instance, the unit cells in chapters 4 and 5 are around $\lambda_0/5$, which represents what seems to be a good compromise between strong interaction and small size. This restriction in turn implies that wave transformations requiring susceptibilities rapid spatial variations might not be implementable due to the restriction of the minimum size of the resonators composing the different discretized unit cells.

Nonreciprocal Metasurfaces

Throughout chapter 6 and 7, we presented a few nonreciprocal metasurface operations that leveraged different nonreciprocal susceptibility responses and proposed transistor-loaded implementations for some of them. For linear time-invariant metasurfaces, nonreciprocity implies breaking at least one of the three tensorial relations from Eqs. (3.6) and we presented examples of distinct metasurfaces breaking all three of those tensorial conditions, which yielded different and complementary nonreciprocal responses.
First, in chapter 6 with the gyrotropic reflective isolator and in Sec. 7.1 with the transmissive Faraday rotator, we investigated tangential *gyrotropic* nonreciprocal responses related to asymmetric $\overline{\overline{\chi}}_{\text{ee}}$ and $\overline{\overline{\chi}}_{\text{mm}}$ tensors, which specifically meant $\chi_{\text{ee}}^{xy} \neq \chi_{\text{ee}}^{yx}$ and $\chi_{\text{mm}}^{xy} \neq \chi_{\text{mm}}^{yx}$. We discussed an example of a transistor-loaded metaparticle realizing simultaneous electric and magnetic nonreciprocal responses in chapter 6 and also presented a mirror-backed metasur-

face with only an electric response $\chi_{\text{ee}}^{xy} \neq \chi_{\text{ee}}^{yx}$ to realize the gyrotropic reflective isolator. This type of gyrotropic nonreciprocity with transistor-loaded resonators was first demonstrated in [197] with unilateral ring resonators and in [198] with cross-polarized dipoles for transmissive nonreciprocal gyrotropy. Note that this type of nonreciprocal response will always provide a rotation of the polarization due to its gyrotropic nature, which can be undesired for certain applications. In chapter 6 and in Sec. 7.1, we also theoretically investigated realizing the same metasurface operations but using alternative gyrotropic bianisotropic nonreciprocal responses of the type $\chi_{\text{em}}^{xx} \neq -\chi_{\text{me}}^{xx}$ and $\chi_{\text{em}}^{yy} \neq -\chi_{\text{me}}^{yy}$ (Tellegen-type). This type of nonreciprocal has yet to be experimentally demonstrated using transistor-loaded metasurfaces, but a potential metaparticle was proposed in [201]. The investigation of Tellegen-type nonreciprocal metasurfaces using transistor-loaded metaparticles remains a potential route for future research.

Next, in Sec. 7.2 with the nonreciprocal phase gradient metasurface, we investigated the tangential bianisotropic nonreciprocal responses of the type $\chi_{\text{em}}^{xy} \neq -\chi_{\text{me}}^{yx}$ and $\chi_{\text{em}}^{yx} \neq -\chi_{\text{me}}^{xy}$ (moving-type). This type of response is of particular interest since it represents the only tangential *nongyrotropic* nonreciprocal response, which can be desirable for metasurface applications where polarization rotation of the incident field is not needed. It can be used for nonreciprocal transmissive isolation with a transistor-loaded implementation as shown in [151, 205] and for nonreciprocal phase shifting as shown in Sec. 7.2, which can realize spatial circulation and nonreciprocal radiation patterns.

Finally, we also investigated *normal* nonreciprocal susceptibility responses in Sec. 7.3 with the realization of the nongyrotropic specular isolator. As far as we know, this work, which leveraged the responses $\chi_{\text{ee}}^{xz} \neq \chi_{\text{ee}}^{zx}$ and $\chi_{\text{em}}^{zy} \neq -\chi_{\text{me}}^{yz}$, represented the first demonstration of a metasurface with normal nonreciprocal responses. The demonstration of this novel type of nonreciprocal response which is able to provide an asymmetric angular reflection response [131] has the potential to unable different metasurface applications. A potentially particularly interesting area of application is in analog computing with metasurfaces, where realizing certain signal processing operations in reflection, such as differentiation and integration, have been shown to require this type of nonreciprocal response [104]. The investigation and design of appropriate transistor-loaded metaparticle to realize other normal nonreciprocal responses, including the ones required to realize the specular isolation operation for the s-polarization (specifically $\chi_{\text{mm}}^{xz} \neq \chi_{\text{mm}}^{zx}$ and $\chi_{\text{em}}^{yz} \neq -\chi_{\text{me}}^{zy}$), still represents an avenue for future research.

The main limitation of the transistor-loaded technology for metasurface applications is being restricted to microwave and mmWave frequencies for the foreseeable future. At this point, leveraging nonlinearity or space-time modulation appears to be the better suited non-

reciprocal technologies for nonreciprocal metasurfaces at optical frequencies. At microwave frequencies, a common critique of transistor-loaded structures for nonreciprociy is that they come with relatively high noise figures [182]. However, in many applications, such as for communications, the important factor is the signal to noise ratio (SNR). A transistor-loaded structure has the intrinsic ability of providing gain which could maintain a good SNR or even improve it. The investigation of metasurfaces with transistor-loaded resonators providing gain still represents an area for future research, where the issue of ensuring stability might prove practically challenging.

CHAPTER 9 CONCLUSION AND RECOMMENDATIONS

Summary of Works

This thesis presented several works related to the development of bianisotropic metasurfaces realizing both reciprocal and nonreciprocal responses.

Chapter 3 introduced the susceptibility-based generalized sheet transition conditions that were subsequently used to model and synthesize the metasurfaces in the rest of the thesis.

Chapter 4 presented bianisotropic metasurfaces realizing large-angle refraction with optimal efficiency. The corresponding susceptibility tensors were derived for the p-polarization problem and two related metasurfaces were designed. This work experimentally demonstrated that properly designed bianisotropic metasurfaces resolve the limited efficiency issue of previous phase gradient metasurfaces for generalized refraction.

Chapter 5 presented a generalization of the Brewster effect using bianisotropic metasurfaces placed at the interface between two media. The corresponding susceptibility tensors were derived to allow arbitrary control of the angle of incidence and polarization of the Brewster effect. The bianisotropic metasurfaces were demonstrated by full-wave simulations in the microwave regime. The proposed bianisotropic metasurfaces provided deeply subwavelength matching solutions for initially mismatched media.

Chapter 6 presented a metasurface realizing reflection isolation between the two orthogonal polarizations. A birefringent metasurface with its corresponding susceptibility tensors was designed to reflect vertically polarized incident waves into horizontally polarized waves, and absorb horizontally polarized incident waves. A mirror-backed transistor-loaded metaparticle implementation was proposed and the metasurface was demonstrated by full-wave simulations.

Chapter 7 presented complementary results related to nonreciprocal metasurfaces. First, the problem of a transmissive Faraday rotation metasurface was analyzed and two sets of susceptibility tensors realizing this operation were derived. Second, the concept of a nonreciprocal phase gradient metasurface composed of bianisotropic nonreciprocal phase shifting unit cells was presented with an implementation using an antenna-circuit-antenna architecture and its related full-wave simulation. Third, a nongyrotropic specular isolator metasurface was presented and its corresponding susceptibility tensors, which were required to include normal nonreciprocal components, were derived. A related transistor-loaded metaparticle was presented and validated by both full-wave simulations and experimental demonstration.

Future Research

Metasurfaces are part of a thriving area of research that will surely lead to a plethora of new applications and concepts in the future. Here, we provide a non-exhaustive list of possible future research directions:

- Investigate the problem of the limited bandwidth of metasurfaces with the aim to realize broadband metasurface operations. This would allow the realization of many practical applications requiring broadband responses.
- Develop a better understanding and techniques to relate the susceptibilities to the geometry of the scattering particles for both reciprocal and nonreciprocal metasurfaces.
- Investigate more deeply metasurfaces that include normal susceptibility responses. Due to the added complexity of synthesizing metasurfaces with normal components, few works have reported this type of response, particularly in the case of nonuniform metasurfaces. More complicated designs of this kind have the potential to realize multipurpose operations that would depend on the direction of propagation of the incident wave.
- Investigate still unreported nonreciprocal susceptibility responses with transistor-loaded metasurfaces. This includes Tellegen-type nonreciprocity and many nonreciprocal normal susceptibility responses beyond those presented in Sec. 7.3.
- Design transistor-loaded metasurfaces with the specific aim of providing gain. Active metasurfaces would provide potentially many useful responses, but could be practically challenging due to the issue of stability.

REFERENCES

[1] N. I. Zheludev and Y. S. Kivshar, "From metamaterials to metadevices," *Nat. Mater.*, vol. 11, no. 11, pp. 917–924, 2012.

[2] D. Schurig, J. J. Mock, B. Justice, S. A. Cummer, J. B. Pendry, A. F. Starr, and D. R. Smith, "Metamaterial electromagnetic cloak at microwave frequencies," *Science*, vol. 314, no. 5801, pp. 977–980, 2006.

[3] J. B. Pendry, "Negative refraction makes a perfect lens," *Phys. Rev. Lett.*, vol. 85, no. 18, p. 3966, 2000.

[4] C. L. Holloway, E. F. Kuester, J. A. Gordon, J. O'Hara, J. Booth, and D. R. Smith, "An overview of the theory and applications of metasurfaces: The two-dimensional equivalents of metamaterials," *IEEE Antennas and Propagation Magazine*, vol. 54, no. 2, pp. 10–35, 2012.

[5] N. Yu and F. Capasso, "Flat optics with designer metasurfaces," *Nat. Mater.*, vol. 13, no. 2, pp. 139–150, 2014.

[6] Y. Ra'di, C. R. Simovski, and S. A. Tretyakov, "Thin perfect absorbers for electromagnetic waves: theory, design, and realizations," *Phys. Rev. Appl.*, vol. 3, no. 3, p. 037001, 2015.

[7] C. Pfeiffer and A. Grbic, "Bianisotropic metasurfaces for optimal polarization control: analysis and synthesis," *Phys. Rev. Applied*, vol. 2, no. 4, p. 044011, 2014.

[8] X. Ni, A. V. Kildishev, and V. M. Shalaev, "Metasurface holograms for visible light," *Nature communications*, vol. 4, p. 2807, 2013.

[9] F. Monticone, N. M. Estakhri, and A. Alù, "Full control of nanoscale optical transmission with a composite metascreen," *Phys. Rev.letters*, vol. 110, no. 20, p. 203903, 2013.

[10] M. Selvanayagam and G. V. Eleftheriades, "Discontinuous electromagnetic fields using orthogonal electric and magnetic currents for wavefront manipulation," *Optics express*, vol. 21, no. 12, pp. 14 409–14 429, 2013.

[11] V. S. Asadchy, M. Albooyeh, S. N. Tcvetkova, A. Díaz-Rubio, Y. Ra'di, and S. Tretyakov, "Perfect control of reflection and refraction using spatially dispersive metasurfaces," *Phys. Rev. B*, vol. 94, no. 7, p. 075142, 2016.

[12] V. S. Asadchy, A. Díaz-Rubio, and S. A. Tretyakov, "Bianisotropic metasurfaces: physics and applications," *Nanophotonics*, vol. 7, no. 6, pp. 1069–1094, 2018.

[13] A. Epstein and G. V. Eleftheriades, "Arbitrary power-conserving field transformations with passive lossless omega-type bianisotropic metasurfaces," *IEEE Trans. Antennas Propag.*, vol. 64, no. 9, pp. 3880–3895, 2016.

[14] C. Caloz, A. Alù, S. Tretyakov, D. Sounas, K. Achouri, and Z.-L. Deck-Léger, "Electromagnetic nonreciprocity," *Phys. Rev. Appl.*, vol. 10, no. 4, p. 047001, 2018.

[15] B. Lax and K. J. Button, "Microwave ferrites and ferrimagnetics," 1962.

[16] C. Caloz and A. Alù, "Guest editorial special cluster on magnetless nonreciprocity in electromagnetics," *IEEE Antennas Wirel. Propag. Lett*, vol. 17, no. 11, pp. 1931–1937, 2018.

[17] A. V. Kildishev, A. Boltasseva, and V. M. Shalaev, "Planar photonics with metasurfaces," *Science*, vol. 339, no. 6125, p. 1232009, 2013.

[18] V. K. Valev, J. J. Baumberg, C. Sibilia, and T. Verbiest, "Chirality and chiroptical effects in plasmonic nanostructures: fundamentals, recent progress, and outlook," *Adv. Mater.*, vol. 25, no. 18, pp. 2517–2534, 2013.

[19] A. E. Minovich, A. E. Miroshnichenko, A. Y. Bykov, T. V. Murzina, D. N. Neshev, and Y. S. Kivshar, "Functional and nonlinear optical metasurfaces," *Laser & Photonics Reviews*, vol. 9, no. 2, pp. 195–213, 2015.

[20] S. Tretyakov, "Metasurfaces for general transformations of electromagnetic fields," *Philosophical Transactions of the Royal Society A: Mathematical, Physical and Engineering Sciences*, vol. 373, no. 2049, p. 20140362, 2015.

[21] S. B. Glybovski, S. A. Tretyakov, P. A. Belov, Y. S. Kivshar, and C. R. Simovski, "Metasurfaces: From microwaves to visible," *Phys. Rep*, vol. 634, pp. 1–72, 2016.

[22] H.-T. Chen, A. J. Taylor, and N. Yu, "A review of metasurfaces: physics and applications," *Rep. Prog. Phys.*, vol. 79, no. 7, p. 076401, 2016.

[23] A. Epstein and G. V. Eleftheriades, "Huygens' metasurfaces via the equivalence principle: design and applications," *JOSA B*, vol. 33, no. 2, pp. A31–A50, 2016.

[24] F. Monticone and A. Alu, "Metamaterial, plasmonic and nanophotonic devices," *Rep. Prog. Phys.*, vol. 80, no. 3, p. 036401, 2017.

[25] K. Achouri and C. Caloz, "Design, concepts, and applications of electromagnetic metasurfaces," *Nanophotonics*, vol. 7, no. 6, pp. 1095–1116, 2018.

[26] M. Chen, M. Kim, A. M. Wong, and G. V. Eleftheriades, "Huygens' metasurfaces from microwaves to optics: a review," *Nanophotonics*, vol. 7, no. 6, pp. 1207–1231, 2018.

[27] B. A. Munk, *Finite antenna arrays and FSS*. John Wiley & Sons, 2003.

[28] B. A. Munk, *Frequency selective surfaces: theory and design*. John Wiley & Sons, 2005.

[29] M. Li, M. A. Al-Joumayly, and N. Behdad, "Broadband true-time-delay microwave lenses based on miniaturized element frequency selective surfaces," *IEEE Trans. Antennas Propag.*, vol. 61, no. 3, pp. 1166–1179, 2012.

[30] M. Li and N. Behdad, "Wideband true-time-delay microwave lenses based on metallo-dielectric and all-dielectric lowpass frequency selective surfaces," *IEEE Trans. Antennas Propag.*, vol. 61, no. 8, pp. 4109–4119, 2013.

[31] A. K. Rashid, B. Li, and Z. Shen, "An overview of three-dimensional frequency-selective structures," *IEEE Antennas Propag. Mag.*, vol. 56, no. 3, pp. 43–67, 2014.

[32] D. Berry, R. Malech, and W. Kennedy, "The reflectarray antenna," *IEEE Trans. Antennas Propag.*, vol. 11, no. 6, pp. 645–651, 1963.

[33] J. Huang and J. A. Encinar, *Reflectarray antennas*. John Wiley & Sons, 2007.

[34] S. V. Hum and J. Perruisseau-Carrier, "Reconfigurable reflectarrays and array lenses for dynamic antenna beam control: A review," *IEEE Trans. Antennas Propag.*, vol. 62, no. 1, pp. 183–198, 2013.

[35] D. Pozar, "Flat lens antenna concept using aperture coupled microstrip patches," *Electron. Lett.*, vol. 32, no. 23, pp. 2109–2111, 1996.

[36] C. G. Ryan, M. R. Chaharmir, J. Shaker, J. R. Bray, Y. M. Antar, and A. Ittipiboon, "A wideband transmitarray using dual-resonant double square rings," *IEEE Trans. Antennas Propag.*, vol. 58, no. 5, pp. 1486–1493, 2010.

[37] T. K. Gaylord and M. Moharam, "Analysis and applications of optical diffraction by gratings," *Proc. IEEE*, vol. 73, no. 5, pp. 894–937, 1985.

[38] M. Neviere, "Electromagnetic study of transmission gratings," *Appl. Opt.*, vol. 30, no. 31, pp. 4540–4547, 1991.

[39] N. Destouches, A. Tishchenko, J. Pommier, S. Reynaud, O. Parriaux, S. Tonchev, and M. A. Ahmed, "99% efficiency measured in the-1 st order of a resonant grating," *Opt. Express*, vol. 13, no. 9, pp. 3230–3235, 2005.

[40] C. Pfeiffer and A. Grbic, "Millimeter-wave transmitarrays for wavefront and polarization control," *IEEE Trans. Microw. Theory Tech.*, vol. 61, no. 12, pp. 4407–4417, 2013.

[41] C. Pfeiffer and A. Grbic, "Cascaded metasurfaces for complete phase and polarization control," *Appl. Phys. Lett.*, vol. 102, no. 23, p. 231116, 2013.

[42] T. Niemi, A. O. Karilainen, and S. A. Tretyakov, "Synthesis of polarization transformers," *IEEE Trans. Antennas Propag.*, vol. 61, no. 6, pp. 3102–3111, 2013.

[43] C. Pfeiffer, C. Zhang, V. Ray, L. J. Guo, and A. Grbic, "High performance bianisotropic metasurfaces: asymmetric transmission of light," *Phys. Rev.letters*, vol. 113, no. 2, p. 023902, 2014.

[44] M. Selvanayagam and G. V. Eleftheriades, "Polarization control using tensor huygens surfaces," *IEEE Trans. Antennas Propag.*, vol. 62, no. 12, pp. 6155–6168, 2014.

[45] A. Arbabi, Y. Horie, M. Bagheri, and A. Faraon, "Dielectric metasurfaces for complete control of phase and polarization with subwavelength spatial resolution and high transmission," *Nature nanotechnology*, vol. 10, no. 11, p. 937, 2015.

[46] M. Selvanayagam and G. V. Eleftheriades, "Design and measurement of tensor impedance transmitarrays for chiral polarization control," *IEEE Trans. Microw. Theory Tech.*, vol. 64, no. 2, pp. 414–428, 2015.

[47] A. Díaz-Rubio, V. S. Asadchy, A. Elsakka, and S. A. Tretyakov, "From the generalized reflection law to the realization of perfect anomalous reflectors," *Science advances*, vol. 3, no. 8, p. e1602714, 2017.

[48] V. S. Asadchy, A. Wickberg, A. Díaz-Rubio, and M. Wegener, "Eliminating scattering loss in anomalously reflecting optical metasurfaces," *ACS Photonics*, vol. 4, no. 5, pp. 1264–1270, 2017.

[49] N. Yu, P. Genevet, M. A. Kats, F. Aieta, J.-P. Tetienne, F. Capasso, and Z. Gaburro, "Light propagation with phase discontinuities: generalized laws of reflection and refraction," *science*, vol. 334, no. 6054, pp. 333–337, 2011.

[50] H. Shi, J. Li, A. Zhang, Y. Jiang, J. Wang, Z. Xu, and S. Xia, "Gradient metasurface with both polarization-controlled directional surface wave coupling and anomalous reflection," *IEEE Antennas and Wireless Propagation Letters*, vol. 14, pp. 104–107, 2014.

[51] S. Sun, K.-Y. Yang, C.-M. Wang, T.-K. Juan, W. T. Chen, C. Y. Liao, Q. He, S. Xiao, W.-T. Kung, G.-Y. Guo *et al.*, "High-efficiency broadband anomalous reflection by gradient meta-surfaces," *Nano letters*, vol. 12, no. 12, pp. 6223–6229, 2012.

[52] C. Pfeiffer, N. K. Emani, A. M. Shaltout, A. Boltasseva, V. M. Shalaev, and A. Grbic, "Efficient light bending with isotropic metamaterial huygens' surfaces," *Nano letters*, vol. 14, no. 5, pp. 2491–2497, 2014.

[53] J. Shi, X. Fang, E. T. Rogers, E. Plum, K. F. MacDonald, and N. I. Zheludev, "Coherent control of snell's law at metasurfaces," *Optics express*, vol. 22, no. 17, pp. 21 051–21 060, 2014.

[54] Y. Ra'di, V. S. Asadchy, and S. A. Tretyakov, "Total absorption of electromagnetic waves in ultimately thin layers," *IEEE Trans. Antennas Propag.*, vol. 61, no. 9, pp. 4606–4614, 2013.

[55] M. Yazdi, M. Albooyeh, R. Alaee, V. Asadchy, N. Komjani, C. Rockstuhl, C. R. Simovski, and S. Tretyakov, "A bianisotropic metasurface with resonant asymmetric absorption," *IEEE Trans. Antennas Propag.*, vol. 63, no. 7, pp. 3004–3015, 2015.

[56] A. Li, S. Kim, Y. Luo, Y. Li, J. Long, and D. F. Sievenpiper, "High-power transistor-based tunable and switchable metasurface absorber," *IEEE Trans. Microw. Theory Tech.*, vol. 65, no. 8, pp. 2810–2818, 2017.

[57] V. S. Asadchy, I. A. Faniayeu, Y. Ra'Di, S. Khakhomov, I. Semchenko, and S. Tretyakov, "Broadband reflectionless metasheets: frequency-selective transmission and perfect absorption," *Phys. Rev.X*, vol. 5, no. 3, p. 031005, 2015.

[58] X. Wang, A. Díaz-Rubio, V. S. Asadchy, G. Ptitcyn, A. A. Generalov, J. Ala-Laurinaho, and S. A. Tretyakov, "Extreme asymmetry in metasurfaces via evanescent fields engineering: Angular-asymmetric absorption," *Phys. Rev.letters*, vol. 121, no. 25, p. 256802, 2018.

[59] F. Cuesta, A. Kuznetsov, G. Ptitcyn, X. Wang, and S. Tretyakov, "Coherent asymmetric absorbers," *arXiv preprint arXiv:2112.04916*, 2021.

[60] F. Aieta, P. Genevet, M. A. Kats, N. Yu, R. Blanchard, Z. Gaburro, and F. Capasso, "Aberration-free ultrathin flat lenses and axicons at telecom wavelengths based on plasmonic metasurfaces," *Nano letters*, vol. 12, no. 9, pp. 4932–4936, 2012.

[61] F. Aieta, P. Genevet, M. Kats, and F. Capasso, "Aberrations of flat lenses and aplanatic metasurfaces," *Optics express*, vol. 21, no. 25, pp. 31 530–31 539, 2013.

[62] M. Khorasaninejad, F. Aieta, P. Kanhaiya, M. A. Kats, P. Genevet, D. Rousso, and F. Capasso, "Achromatic metasurface lens at telecommunication wavelengths," *Nano letters*, vol. 15, no. 8, pp. 5358–5362, 2015.

[63] F. Aieta, M. A. Kats, P. Genevet, and F. Capasso, "Multiwavelength achromatic metasurfaces by dispersive phase compensation," *Science*, vol. 347, no. 6228, pp. 1342–1345, 2015.

[64] S. Zhang, M.-H. Kim, F. Aieta, A. She, T. Mansuripur, I. Gabay, M. Khorasaninejad, D. Rousso, X. Wang, M. Troccoli *et al.*, "High efficiency near diffraction-limited mid-infrared flat lenses based on metasurface reflectarrays," *Optics express*, vol. 24, no. 16, pp. 18 024–18 034, 2016.

[65] J. Scheuer, "Metasurfaces-based holography and beam shaping: engineering the phase profile of light," *Nanophotonics*, vol. 6, no. 1, pp. 137–152, 2017.

[66] L. Huang, S. Zhang, and T. Zentgraf, "Metasurface holography: from fundamentals to applications," *Nanophotonics*, vol. 7, no. 6, pp. 1169–1190, 2018.

[67] L. Chen, S. Kanwal, B. Yu, J. Feng, C. Tao, J. Wen, and D. Zhang, "Generation of high-uniformity and high-resolution bessel beam arrays through all-dielectric metasurfaces," *Nanophotonics*, 2022.

[68] K. Achouri, B. A. Khan, S. Gupta, G. Lavigne, M. A. Salem, and C. Caloz, "Synthesis of electromagnetic metasurfaces: principles and illustrations," *EPJ Appl. Metamater.*, vol. 2, p. 12, 2015.

[69] P. Genevet, N. Yu, F. Aieta, J. Lin, M. A. Kats, R. Blanchard, M. O. Scully, Z. Gaburro, and F. Capasso, "Ultra-thin plasmonic optical vortex plate based on phase discontinuities," *Appl. Phys. Lett.*, vol. 100, no. 1, p. 013101, 2012.

[70] X. Yi, X. Ling, Z. Zhang, Y. Li, X. Zhou, Y. Liu, S. Chen, H. Luo, and S. Wen, "Generation of cylindrical vector vortex beams by two cascaded metasurfaces," *Optics express*, vol. 22, no. 14, pp. 17 207–17 215, 2014.

[71] C. Pfeiffer and A. Grbic, "Controlling vector bessel beams with metasurfaces," *Phys. Rev. Appl.*, vol. 2, no. 4, p. 044012, 2014.

[72] E. Karimi, S. A. Schulz, I. De Leon, H. Qassim, J. Upham, and R. W. Boyd, "Generating optical orbital angular momentum at visible wavelengths using a plasmonic metasurface," *Light: Science & Applications*, vol. 3, no. 5, p. e167, 2014.

[73] C. Pfeiffer and A. Grbic, "Generating stable tractor beams with dielectric metasurfaces," *Phys. Rev.B*, vol. 91, no. 11, p. 115408, 2015.

[74] M. Veysi, C. Guclu, and F. Capolino, "Vortex beams with strong longitudinally polarized magnetic field and their generation by using metasurfaces," *JOSA B*, vol. 32, no. 2, pp. 345–354, 2015.

[75] G. Zheng, H. Mühlenbernd, M. Kenney, G. Li, T. Zentgraf, and S. Zhang, "Metasurface holograms reaching 80% efficiency," *Nature nanotechnology*, vol. 10, no. 4, p. 308, 2015.

[76] P. Genevet and F. Capasso, "Holographic optical metasurfaces: a review of current progress," *Rep. Prog. Phys.*, vol. 78, no. 2, p. 024401, 2015.

[77] W. Wan, J. Gao, and X. Yang, "Metasurface holograms for holographic imaging," *Adv. Opt. Mater.*, vol. 5, no. 21, p. 1700541, 2017.

[78] G. Minatti, F. Caminita, M. Casaletti, and S. Maci, "Spiral leaky-wave antennas based on modulated surface impedance," *IEEE Trans. Antennas Propag.*, vol. 59, no. 12, pp. 4436–4444, 2011.

[79] G. Minatti, F. Caminita, E. Martini, M. Sabbadini, and S. Maci, "Synthesis of modulated-metasurface antennas with amplitude, phase, and polarization control," *IEEE Trans. Antennas Propag.*, vol. 64, no. 9, pp. 3907–3919, 2016.

[80] A. Epstein, J. P. Wong, and G. V. Eleftheriades, "Cavity-excited huygens' metasurface antennas for near-unity aperture illumination efficiency from arbitrarily large apertures," *Nat.comm.*, vol. 7, no. 1, pp. 1–10, 2016.

[81] A. Epstein and G. V. Eleftheriades, "Arbitrary antenna arrays without feed networks based on cavity-excited omega-bianisotropic metasurfaces," *IEEE Trans. Antennas Propag.*, vol. 65, no. 4, pp. 1749–1756, 2017.

[82] G. Minatti, M. Faenzi, E. Martini, F. Caminita, P. De Vita, D. González-Ovejero, M. Sabbadini, and S. Maci, "Modulated metasurface antennas for space: Synthesis,

analysis and realizations," *IEEE Trans. Antennas Propag.*, vol. 63, no. 4, pp. 1288–1300, 2014.

[83] A. H. Abdelrahman, A. Z. Elsherbeni, and F. Yang, "Transmitarray antenna design using cross-slot elements with no dielectric substrate," *IEEE Antennas and Wireless Propagation Letters*, vol. 13, pp. 177–180, 2014.

[84] M. Farmahini-Farahani and H. Mosallaei, "Birefringent reflectarray metasurface for beam engineering in infrared," *Optics letters*, vol. 38, no. 4, pp. 462–464, 2013.

[85] M. Faenzi, G. Minatti, D. González-Ovejero, F. Caminita, E. Martini, C. Della Giovampaola, and S. Maci, "Metasurface antennas: New models, applications and realizations," *Sci. Rep.*, vol. 9, no. 1, pp. 1–14, 2019.

[86] E. Basar, M. Di Renzo, J. De Rosny, M. Debbah, M.-S. Alouini, and R. Zhang, "Wireless communications through reconfigurable intelligent surfaces," *IEEE Access*, vol. 7, pp. 116 753–116 773, 2019.

[87] M. Di Renzo, M. Debbah, D.-T. Phan-Huy, A. Zappone, M.-S. Alouini, C. Yuen, V. Sciancalepore, G. C. Alexandropoulos, J. Hoydis, H. Gacanin *et al.*, "Smart radio environments empowered by reconfigurable ai meta-surfaces: An idea whose time has come," *EURASIP J. Wirel. Commun. Netw.*, vol. 2019, no. 1, pp. 1–20, 2019.

[88] M. Di Renzo, A. Zappone, M. Debbah, M.-S. Alouini, C. Yuen, J. De Rosny, and S. Tretyakov, "Smart radio environments empowered by reconfigurable intelligent surfaces: How it works, state of research, and the road ahead," *IEEE J. Sel. Areas Commun.*, vol. 38, no. 11, pp. 2450–2525, 2020.

[89] T. S. Almoneef and O. M. Ramahi, "Metamaterial electromagnetic energy harvester with near unity efficiency," *Appl. Phys. Lett.*, vol. 106, no. 15, p. 153902, 2015.

[90] L. Li, X. Zhang, C. Song, and Y. Huang, "Progress, challenges, and perspective on metasurfaces for ambient radio frequency energy harvesting," *Appl. Phys. Lett.*, vol. 116, no. 6, p. 060501, 2020.

[91] J. Zhou, P. Zhang, J. Han, L. Li, and Y. Huang, "Metamaterials and metasurfaces for wireless power transfer and energy harvesting," *Proc. IEEE*, 2021.

[92] P. Su, Y. Zhao, S. Jia, W. Shi, and H. Wang, "An ultra-wideband and polarization-independent metasurface for rcs reduction," *Sci. Rep.*, vol. 6, no. 1, pp. 1–8, 2016.

[93] X. Liu, J. Gao, L. Xu, X. Cao, Y. Zhao, and S. Li, "A coding diffuse metasurface for rcs reduction," *IEEE Antennas Wirel. Propag. Lett.*, vol. 16, pp. 724–727, 2016.

[94] H. Sun, C. Gu, X. Chen, Z. Li, L. Liu, B. Xu, and Z. Zhou, "Broadband and broad-angle polarization-independent metasurface for radar cross section reduction," *Sci. Rep.*, vol. 7, no. 1, pp. 1–9, 2017.

[95] A. Alù, "Mantle cloak: Invisibility induced by a surface," *Phys. Rev. B*, vol. 80, no. 24, p. 245115, 2009.

[96] P.-Y. Chen and A. Alù, "Mantle cloaking using thin patterned metasurfaces," *Phys. Rev. B*, vol. 84, no. 20, p. 205110, 2011.

[97] P.-Y. Chen, J. Soric, and A. Alù, "Invisibility and cloaking based on scattering cancellation," *Adv. Mater.*, vol. 24, no. 44, pp. OP281–OP304, 2012.

[98] P.-Y. Chen, C. Argyropoulos, and A. Alù, "Broadening the cloaking bandwidth with non-foster metasurfaces," *Phys. Rev. Lett.*, vol. 111, no. 23, p. 233001, 2013.

[99] D. L. Sounas, R. Fleury, and A. Alù, "Unidirectional cloaking based on metasurfaces with balanced loss and gain," *Phys. Rev. Appl.*, vol. 4, no. 1, p. 014005, 2015.

[100] R. Fleury, F. Monticone, and A. Alù, "Invisibility and cloaking: Origins, present, and future perspectives," *Phys. Rev. Appl.*, vol. 4, no. 3, p. 037001, 2015.

[101] M. Dehmollaian and C. Caloz, "Concentric metawaveguide cloaking," in *2021 Fifteenth International Congress on Artificial Materials for Novel Wave Phenomena (Metamaterials)*. IEEE, 2021, pp. 111–113.

[102] F. Zangeneh-Nejad, D. L. Sounas, A. Alù, and R. Fleury, "Analogue computing with metamaterials," *Nat. Rev. Mater.*, vol. 6, no. 3, pp. 207–225, 2021.

[103] A. Pors, M. G. Nielsen, and S. I. Bozhevolnyi, "Analog computing using reflective plasmonic metasurfaces," *Nano letters*, vol. 15, no. 1, pp. 791–797, 2014.

[104] A. Momeni, H. Rajabalipanah, A. Abdolali, and K. Achouri, "Generalized optical signal processing based on multioperator metasurfaces synthesized by susceptibility tensors," *Phys. Rev. Appl.*, vol. 11, no. 6, p. 064042, 2019.

[105] H. Kwon, D. Sounas, A. Cordaro, A. Polman, and A. Alù, "Nonlocal metasurfaces for optical signal processing," *Phys. Rev. Lett.*, vol. 121, no. 17, p. 173004, 2018.

[106] T. Zhu, Y. Lou, Y. Zhou, J. Zhang, J. Huang, Y. Li, H. Luo, S. Wen, S. Zhu, Q. Gong *et al.*, "Generalized spatial differentiation from the spin hall effect of light and its application in image processing of edge detection," *Phys. Rev. Appl.*, vol. 11, no. 3, p. 034043, 2019.

[107] A. Silva, F. Monticone, G. Castaldi, V. Galdi, A. Alù, and N. Engheta, "Performing mathematical operations with metamaterials," *Science*, vol. 343, no. 6167, pp. 160–163, 2014.

[108] A. Abdolali, A. Momeni, H. Rajabalipanah, and K. Achouri, "Parallel integro-differential equation solving via multi-channel reciprocal bianisotropic metasurface augmented by normal susceptibilities," *New J. Phys.*, vol. 21, no. 11, p. 113048, 2019.

[109] M. F. Imani, J. N. Gollub, O. Yurduseven, A. V. Diebold, M. Boyarsky, T. Fromenteze, L. Pulido-Mancera, T. Sleasman, and D. R. Smith, "Review of metasurface antennas for computational microwave imaging," *IEEE Trans. Antennas Propag.*, vol. 68, no. 3, pp. 1860–1875, 2020.

[110] X. Lin, Y. Rivenson, N. T. Yardimci, M. Veli, Y. Luo, M. Jarrahi, and A. Ozcan, "All-optical machine learning using diffractive deep neural networks," *Science*, vol. 361, no. 6406, pp. 1004–1008, 2018.

[111] C. Qian, X. Lin, X. Lin, J. Xu, Y. Sun, E. Li, B. Zhang, and H. Chen, "Performing optical logic operations by a diffractive neural network," *Light Sci. Appl.*, vol. 9, no. 1, pp. 1–7, 2020.

[112] C. M. V. Burgos, T. Yang, Y. Zhu, and A. N. Vamivakas, "Design framework for metasurface optics-based convolutional neural networks," *Appl. Opt.*, vol. 60, no. 15, pp. 4356–4365, 2021.

[113] C. Liu, Q. Ma, Z. J. Luo, Q. R. Hong, Q. Xiao, H. C. Zhang, L. Miao, W. M. Yu, Q. Cheng, L. Li *et al.*, "A programmable diffractive deep neural network based on a digital-coding metasurface array," *Nat. Electron.*, pp. 1–10, 2022.

[114] C. Pfeiffer and A. Grbic, "Metamaterial Huygens' surfaces: tailoring wave fronts with reflectionless sheets," *Phys. Rev. Lett.*, vol. 110, no. 19, p. 197401, 2013.

[115] A. Epstein and G. V. Eleftheriades, "Synthesis of passive lossless metasurfaces using auxiliary fields for reflectionless beam splitting and perfect reflection," *Phys. Rev.letters*, vol. 117, no. 25, p. 256103, 2016.

[116] C. R. Simovski, M. S. Kondratjev, P. A. Belov, and S. A. Tretyakov, "Interaction effects in two-dimensional bianisotropic arrays," *IEEE Trans. Antennas Propag.*, vol. 47, no. 9, pp. 1429–1439, 1999.

[117] S. I. Maslovski and S. Tretyakov, "Full-wave interaction field in two-dimensional arrays of dipole scatterers," *Int. J. Electron Commun. (AEU)*, vol. 53, no. 3, pp. 135–139, 1999.

[118] S. A. Tretyakov, A. J. Viitanen, S. I. Maslovski, and I. E. Saarela, "Impedance boundary conditions for regular dense arrays of dipole scatterers," *IEEE Trans. Antennas Propag.*, vol. 51, no. 8, pp. 2073–2078, 2003.

[119] S. Tretyakov, *Analytical modeling in applied electromagnetics*. Artech House, 2003.

[120] C. L. Holloway, M. A. Mohamed, E. F. Kuester, and A. Dienstfrey, "Reflection and transmission properties of a metafilm: With an application to a controllable surface composed of resonant particles," *IEEE Trans. Electromagn. Compat.*, vol. 47, no. 4, pp. 853–865, 2005.

[121] M. Albooyeh, S. Tretyakov, and C. Simovski, "Electromagnetic characterization of bianisotropic metasurfaces on refractive substrates: General theoretical framework," *Ann. Phys.*, vol. 528, no. 9-10, pp. 721–737, 2016.

[122] V. Asadchy, Y. Ra'di, J. Vehmas, and S. Tretyakov, "Functional metamirrors using bianisotropic elements," *Phys. Rev. Lett.*, vol. 114, no. 9, p. 095503, 2015.

[123] E. F. Kuester, M. A. Mohamed, M. Piket-May, and C. L. Holloway, "Averaged transition conditions for electromagnetic fields at a metafilm," *IEEE Trans. Antennas Propag.*, vol. 51, no. 10, pp. 2641–2651, 2003.

[124] K. Achouri, M. A. Salem, and C. Caloz, "General metasurface synthesis based on susceptibility tensors," *IEEE Trans. Antennas Propag.*, vol. 63, no. 7, pp. 2977–2991, 2015.

[125] A. I. Dimitriadis, N. V. Kantartzis, T. D. Tsiboukis, and C. Hafner, "Generalized non-local surface susceptibility model and fresnel coefficients for the characterization of periodic metafilms with bianisotropic scatterers," *J. Comput. Phys.*, vol. 281, pp. 251–268, 2015.

[126] K. Achouri, G. Lavigne, and C. Caloz, "Comparison of two synthesis methods for birefringent metasurfaces," *Journal of Applied Physics*, vol. 120, no. 23, p. 235305, 2016.

[127] M. Dehmollaian, G. Lavigne, and C. Caloz, "Comparison of tensor boundary conditions with generalized sheet transition conditions," *IEEE Trans. Antennas Propag.*, vol. 67, no. 12, pp. 7396–7406, 2019.

[128] K. Achouri and C. Caloz, *Electromagnetic Metasurfaces: Theory and Applications*. Wiley-IEEE Press, 2020.

[129] M. Albooyeh, D.-H. Kwon, F. Capolino, and S. Tretyakov, "Equivalent realizations of reciprocal metasurfaces: Role of tangential and normal polarization," *Phys. Rev. B*, vol. 95, no. 11, p. 115435, 2017.

[130] K. Achouri and C. Caloz, "Controllable angular scattering with a bianisotropic metasurface," *2017 IEEE APS*, pp. 1489–1490, 2017.

[131] K. Achouri and O. J. Martin, "Angular scattering properties of metasurfaces," *IEEE Trans. Antennas Propag.*, vol. 68, no. 1, pp. 432–442, 2019.

[132] T. Smy, V. Tiukuvaara, S. Gupta *et al.*, "Ie-gstc metasurface field solver using surface susceptibility tensors with normal polarizabilities," *arXiv preprint arXiv:2105.05875*, 2021.

[133] K. Achouri, Y. Vahabzadeh, and C. Caloz, "Mathematical synthesis and analysis of a second-order magneto-electrically nonlinear metasurface," *Opt. Exp.*, vol. 25, no. 16, pp. 19 013–19 022, 2017.

[134] K. Achouri, A. Kiselev, and O. J. Martin, "Modeling of second-order nonlinear metasurfaces," *New J. Phys.*, 2022.

[135] N. Chamanara, Y. Vahabzadeh, and C. Caloz, "Simultaneous control of the spatial and temporal spectra of light with space-time varying metasurfaces," *IEEE Trans. Antennas Propag.*, vol. 67, no. 4, pp. 2430–2441, 2019.

[136] M. M. Idemen, *Discontinuities in the electromagnetic field*. John Wiley & Sons, 2011, vol. 40.

[137] C. L. Holloway, A. Dienstfrey, E. F. Kuester, J. F. O'Hara, A. K. Azad, and A. J. Taylor, "A discussion on the interpretation and characterization of metafilms/metasurfaces: The two-dimensional equivalent of metamaterials," *Metamaterials*, vol. 3, no. 2, pp. 100–112, 2009.

[138] G. Lavigne and C. Caloz, "Angle-independent nongyrotropic metasurfaces," in *2019 Thirteenth International Congress on Artificial Materials for Novel Wave Phenomena (Metamaterials)*. IEEE, 2019, pp. X–209.

[139] K. Achouri and O. J. Martin, "Fundamental properties and classification of polarization converting bianisotropic metasurfaces," *IEEE Trans. Antennas Propag.*, vol. 69, no. 9, pp. 5653–5663, 2021.

[140] Y. Vahabzadeh, K. Achouri, and C. Caloz, "Simulation of metasurfaces in finite difference techniques," *IEEE Trans. Antennas Propag.*, vol. 64, no. 11, pp. 4753–4759, 2016.

[141] Y. Vahabzadeh, N. Chamanara, K. Achouri, and C. Caloz, "Computational analysis of metasurfaces," *IEEE J. Multiscale Multiphysics Comput. Tech.*, vol. 3, pp. 37–49, 2018.

[142] Y. Vahabzadeh, N. Chamanara, and C. Caloz, "Generalized sheet transition condition fdtd simulation of metasurface," *IEEE Trans. Antennas Propag.*, vol. 66, no. 1, pp. 271–280, 2017.

[143] S. Sandeep, J.-M. Jin, and C. Caloz, "Finite-element modeling of metasurfaces with generalized sheet transition conditions," *IEEE Trans. Antennas Propag.*, vol. 65, no. 5, pp. 2413–2420, 2017.

[144] M. Dehmollaian, N. Chamanara, and C. Caloz, "Wave scattering by a cylindrical metasurface cavity of arbitrary cross section: Theory and applications," *IEEE Trans. Antennas Propag.*, vol. 67, no. 6, pp. 4059–4072, 2019.

[145] J. A. Kong, *Electromagnetic wave theory*. Wiley-Interscience, 1990.

[146] J. Budhu and A. Grbic, "Recent advances in bianisotropic boundary conditions: theory, capabilities, realizations, and applications," *Nanophotonics*, 2021.

[147] J. P. Wong, A. Epstein, and G. V. Eleftheriades, "Reflectionless wide-angle refracting metasurfaces," *IEEE Trans. Antennas Propag.*, vol. 15, pp. 1293–1296, 2016.

[148] M. Chen, E. Abdo-Sánchez, A. Epstein, and G. V. Eleftheriades, "Experimental verification of reflectionless wide-angle refraction via a bianisotropic huygens' metasurface," in *2017 XXXIInd General Assembly and Scientific Symposium of the International Union of Radio Science (URSI GASS)*. IEEE, 2017, pp. 1–4.

[149] M. Chen, E. Abdo-Sánchez, A. Epstein, and G. V. Eleftheriades, "Theory, design, and experimental verification of a reflectionless bianisotropic Huygens' metasurface for wide-angle refraction," *Phys. Rev. B*, vol. 97, no. 12, p. 125433, 2018.

[150] V. Popov, A. Díaz-Rubio, V. Asadchy, S. Tcvetkova, F. Boust, S. Tretyakov, and S. N. Burokur, "Omega-bianisotropic metasurface for converting a propagating wave into a surface wave," *Phys. Rev. B*, vol. 100, no. 12, p. 125103, 2019.

[151] S. Taravati, B. A. Khan, S. Gupta, K. Achouri, and C. Caloz, "Nonreciprocal nongyrotropic magnetless metasurface," *IEEE Trans. Antennas Propag.*, vol. 65, no. 7, pp. 3589–3597, 2017.

[152] A. H. Dorrah and G. V. Eleftheriades, "Bianisotropic huygens' metasurface pairs for nonlocal power-conserving wave transformations," *IEEE Antennas Wirel. Propag. Lett.*, vol. 17, no. 10, pp. 1788–1792, 2018.

[153] V. G. Ataloglou, A. H. Dorrah, and G. V. Eleftheriades, "Design of compact huygens' metasurface pairs with multiple reflections for arbitrary wave transformations," *IEEE Trans. Antennas Propag.*, vol. 68, no. 11, pp. 7382–7394, 2020.

[154] D. Lin, P. Fan, E. Hasman, and M. L. Brongersma, "Dielectric gradient metasurface optical elements," *science*, vol. 345, no. 6194, pp. 298–302, 2014.

[155] Y. F. Yu, A. Y. Zhu, R. Paniagua-Domínguez, Y. H. Fu, B. Luk'yanchuk, and A. I. Kuznetsov, "High-transmission dielectric metasurface with 2π phase control at visible wavelengths," *Laser & Photonics Reviews*, vol. 9, no. 4, pp. 412–418, 2015.

[156] M. Decker, I. Staude, M. Falkner, J. Dominguez, D. N. Neshev, I. Brener, T. Pertsch, and Y. S. Kivshar, "High-efficiency dielectric huygens' surfaces," *Advanced Optical Materials*, vol. 3, no. 6, pp. 813–820, 2015.

[157] K. Achouri, A. Yahyaoui, S. Gupta, H. Rmili, and C. Caloz, "Dielectric resonator metasurface for dispersion engineering," *IEEE Trans. Antennas Propag.*, vol. 65, no. 2, pp. 673–680, 2016.

[158] A. E. Olk and D. A. Powell, "Accurate metasurface synthesis incorporating near-field coupling effects," *Phys. Rev. Appl.*, vol. 11, no. 6, p. 064007, 2019.

[159] F. Ding, A. Pors, and S. I. Bozhevolnyi, "Gradient metasurfaces: a review of fundamentals and applications," *Rep. Prog. Phys.*, vol. 81, no. 2, p. 026401, 2017.

[160] N. M. Estakhri and A. Alù, "Wave-front transformation with gradient metasurfaces," *Phys. Rev. X*, vol. 6, no. 4, p. 041008, 2016.

[161] W. L. Stutzman and G. A. Thiele, *Antenna theory and design*. John Wiley & Sons, 2012.

[162] M. W. Farn, "Binary gratings with increased efficiency," *Applied optics*, vol. 31, no. 22, pp. 4453–4458, 1992.

[163] B. O. Zhu and Y. Feng, "Passive metasurface for reflectionless and arbitary control of electromagnetic wave transmission," *IEEE Trans. Antennas Propag.*, vol. 63, no. 12, pp. 5500–5511, 2015.

[164] D. Sell, J. Yang, S. Doshay, R. Yang, and J. A. Fan, "Large-angle, multifunctional metagratings based on freeform multimode geometries," *Nano Lett.*, vol. 17, no. 6, pp. 3752–3757, 2017.

[165] Y. Ra'di, D. L. Sounas, and A. Alu, "Metagratings: beyond the limits of graded metasurfaces for wave front control," *Phys. Rev.letters*, vol. 119, no. 6, p. 067404, 2017.

[166] A. Epstein and O. Rabinovich, "Unveiling the properties of metagratings via a detailed analytical model for synthesis and analysis," *Phys. Rev. Appl.*, vol. 8, no. 5, p. 054037, 2017.

[167] V. Popov, F. Boust, and S. N. Burokur, "Controlling diffraction patterns with metagratings," *Phys. Rev. Appl.*, vol. 10, no. 1, p. 011002, 2018.

[168] V. Neder, Y. Ra'di, A. Alù, and A. Polman, "Combined metagratings for efficient broad-angle scattering metasurface," *ACS photonics*, vol. 6, no. 4, pp. 1010–1017, 2019.

[169] B. E. Saleh, M. C. Teich, and B. E. Saleh, *Fundamentals of photonics*. Wiley New York, 1991, vol. 22.

[170] E. Malus, "Sur une propriété de la lumière réfléchie," *Mém. Phys. Chim. Soc. d'Arcueil*, vol. 2, pp. 143–158, 1809.

[171] D. Brewster, "On the laws which regulate the polarisation of light by reflexion from transparent bodies," *Philos. Trans. R. Soc.*, vol. 105, pp. 125–159, 1815.

[172] A. J. Fresnel, *Mémoire sur la loi des modifications que la réflexion imprime à la lumière polarisée*. De l'Imprimerie De Firmin Didot Fréres, 1834.

[173] C. L. Giles and W. J. Wild, "Brewster angles for magnetic media," *J. Infrared Millim. Terahertz Waves*, vol. 6, no. 3, pp. 187–197, 1985.

[174] R. Paniagua-Domínguez, Y. F. Yu, A. E. Miroshnichenko, L. A. Krivitsky, Y. H. Fu, V. Valuckas, L. Gonzaga, Y. T. Toh, A. Y. S. Kay, B. Luk'yanchuk *et al.*, "Generalized Brewster effect in dielectric metasurfaces," *Nature Comm.*, vol. 7, no. 1, pp. 1–9, 2016.

[175] D. R. Abujetas, J. A. Sanchez-Gil, and J. J. Sáenz, "Generalized brewster effect in high-refractive-index nanorod-based metasurfaces," *Opt. Express*, vol. 26, no. 24, pp. 31 523–31 541, 2018.

[176] Y. Tamayama, "Brewster effect in metafilms composed of bi-anisotropic split-ring resonators," *Opt. Let.*, vol. 40, no. 7, pp. 1382–1385, 2015.

[177] S. Yin and J. Qi, "Metagrating-enabled Brewster's angle for arbitrary polarized electromagnetic waves and its manipulation," *Opt. Express*, vol. 27, no. 13, pp. 18 113–18 122, 2019.

[178] C. Wang, Z. Zhu, W. Cui, Y. Yang, L. Ran, and D. Ye, "All-angle brewster effect observed on a terahertz metasurface," *Appl. Phys. Lett.*, vol. 114, no. 19, p. 191902, 2019.

[179] Z. Zhang, Z. Che, X. Liang, J. Chu, J. Zeng, H. Huang, F. Guan, L. Shi, X. Liu, and J. Zi, "Realizing generalized brewster effect by generalized kerker effect," *Phys. Rev. Appl.*, vol. 16, no. 5, p. 054017, 2021.

[180] V. S. Asadchy, M. S. Mirmoosa, A. Díaz-Rubio, S. Fan, and S. A. Tretyakov, "Tutorial on electromagnetic nonreciprocity and its origins," *Proc. IEEE*, vol. 108, no. 10, pp. 1684–1727, 2020.

[181] A. B. Villaverde, D. Donatti, and D. Bozinis, "Terbium gallium garnet verdet constant measurements with pulsed magnetic field," *J. Phys. C: Solid State Phys.*, vol. 11, no. 12, p. L495, 1978.

[182] N. Reiskarimian, "A review of nonmagnetic nonreciprocal electronic devices: Recent advances in nonmagnetic nonreciprocal components," *IEEE J. Solid-State Circuits*, vol. 13, no. 4, pp. 112–121, 2021.

[183] Y. Shi, Z. Yu, and S. Fan, "Limitations of nonlinear optical isolators due to dynamic reciprocity," *Nat. Photonics*, vol. 9, no. 6, pp. 388–392, 2015.

[184] D. L. Sounas, J. Soric, and A. Alù, "Broadband passive isolators based on coupled nonlinear resonances," *Nat. Electron.*, vol. 1, no. 2, pp. 113–119, 2018.

[185] D. E. Fernandes and M. G. Silveirinha, "Asymmetric transmission and isolation in nonlinear devices: why they are different," *IEEE Antennas Wirel. Propag. Lett.*, vol. 17, no. 11, pp. 1953–1957, 2018.

[186] Y. Hadad, J. C. Soric, and A. Alù, "Breaking temporal symmetries for emission and absorption," *Proc. Natl. Acad. Sci. U.S.A.*, vol. 113, no. 13, pp. 3471–3475, 2016.

[187] Y. Shi, S. Han, and S. Fan, "Optical circulation and isolation based on indirect photonic transitions of guided resonance modes," *ACS Photonics*, vol. 4, no. 7, pp. 1639–1645, 2017.

[188] D. L. Sounas, C. Caloz, and A. Alu, "Giant non-reciprocity at the subwavelength scale using angular momentum-biased metamaterials," *Nature communications*, vol. 4, p. 2407, 2013.

[189] D. L. Sounas, N. A. Estep, A. Kord, and A. Alù, "Angular-momentum biased circulators and their power consumption," *IEEE Antennas Wirel. Propag. Lett*, vol. 17, no. 11, pp. 1963–1967, 2018.

[190] Y. E. Wang, "On time-modulation-enabled nonreciprocity," *IEEE Antennas Wirel. Propag. Lett*, vol. 17, no. 11, pp. 1973–1977, 2018.

[191] A. Shaltout, A. Kildishev, and V. Shalaev, "Time-varying metasurfaces and lorentz non-reciprocity," *Opt. Mater. Exp.*, vol. 5, no. 11, pp. 2459–2467, 2015.

[192] S. Taravati and A. A. Kishk, "Space-time modulation: Principles and applications," *IEEE Microw. Mag.*, vol. 21, no. 4, pp. 30–56, 2020.

[193] S. Taravati and G. V. Eleftheriades, "Full-duplex nonreciprocal beam steering by time-modulated phase-gradient metasurfaces," *Phys. Rev. Appl.*, vol. 14, no. 1, p. 014027, 2020.

[194] B.-I. Popa and S. A. Cummer, "An architecture for active metamaterial particles and experimental validation at rf," *Microw. Opt. Technol. Lett*, vol. 49, no. 10, pp. 2574–2577, 2007.

[195] Y. Yuan, B.-I. Popa, and S. A. Cummer, "Zero loss magnetic metamaterials using powered active unit cells," *Opt. Express*, vol. 17, no. 18, pp. 16 135–16 143, 2009.

[196] B.-I. Popa and S. A. Cummer, "Nonreciprocal active metamaterials," *Phys. Rev. B*, vol. 85, no. 20, p. 205101, 2012.

[197] T. Kodera, D. L. Sounas, and C. Caloz, "Artificial Faraday rotation using a ring metamaterial structure without static magnetic field," *Appl. Phys. Lett*, vol. 99, no. 3, p. 031114, 2011.

[198] Z. Wang, Z. Wang, J. Wang, B. Zhang, J. Huangfu, J. D. Joannopoulos, M. Soljačić, and L. Ran, "Gyrotropic response in the absence of a bias field," *Proceedings of the National Academy of Sciences*, vol. 109, no. 33, pp. 13 194–13 197, 2012.

[199] D. L. Sounas, T. Kodera, and C. Caloz, "Electromagnetic modeling of a magnetless nonreciprocal gyrotropic metasurface," *IEEE Trans. Antennas Propag*, vol. 61, no. 1, pp. 221–231, 2012.

[200] T. Kodera, D. L. Sounas, and C. Caloz, "Magnetless nonreciprocal metamaterial (mnm) technology: application to microwave components," *IEEE Trans. Microw. Theory Tech*, vol. 61, no. 3, pp. 1030–1042, 2013.

[201] Y. Ra'di and A. Grbic, "Magnet-free nonreciprocal bianisotropic metasurfaces," *Phys. Rev.B*, vol. 94, no. 19, p. 195432, 2016.

[202] T. Kodera and C. Caloz, "Unidirectional loop metamaterials (ulm) as magnetless artificial ferrimagnetic materials: principles and applications," *IEEE Antennas Wirel. Propag. Lett*, vol. 17, no. 11, pp. 1943–1947, 2018.

[203] Y. Ra'di and A. Alù, "Nonreciprocal wavefront manipulation in synthetically moving metagratings," in *Photonics*, vol. 7, no. 2. Multidisciplinary Digital Publishing Institute, 2020, p. 28.

[204] S. Taravati and G. V. Eleftheriades, "Full-duplex reflective beamsteering metasurface featuring magnetless nonreciprocal amplification," *Nat. Commun.*, vol. 12, p. 4414, 2021.

[205] S. Taravati and G. V. Eleftheriades, "Programmable nonreciprocal meta-prism," *Sci. Rep.*, vol. 11, no. 1, pp. 1–12, 2021.

[206] Y. B. Li, S. Y. Wang, H. P. Wang, H. Li, J. L. Shen, and T. J. Cui, "Nonreciprocal control of electromagnetic polarizations applying active metasurfaces," *Adv. Opt. Mater.*, p. 2102154, 2022.

[207] D. Ramaccia, D. L. Sounas, A. Alu, A. Toscano, and F. Bilotti, "Phase-induced frequency conversion and doppler effect with time-modulated metasurfaces," *IEEE Trans. Antennas Propag.*, vol. 68, no. 3, pp. 1607–1617, 2019.

[208] X. Guo, Y. Ding, Y. Duan, and X. Ni, "Nonreciprocal metasurface with space–time phase modulation," *Light Sci. Appl.*, vol. 8, no. 1, pp. 1–9, 2019.

[209] L. Zhang, X. Q. Chen, S. Liu, Q. Zhang, J. Zhao, J. Y. Dai, G. D. Bai, X. Wan, Q. Cheng, G. Castaldi *et al.*, "Space-time-coding digital metasurfaces," *Nat. Comm.*, vol. 9, no. 1, pp. 1–11, 2018.

[210] A. M. Shaltout, V. M. Shalaev, and M. L. Brongersma, "Spatiotemporal light control with active metasurfaces," *Science*, vol. 364, no. 6441, p. eaat3100, 2019.

[211] X. Wang and C. Caloz, "Spread-spectrum selective camouflaging based on time-modulated metasurface," *IEEE Trans. Antennas Propag.*, vol. 69, no. 1, pp. 286–295, 2020.

[212] X. Wang, A. Diaz-Rubio, H. Li, S. A. Tretyakov, and A. Alu, "Theory and design of multifunctional space-time metasurfaces," *Phys. Rev. Appl.*, vol. 13, no. 4, p. 044040, 2020.

[213] A. M. Urbas, Z. Jacob, L. Dal Negro, N. Engheta, A. Boardman, P. Egan, A. B. Khanikaev, V. Menon, M. Ferrera, N. Kinsey *et al.*, "Roadmap on optical metamaterials," *J. Opt.*, vol. 18, no. 9, p. 093005, 2016.

[214] H. Shi, A. Zhang, S. Zheng, J. Li, and Y. Jiang, "Dual-band polarization angle independent 90 polarization rotator using twisted electric-field-coupled resonators," *Appl. Phys. Lett.*, vol. 104, no. 3, p. 034102, 2014.

[215] K. Achouri, G. Lavigne, M. A. Salem, and C. Caloz, "Metasurface spatial processor for electromagnetic remote control," *IEEE Trans. Antennas Propag.*, vol. 64, no. 5, pp. 1759–1767, 2016.

[216] M. Khorasaninejad, W. T. Chen, R. C. Devlin, J. Oh, A. Y. Zhu, and F. Capasso, "Metalenses at visible wavelengths: Diffraction-limited focusing and subwavelength resolution imaging," *Science*, vol. 352, no. 6290, pp. 1190–1194, 2016.

[217] G. Lavigne, K. Achouri, C. Caloz, V. Asadchy, and S. Tretyakov, "Perfectly refractive metasurface using bianisotropy," in *2017 IEEE International Symposium on Antennas*

and Propagation & USNC/URSI National Radio Science Meeting. IEEE, 2017, pp. 1713–1714.

[218] E. J. Rothwell and M. J. Cloud, *Electromagnetics*. CRC press, 2018.

[219] M. A. Salem and C. Caloz, "Manipulating light at distance by a metasurface using momentum transformation," *Opt. Express*, vol. 22, no. 12, pp. 14 530–14 543, 2014.

[220] D. M. Pozar, *Microwave engineering*. John Wiley & Sons, 2009.

[221] C. A. Balanis, *Antenna theory: analysis and design*. John wiley & sons, 2016.

[222] G. Lavigne, K. Achouri, V. S. Asadchy, S. A. Tretyakov, and C. Caloz, "Susceptibility derivation and experimental demonstration of refracting metasurfaces without spurious diffraction," *IEEE Trans. Antennas Propag.*, vol. 66, no. 3, pp. 1321–1330, 2018.

[223] G. Lavigne and C. Caloz, "Extending the Brewster effect to arbitrary angle and polarization using bianisotropic metasurfaces," in *2018 IEEE International Symposium on Antennas and Propagation & USNC/URSI National Radio Science Meeting*. IEEE, 2018, pp. 771–772.

[224] J. D. Jackson, *Classical electrodynamics*. American Association of Physics Teachers, 1999.

[225] R. Alaee, M. Albooyeh, A. Rahimzadegan, M. S. Mirmoosa, Y. S. Kivshar, and C. Rockstuhl, "All-dielectric reciprocal bianisotropic nanoparticles," *Phys. Rev. B*, vol. 92, no. 24, p. 245130, 2015.

[226] M. Odit, P. Kapitanova, P. Belov, R. Alaee, C. Rockstuhl, and Y. S. Kivshar, "Experimental realisation of all-dielectric bianisotropic metasurfaces," *Appl. Phys. Lett.*, vol. 108, no. 22, p. 221903, 2016.

[227] D. L. Sounas and A. Alù, "Nonreciprocity based on nonlinear resonances," *IEEE Antennas Wirel. Propag. Lett*, vol. 17, no. 11, pp. 1958–1962, 2018.

[228] M. Dehmollaian, G. Lavigne, and C. Caloz, "Comparison of tensor boundary conditions with generalized sheet transition conditions," *IEEE Trans. Antennas Propag.*, vol. 67, no. 12, pp. 7396–7406, 2019.

[229] J. A. Kong, "Theorems of bianisotropic media," *Proc. IEEE*, vol. 60, no. 9, pp. 1036–1046, 1972.

[230] D. M. Pozar, *Microwave Engineering*, 4th ed. Wiley, 2011, chap. 9.

[231] C. Caloz and A. Sihvola, "Electromagnetic chirality, Part I: Microscopic perspective," *IEEE Antennas Propag. Mag.*, vol. 62, no. 1, pp. 58–71, 2020.

[232] C. Caloz and A. Sihvola, "Electromagnetic chirality, Part II: Macroscopic perspective," *IEEE Antennas Propag. Mag.*, vol. 62, no. 2, pp. 89–98, 2020.

[233] Y. Cheng, W. Li, and X. Mao, "Triple-band polarization angle independent 90° polarization rotator based on fermat's spiral structure planar chiral metamaterial," *Prog. Electromagn. Res*, vol. 165, pp. 35–45, 2019.

[234] T. Kodera, G. Lavigne, and C. Caloz, "Transistor-based magnetless faraday metasurface and spatial isolator," in *2020 IEEE APS*. IEEE, 2020, pp. 713–714.

[235] A. Ishimaru, *Electromagnetic wave propagation, radiation, and scattering: from fundamentals to applications*. John Wiley & Sons, 2017.

[236] S. Tretyakov, A. Sihvola, A. Sochava, and C. Simovski, "Magnetoelectric interactions in bi-anisotropic media," *J. Electromagn. Waves Appl.*, vol. 12, no. 4, pp. 481–497, 1998.

APPENDIX A GENERALIZED SHEET TRANSITION CONDITIONS DERIVATION FOR FLAT METASURFACES

Assuming the time-harmonic conventional $e^{+j\omega t}$, the sourceless Maxwell equations take the form

$$\nabla \times \mathbf{E} = -j\omega\mathbf{B}, \tag{A.1a}$$

$$\nabla \times \mathbf{H} = j\omega\mathbf{D}, \tag{A.1b}$$

where the fields are related to the induced electric polarization density $\mathbf{P}$ and the induced magnetic polarization density $\mathbf{M}$ by the constitutive relations

$$\mathbf{D} = \epsilon_0\mathbf{E} + \mathbf{P} \quad \text{or} \quad \mathbf{E} = (\mathbf{D} - \mathbf{P})/\epsilon_0, \tag{A.2a}$$

$$\mathbf{B} = \mu_0(\mathbf{H} + \mathbf{M}) \quad \text{or} \quad \mathbf{H} = \mathbf{B}/\mu_0 - \mathbf{M}. \tag{A.2b}$$

The GSTCs aim to model the response of the metasurface in term of effective polarizations. To do so, we shall express the fields $\mathbf{D}$ and $\mathbf{E}$ in terms of $\mathbf{P}$ and the fields $\mathbf{B}$ and $\mathbf{H}$ in terms of $\mathbf{M}$ using (A.2). Inserting (A.2) into (A.1) yields

$$\nabla \times [(\mathbf{D} - \mathbf{P})/\epsilon_0] = -j\omega\mu_0(\mathbf{H} + \mathbf{M}), \tag{A.3a}$$

$$\nabla \times (\mathbf{B}/\mu_0 - \mathbf{M}) = j\omega(\epsilon_0\mathbf{E} + \mathbf{P}). \tag{A.3b}$$

Assuming the first-order metasurface discontinuity [124], we can split the polarization densities into volume and surface components as

$$\mathbf{P} = \mathbf{P}_\mathrm{v} + \mathbf{P}_\mathrm{s}\delta(z), \tag{A.4a}$$

$$\mathbf{M} = \mathbf{M}_\mathrm{v} + \mathbf{M}_\mathrm{s}\delta(z), \tag{A.4b}$$

where the $\delta(z)$ is the Dirac delta distribution. Inserting (A.4) into (A.3), and rearranging the parts related to the surface polarization densities on the right-hand side leads to

$$\nabla \times [(\mathbf{D} - \mathbf{P}_\mathrm{v})/\epsilon_0] = -j\omega\mu_0\mathbf{H} - j\omega\mu_0\mathbf{M}_\mathrm{v} - j\omega\mu_0\mathbf{M}_\mathrm{s}\delta(z) + \nabla \times (\mathbf{P}_\mathrm{s}\delta(z)/\epsilon_0), \tag{A.5a}$$

$$\nabla \times (\mathbf{B}/\mu_0 - \mathbf{M}_\mathrm{v}) = j\omega\epsilon_0\mathbf{E} + j\omega\mathbf{P}_\mathrm{v} + j\omega\mathbf{P}_\mathrm{s}\delta(z) + \nabla \times [\mathbf{M}_\mathrm{s}\delta(z)]. \tag{A.5b}$$

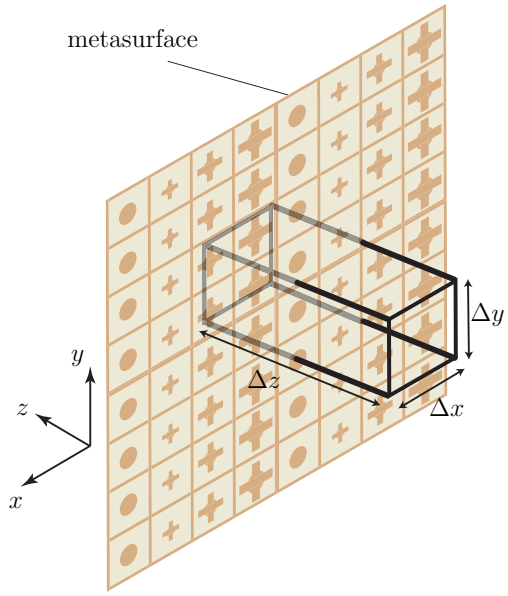

Figure A.1 Flat metasurface placed in the xy-plane with the related integration pillbox

We can now use the conventional pillbox integration technique over a rectangular surface around the metasurface as shown in Fig. A.1 and apply Stokes theorem, which yields

$$\oint[(\mathbf{D}-\mathbf{P}_{\mathrm{v}})/\epsilon_0]\cdot d\mathbf{l} = -j\omega\mu_0 \iint(\mathbf{H}+\mathbf{M}_{\mathrm{v}})\cdot d\mathbf{S} - j\omega\mu_0 \iint \delta(z)\mathbf{M}_{\mathrm{s}}\cdot d\mathbf{S} + \oint(\delta(z)\mathbf{P}_{\mathrm{s}}/\epsilon_0)\cdot d\mathbf{l}, \quad \text{(A.6a)}$$

$$\oint(\mathbf{B}/\mu_0 - \mathbf{M}_{\mathrm{v}})\cdot d\mathbf{l} = j\omega\epsilon_0 \iint(\mathbf{E}+\mathbf{P}_{\mathrm{v}}/\epsilon_0)\cdot d\mathbf{S} + j\omega \iint \delta(z)\mathbf{P}_{\mathrm{s}}\cdot d\mathbf{S} + \oint \mathbf{M}_{\mathrm{s}}\delta(z)\cdot d\mathbf{l}, \quad \text{(A.6b)}$$

where $d\mathbf{S}$ and $d\mathbf{l}$ are the surfaces and contours of the pillbox integration domain of Fig. A.1. The integrands in the left-hand sides of (A.6) can be simplified through the constitutive relations (A.3) as

$$(\mathbf{D}^{\pm} - \mathbf{P}_{\mathrm{v}}^{\pm})/\epsilon_0 = \mathbf{E}^{\pm}, \quad \mathbf{B}^{\pm}/\mu_0 - \mathbf{M}_{\mathrm{v}}^{\pm} = \mathbf{H}^{\pm}, \quad \text{(A.7)}$$

where the $+$ and $-$ signs respectively represent the $+z$ and $-z$ regions in Fig. A.1. Next, we substitute (A.7) into (A.6) and integrate these relations over one of the xz-plane of the pillbox which yields

$$\begin{aligned}&(E_x^+ - E_x^-)\Delta x + (E_z^{\mathrm{left}} + E_z^{\mathrm{right}})\Delta z = \\ &-j\omega\mu_0(H_y + M_{\mathrm{v},y})\Delta x\Delta z - j\omega\mu_0 M_{\mathrm{s},y}\delta(z)\Delta x\Delta z - (P_{\mathrm{s},z}^{\mathrm{right}} - P_{\mathrm{s},z}^{\mathrm{left}})\delta(z)\Delta z/\epsilon_0,\end{aligned} \quad \text{(A.8a)}$$

$$\begin{aligned}&(H_x^+ - H_x^-)\Delta x + (H_z^{\mathrm{left}} + H_z^{\mathrm{right}})\Delta z = \\ &j\omega\epsilon_0(E_y + P_{\mathrm{v},y}/\epsilon_0)\Delta x\Delta z + j\omega P_{\mathrm{s},y}\delta(z)\Delta x\Delta z - (M_{\mathrm{s},z}^{\mathrm{right}} - M_{\mathrm{s},z}^{\mathrm{left}})\delta(z)\Delta z.\end{aligned} \quad \text{(A.8b)}$$

We then take the limit $\Delta z \to 0$, replace $\delta(z)\Delta z \to 1$ and divide by Δx which reduces (A.8) to

$$E_x^+ - E_x^- = -j\omega\mu_0 M_{\mathrm{s},y} - (P_{\mathrm{s},z,\mathrm{right}} - P_{\mathrm{s},z,\mathrm{left}})/(\epsilon_0 \Delta x), \tag{A.9a}$$

$$H_x^+ - H_x^- = -j\omega P_{\mathrm{s},y} - (M_{\mathrm{s},z,\mathrm{right}} - M_{\mathrm{s},z,\mathrm{left}})/\Delta x, \tag{A.9b}$$

which, by taking the limit $\Delta x \to 0$ reduces to

$$\Delta E_x = -j\omega\mu_0 M_{\mathrm{s},y} - \frac{\partial(P_{\mathrm{s},z}/\epsilon_0)}{\partial_x}, \tag{A.10a}$$

$$\Delta H_x = -j\omega P_{\mathrm{s},y} - \frac{\partial M_{\mathrm{s},z}}{\partial_x}, \tag{A.10b}$$

where $\Delta E_x = E_x^+ - E_x^-$ and $\Delta H_x = H_x^+ - H_x^-$. Similarly, by integrating (A.6) over one of the yz-plane of the pillbox, we obtain

$$\Delta E_y = j\omega\mu_0 M_{\mathrm{s},x} - \frac{\partial(P_{\mathrm{s},z}/\epsilon_0)}{\partial_y}, \tag{A.11a}$$

$$\Delta H_y = -j\omega P_{\mathrm{s},x} - \frac{\partial M_{\mathrm{s},z}}{\partial_y}, \tag{A.11b}$$

where $\Delta E_y = E_y^+ - E_y^-$ and $\Delta H_y = H_y^+ - H_y^-$.
Finally, by combining (A.10) and (A.11), we obtain the GSTCs for a flat metasurface as

$$\hat{z} \times \Delta\mathbf{E} = -j\omega\mu\mathbf{M}_{\parallel} - \frac{1}{\epsilon}\hat{z} \times \nabla P_z, \tag{A.12a}$$

$$\hat{z} \times \Delta\mathbf{H} = j\omega\mathbf{P}_{\parallel} - \hat{z} \times \nabla M_z, \tag{A.12b}$$

where $\parallel$ refer to the tangential components x and y.

APPENDIX B LIST OF PUBLICATIONS

Journal publications

1. Lavigne, G., Achouri, K., Asadchy, V. S., Tretyakov, S. A., and Caloz, C. (2018). Susceptibility derivation and experimental demonstration of refracting metasurfaces without spurious diffraction. IEEE Transactions on Antennas and Propagation, 66(3), 1321-1330.

2. Dehmollaian, M., Lavigne, G., and Caloz, C. (2019). Comparison of tensor boundary conditions with generalized sheet transition conditions. IEEE Transactions on Antennas and Propagation, 67(12), 7396-7406.

3. Lavigne, G., and Caloz, C. (2021). Generalized Brewster effect using bianisotropic metasurfaces. Optics Express, 29(7), 11361-11370.

4. Lavigne, G., and Caloz, C. (2021). Magnetless reflective gyrotropic spatial isolator metasurface. New Journal of Physics, 23, 075006.

5. Lavigne, G., Kodera, T., and Caloz, C. (2022). Metasurface Magnetless Specular Isolator. Scientific Reports, 12, 5652(2022).

Conference publications

1. Lavigne, G., and Caloz, C. (2019, January). Manipulation of Fresnel Coefficients using Crossanisotropic Metasurface Coating. In 2019 United States National Committee of URSI National Radio Science Meeting (USNC-URSI NRSM) (pp. 1-2). IEEE.

2. Patri, A., Lavigne, G., and Caloz, C. (2019, July). Transmissive Suppressed-Order Diffraction Grating (SODG). In 2019 IEEE International Symposium on Antennas and Propagation and USNC-URSI Radio Science Meeting (pp. 1209-1210). IEEE.

3. Lavigne, G., and Caloz, C. (2019, July). Towards Generalized Transistor-based Magnetless Nonreciprocal Metasurface. In 2019 IEEE International Symposium on Antennas and Propagation and USNC-URSI Radio Science Meeting (pp. 1617-1618). IEEE.

4. M. Dehmollaian, G. Lavigne, and C. Caloz, "Electromagnetic sink based on a nonreciprocal metasurface cavity," in META'19, Lisbon, Portugal, Jul. 2019.

5. Lavigne, G., and Caloz, C. (2019, September). Nonreciprocal phase gradient metasurface: Principle and transistor implementation. In 2019 Thirteenth International Congress on Artificial Materials for Novel Wave Phenomena (Metamaterials) (pp. X-212). IEEE.

6. Lavigne, G., and Caloz, C. (2019, September). Angle-independent nongyrotropic metasurfaces. In 2019 Thirteenth International Congress on Artificial Materials for Novel Wave Phenomena (Metamaterials) (pp. X-209). IEEE.

7. Kodera, T., Lavigne, G., and Caloz, C. (2020, July). Transistor-based Magnetless Faraday Metasurface and Spatial Isolator. In 2020 IEEE International Symposium on Antennas and Propagation and North American Radio Science Meeting (pp. 713-714). IEEE.

8. Lavigne, G., and Caloz, C. (2020, July). Metasurface specular isolator. In 2020 IEEE International Symposium on Antennas and Propagation and North American Radio Science Meeting (pp. 951-952). IEEE.

9. G. Lavigne, T. Kodera, and C. Caloz, "'Perfect' Faraday-rotation metasurface," in Metamaterials'2020, Int. Congr. Art. Mat. Nov. Wave. Phenom., New York, USA, Sep. 2020, pp. 156–158.

10. Lavigne, G., and Caloz, C. (2021, March). Nonreciprocal Wavefront Manipulation with Transistor-loaded Metasurfaces. In 2021 15th European Conference on Antennas and Propagation (EuCAP) (pp. 1-3). IEEE.

11. Lavigne, G., and Caloz, C. (2021). Advances in Bianisotropic GSTC-based Metasurfaces. In 2021 IEEE International Symposium on Antennas and Propagation and USNC-URSI Radio Science Meeting. IEEE.